USGS
science for a changing world

Topographic Slope as a Proxy for Seismic Site-Conditions (V_s^{30}) and Amplification Around the Globe

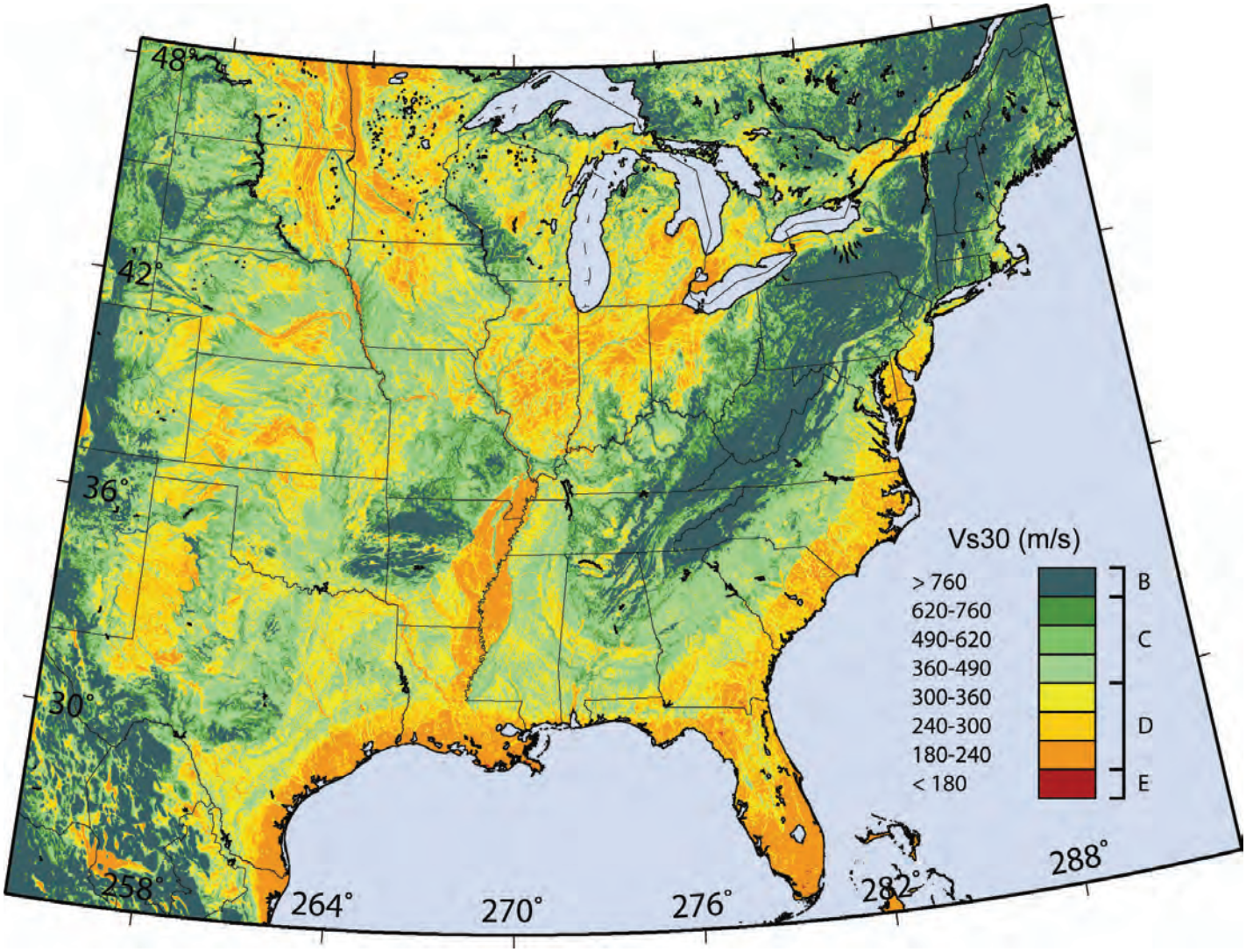

Open-File Report 2007-1357

U.S. Department of the Interior
U.S. Geological Survey

Topographic Slope as a Proxy for Seismic Site-Conditions (V_S^{30}) and Amplification Around the Globe

By Trevor I. Allen and David J. Wald

Open-File Report 2007–1357

U.S. Department of the Interior
U.S. Geological Survey

U.S. Department of the Interior
DIRK KEMPTHORNE, Secretary

U.S. Geological Survey
Mark D. Myers, Director

U.S. Geological Survey, Reston, Virginia 2007

For product and ordering information:
World Wide Web: http://www.usgs.gov/pubprod
Telephone: 1-888-ASK-USGS

For more information on the USGS—the Federal source for science about the Earth,
its natural and living resources, natural hazards, and the environment:
World Wide Web: http://www.usgs.gov
Telephone: 1-888-ASK-USGS

Suggested citation:
Allen, T.I., and Wald, D.J., 2007, Topographic slope as a proxy for global seismic site conditions (V_S^{30}) and amplification around the globe: U.S. Geological Survey Open-File Report 2007-1357, 69 p.

Contents

Figures

Tables

Topographic Slope as a Proxy for Seismic Site-Conditions (V_S^{30}) and Amplification Around the Globe

By Trevor I. Allen and David J. Wald[1]

Executive Summary

It is well-known that large global earthquakes can have a dramatic effect on local communities and the built environment. Moreover, ground motions amplified by surficial materials can exacerbate the situation, often making the difference between minor and major damage. For a real-time earthquake impact alert system, such as Prompt Assessment of Global Earthquakes for Response (PAGER) (Wald and others, 2006), we seek to rapidly evaluate potential ground shaking in the source region and subsequently provide an estimate of the population exposure to potentially fatal levels of ground shaking in any region of the world. The contribution of surficial geology (particularly soft sediments) to the amplification of ground shaking is an important component in predicting the levels of ground motion observed at any site. Unfortunately, the availability of information regarding seismic site-conditions is only available at a few sites around the globe.

Herein, we describe a methodology for deriving maps of seismic site-conditions anywhere in the world using topographic slope as a proxy. Average shear-velocity down to 30 m (or V_S^{30}) measurements are correlated against topographic slope to develop two sets of coefficients for predicting V_S^{30}: one for active tectonic regions that possess dynamic topographic relief, and one for stable continental regions where changes in topography are more subdued. These coefficients have been applied to the continental United States, in addition to other regions around the world. They are subsequently compared to existing site-condition maps based on geology and observed V_S^{30} measurements, where available. The application of the topographic slope method in regions with abundant V_S^{30} measurements (for example California, Memphis, and Taiwan) indicates that this method provides site condition-maps of similar quality, or in some cases, maps superior to those developed from more traditional techniques.

Having a first-order assessment of seismic site-conditions anywhere in the world provides a valuable tool to rapidly estimate ground motions following any global earthquake, the primary motivation for this research. These V_S^{30} maps will enable us to better quantify possible ground shaking and rapidly deliver these predictions to emergency managers and responders. In addition, the V_S^{30} maps for the globe will also have practical applications for numerous related probabilistic- and scenario-based studies. To date, several researchers have requested maps or have used the approach outlined herein for their own applications (for example Cagnan and Kariptas, written commun., 2007; Harmandar and others, 2007).

Given that we anticipate a significant demand for these products, we have developed an internet delivery service so that users can download maps and grids of seismic site-conditions for specified regions. To some extent, these grids can also be customized by the user if they disagree with the predefined correlations derived using the methodologies described within this report.

Finally, this report represents a more comprehensive account of this technique and provides a more fully illustrated global description of results than that given in Wald and Allen (2007), which has been accepted for publication in the Bulletin of the Seismological Society of America.

[1] U.S. Geological Survey, Geologic Hazards Team, 1711 Illinois St., Golden, CO 80401

Introduction

Recognition of the importance of the ground motion amplification from regolith has lead to the development of systematic approaches to mapping seismic site-conditions (for example, Park and Elrick, 1998; Wills and others, 2000; Holzer and others, 2005) as well as to quantifying both amplitude- and frequency-dependent site amplifications (for example, Borcherdt, 1994). A now standardized approach is measuring or mapping the average shear-wave velocity in the upper 30 m, V_S^{30}. Moreover, many U.S. Building Codes now require site characterization to be explicitly in terms of V_S^{30} (for example, Building Seismic Safety Council, 2000; Dobry and others, 2000). In addition, many of the ground motion prediction equations (for example, Boore and others, 1997; Chiou and Youngs, 2006) are calibrated against seismic station site-conditions described with V_S^{30} values.

Maps of seismic site-conditions on regional scales are relatively rare since they require substantial investment in geological and geotechnical data acquisition and interpretation. In many seismically active regions of the world, information about surficial geology and shear velocity either does not exist, varies dramatically in quality, varies spatially, or is not easily accessible. Such maps are available for only a few regions, predominantly in seismically active urban areas of the world. Topographic elevation data, on the other hand, are available at uniform sampling for the globe. Intuitively, topographic variations should be an indicator of near-surface geomorphology and lithology to the first order, with steep mountains indicating rock, nearly-flat basins indicating soil, and a transition between the end members on intermediate slopes. Indeed, the similarity between the topography of California (fig. 1a) and the surficial site-condition map derived from geology (fig. 1b) is striking. In addition, recent studies have confirmed good correlations among V_S^{30} and both slope and geomorphic indicators in Japan (Matsuoka and others, 2005) and between and elevation V_S^{30} in Taiwan (Chiou and Youngs, 2006). Other geoscience disciplines have used similar topography-based techniques to characterize thickness of sediment deposits for hydrologic and geomorphic purposes (for example, Gallant and Dowling, 2003).

Whether topography alone can routinely distinguish between more subtle variations in surficial geology and, in particular, shallow site-conditions (and thus ground motion amplification), is the subject of this analysis. Our primary hypothesis is that the similarity of geology and topography, or more specifically, the slope of topography, may be exploited to provide a first-order assessment of site-dependent features of seismic hazard. This is particularly important in regions that do not possess high-quality surficial geology or regolith maps, or for areas where geology maps have not been sufficiently correlated with V_S^{30} measurements.

Slope of topography, or gradient, should be diagnostic of V_S^{30}, since more competent (high-velocity) materials are more likely to maintain a steep slope, whereas deep basin sediments are deposited primarily in environments with very low gradients. Furthermore, sediment fineness, itself a proxy for lower shear velocity (Park and Elrick, 1998), should relate to slope. For example, steep, coarse, mountain-front alluvial fan material typically grades to finer deposits with distance from the mountain front and is deposited at decreasing slopes by less energetic fluvial and pluvial processes.

The motivation for deriving a relationship between topography and site-condition comes from a practical need to characterize approximate site amplification as part of an effort to rapidly predict ground shaking and earthquake impact globally. The prediction of reliable ground-motions is a key objective for the Prompt Assessment of Global Earthquakes for Response (PAGER) program of the U.S. Geological Survey (USGS) National Earthquake Information Center (Wald and others, 2006). For PAGER, we must compute empirically-based ShakeMaps (Wald and others, 1999b; Wald and others, 2005) that incorporate our best estimate of seismic site-conditions in any region of the world. Relying on ground motion predictions on rock sites rather than considering potential modification of shaking from regolith can result in differences in ground motion of up to 250 percent (see table 1). This

difference can be equivalent to more than a full unit in shaking intensity (Wald and others, 1999a). Consequently, we require at least a first-order approximation of seismic site-conditions to enable modifications to ground motion predictions. Beyond this specific application, we expect that such correlations may be useful for other seismological and geotechnical applications, including introducing site amplification to regional hazard maps.

It should be stressed that V_S^{30} is not the only factor that dictates the ground motion response at a particular site. Deep basins can introduce amplified ground-motion at low frequencies as a result of resonance effects (for example, Campillo and others, 1989). Alternatively, deep low-velocity structures can attenuate much of the high-frequency energy before it reaches near-surface sediments; thus ground motions may be deamplified relative to surrounding regions on firmer sites where seismic waves are transmitted more efficiently. In addition, topographic effects on rock sites may act to enhance ground motions (for example, Dowrick and others, 1995).

In our analysis, we first correlate 30 arc second topographic data with V_S^{30} measurements in areas of active tectonics to develop a set of coefficients to predict V_S^{30}. We then produce V_S^{30} maps, effectively forward predictions of V_S^{30} from topographic slope, in areas where the V_S^{30} measurements originate and compare our estimated V_S^{30} values to the observations, both visually and statistically. In addition, we compare our topographically-based maps with existing V_S^{30} site-condition maps used for ShakeMap and other applications that are based initially on geologic maps. These analyses are then repeated for V_S^{30} data aggregated in stable continental regions. Assuming these correlations can be used in other regions where abundant V_S^{30} are not available, we apply this technique, based primarily on United States and Taiwanese data, to estimate seismic site-conditions to many other regions around the world using the correlation. Finally, we use our active tectonic and stable-continent V_S^{30}-topographic slope correlations to produce regional-scale site-condition maps for the continental United States. Some of the example regions given in this report may not have either measured V_S^{30} data associated to validate the model or a corresponding geologically-based V_S^{30} map. These examples can be considered as forward predictions and are included to illustrate the potential of this technique.

The topographic slope method has several limitations, and we are currently considering various approaches that may improve this technique. For example, remote sensing techniques that estimate composition of surficial materials could be employed in certain geological conditions where slope is a relatively poor predictor (for example unweathered volcanic plateaus or flat-lying carbonates). Cases that we have observed are noted in this report, but overall, this technique does provide a robust first-order assessment of global seismic site-conditions and will be a valuable tool in rapid assessment of ground motion or regional earthquake hazard estimation.

Table 1. Short-period (0.1 to 0.5 s) site amplification factors from equation 7a, and mid-period (0.4 to 2.0 s) from equation 7b of Borcherdt (1994). Class is NEHRP letter classification; V_S is mean V_S30 velocity (m/s) from Wills and others (2000), and PGA is the cutoff input peak acceleration in cm/s^2 (see Borcherdt, 1994, for more details).

Class	V_s	Short-period (PGA)				Mid-period (PGV)			
PGA			150	250	350		150	250	350
B	686	1.00	1.00	1.00	1.00	1.00	1.00	1.00	1.00
C	464	1.15	1.10	1.04	0.98	1.29	1.26	1.23	1.19
D	301	1.33	1.23	1.09	0.96	1.71	1.64	1.55	1.45
E	163	1.65	1.43	1.15	0.93	2.55	2.37	2.14	1.91

Data

Measured V_S^{30} data have been compiled from several sources. We note that V_S^{30} "data" themselves require significant interpretation and that not all approaches for resolving V_S^{30} are equal, nor do they produce equivalent results. We do not appraise the quality of the V_S^{30} measurements herein. However, in our analyses, we do have the opportunity to compare the various data sets with one another within the framework of an independent parameter; namely, slope of topography.

In California, we use some 767 shear-velocity measurements (provided by C. Wills, written commun., 2005). Many of these data were used to develop the current Californian Site-conditions Map (Wills and others, 2000). Values of V_S^{30} for Salt Lake City and the Utah ShakeMap V_S^{30} site-condition map were provided by K. Pankow (written commun., 2006) and represent measurements gathered by the Utah Geological Survey from other sources (Ashland and McDonald, 2003). Central United States V_S^{30} data (432 sites in total) are obtained from R. Street (written commun., 2005). Many of these data were assembled by the work of Street and others (2001) and include sites in Tennessee, Missouri, Kentucky, and Arkansas. We also acquired V_S^{30} maps used for ShakeMap purposes from network operators in California, Utah, and Memphis.

Outside the United States, we use observations from Taiwan (387 sites) and Italy (43 sites) compiled by the Pacific Earthquake Engineering Research Center (PEER) Next Generation Attenuation (NGA) project courtesy of W. Silva (written commun., 2006) and available online at *http://peer.berkeley.edu /products/nga_project.html*. Data for 436 sites across Australia were provided by Geoscience Australia, collected under the auspices of their National Risk Assessments Program for urban areas (for example, Dhu and Jones, 2002; Jones and others, 2005). Additional Australian data were obtained from recent Spectral Analysis of Surface Waves (SASW) surveys (Collins and others, 2006) at several ground motion recording sites. We also obtained national site-condition maps for Taiwan (C.-T. Lee, written commun., 2007), Italy (A. Michelini, written commun., 2006), Puerto Rico (G. Cua, pers. Comm., 2007), and Turkey (Z. Cagnan, written commun., 2007) for comparative purposes.

For topography, we employ the Shuttle Radar Topography Mission 30-sec (SRTM30) global topographic data set (Farr and Kobrick, 2000). The SRTM30 data are considered an upgrade from the commonly-used USGS 30-sec topographic data (GTOPO30). We use the 30-sec data in our analysis rather than some of the higher-resolution data sets available because those data are not available or complete on a global scale. Wald and others (2006) showed that higher-resolution details of site-conditions can indeed be recovered with 9 arc sec data in California, but that finer resolution is not yet uniformly available globally. It is also important to note that different resolution topographic data will result in varying slope values, particularly in areas of high relief, and may require alternative correlations with V_S^{30} than presented herein. It is worth noting that if the resolution of the topography data is lower than the ridge-to-valley wavelength in a particular region, it will tend to artificially flatten the perceived topography on average.

Other data described in this paper include V_S^{30} values from Puerto Rico (J. Odum, written commun., 2006), Seattle, Washington (I. Wong, written commun., 2006), and New Zealand . A subset of V_S^{30} data for Japan was provided by H. Kawase (written commun., 2006) and the corresponding K-Net strong-motion station locations were obtained online at *http://www.kyoshin.bosai.go.jp/k-net/pubdata/sitedb/sitepub_en.csv*.

Methodology

We first correlate V_S^{30} (m/s) with topographic slope (m/m) at each V_S^{30} measurement point for data in active tectonic areas (fig. 2a). Color-coded symbols represent data from different geographic

regions: California, Taiwan, Italy, and Utah. Figure 2b represents the correlation between V_S^{30} and the slope for stable continental regions employing measurements from the Mississippi Embayment region in the central United States, and Australia. The overall trend in both figures illustrates increasing V_S^{30} with increasing slope, indicative of faster, more competent materials holding steeper slopes. There is significant scatter, yet we will show that the trend is sufficient to be used as a reliable predictor of V_S^{30}. However, there are likely biases in data sampling; in particular, the lack of V_S^{30} measurements at steeper gradients. Most of the V_S^{30} data are found to sample relatively low gradients of less than about 7 percent (percent grade is the vertical rise over horizontal distance traversed), or a slope of about 4 degrees. In general, V_S^{30} measurements are collected as an effort to characterize amplification at low V_S^{30} sites rather than hard rock sites, and those data from rock V_S^{30} sites tend to show more scatter (Wills and Clahan, 2006).

One would not expect a direct, physical relationship between slope and V_S^{30}, and in fact no simple analytic formula emerges from the data. Rather, we chose to characterize the relationship in terms of discrete steps in shear velocity values tied to National Earthquake Hazards Reduction Program (NEHRP) V_S^{30} boundaries (Building Seismic Safety Council, 1995). The NEHRP boundaries are further subdivided into narrower velocity windows to increase resolution where possible. Slope ranges for each bin were based on initial regression analysis, but final assignment of starting and ending slope bins required subjective modification where there were fewer data to constrain the regressions. Topographic slope at any site that falls within these windows is assigned a V_S^{30} by interpolating over the subdivided NEHRP boundaries based on that slope value (fig. 2; table 2). This approach differs slightly from the approach used initially by Wald and Allen (2007), who simply take the median velocity of the subdivided NEHRP classifications for those sites that have slope values within the specified range. It should be noted that we did not use the Utah V_S^{30} data in developing these correlations. It is observed that the Utah data possess systematically low shear velocity for a given slope as compared to mean values from the other regions. We discuss the implications of this omission later.

We have also performed multiple linear regression analyses on both slope and elevation, attempting to correlate them jointly with V_S^{30}. Essentially, slope and elevation themselves correlate well, but elevation alone is, in general, a poorer predictor of V_S^{30} than slope. In essence, there are many areas of low slope over a wide range of possible elevations. Hence, the joint analysis proved weaker than using slope alone.

Table 2. Summary of slope ranges for subdivided NEHRP V_S30 categories.

Class	V_s^{30} range (m/s)	Slope range (m/m) – (active tectonic)	Slope range (m/m) – (stable continent)
E	<180	<1.0E-4	<2.0E-5
	180–240	1.0E-4–2.2E-3	2.0E-5–2.0E-3
D	240–300	2.2E-3–6.3E-3	2.0E-3–4.0E-3
	300–360	6.3E-3–0.018	4.0E-3–7.2E-3
	360–490	0.018–0.050	7.2E-3–0.013
C	490–620	0.050–0.10	0.013–0.018
	620–760	0.10–0.138	0.018–0.025
B	>760	>0.138	>0.025

Application in Active Tectonic Regions

California

We compute $V_S{}^{30}$ for all of California, applying the topographic slope ranges shown in figure 2a (tectonic regions) to corresponding $V_S{}^{30}$ values in order to produce the map shown in figure 1c. A direct comparison to the topographic slope-based $V_S{}^{30}$ predictions can be made from the California statewide map, based on surface geology and $V_S{}^{30}$ measurements (fig.1b; modified from Wills and others, 2000). One notable difference between the slope-derived map of $V_S{}^{30}$ (fig. 1c) and the geology-based Wills and others (2000) map (fig. 1b) is that the former allows more continuous variations in $V_S{}^{30}$, whereas the latter assigns $V_S{}^{30}$ values to all occurrences of that geological unit to a constant (mean $V_S{}^{30}$) value. Consequently, the relative few colors of the Wills and others (2000) map are a consequence of the few discrete geologic units that were classified. Wills and Clahan (2006) present further subdivisions based on geological considerations that may provide a more precise assignment of $V_S{}^{30}$ variations.

To provide more quantitative validation for this technique, we present histograms that indicate the (log) ratio of measured $V_S{}^{30}$ values and those estimated from topographic slope for the same sites in California (fig. 3a). Figure 3b shows the equivalent plot when we compare measured $V_S{}^{30}$ to those velocities assigned by Wills and others (2000). Neither comparison have significant bias, and the slope-based and geology-based values have comparable scatter.

To examine the topographic approach in more detail, figures 4 and 5 show more detailed maps centered on the high seismic-risk areas of the San Francisco Bay area and the Los Angeles region, respectively. Owing to the investment of intensive geophysical and geotechnical investigations, significant portions of the $V_s{}^{30}$ data are obtained from these heavily-populated regions. Direct comparison of the measured $V_s{}^{30}$ values (colored circles) on figures 4a and 5a with the Wills and others (2000) map (figs. 4b and 5b) and with corresponding slope-derived values (figs. 4c and 5c) proves informative. There is a favorable agreement between the Wills and others (2000) $V_s{}^{30}$ map and the slope-derived $V_s{}^{30}$ maps. However, the slope-derived maps predict wider ranges in $V_s{}^{30}$ that appear more spatially variable than the geology-based maps. Conversely, geology-based values are typically taken as constants within a specific geological unit, independent of any slope variations that may correlate with changing material properties (mostly particle size) and thus with $V_s{}^{30}$ values.

Even at this scale, in the San Francisco Bay area many of the details of the geology-based (fig. 4b) and topography-based (fig. 4c) maps are recovered, and the automated assignment of velocities near the DE boundary to near sea-level elevations seems to mimic the mapped extent of this site class on the Wills and others (2000) map. Correspondence between classes C near the BC boundary are less well recovered, but fortunately the overall error in site amplification introduced by misclassifying C for BC, or vice versa, is only about 10 percent (see table 1). Similar correlation is seen in the maps for the Los Angeles region (fig. 5). Here, additional surficial materials near the DE boundary are present in the slope map (fig. 5c) that are not seen on the geology map (fig. 5b). The abundance of surficial material near the DE boundary on the topographically-based $V_s{}^{30}$ map appears consistent with the measured data that are superimposed onto the elevation map (fig. 5a). Many of these areas on the Wills and others (Wills and others, 2000) map could likely be classified near the DE boundary, based on both border line low $V_s{}^{30}$ (for class D) observations and small particle sizes (C. Wills, written commun., 2005).

Next we compare the geologically- and topographically-based $V_s{}^{30}$ maps for the San Francisco Bay area and Los Angeles (figs. 4d and 5d, respectively) more quantitatively. The ratio of the amplification for the $V_s{}^{30}$ maps is calculated. Amplification at mid-periods is assigned to each grid cell by applying the amplification factors of Borcherdt (1994), assuming a uniform peak ground

acceleration (PGA) of 250 cm/s^2. The ratio of amplifications for the San Francisco Bay area (fig. 4d) for the two maps indicates relatively neutral differences in amplification around the bay itself. However, the topographically-based $V_S{}^{30}$ map predicts consistently higher amplification in the Central Valley in the northeast margin of the map. In the Los Angeles region the Wills *et al*. (2000) map tends to predict slightly higher amplifications over a larger area than does the topographically-based map (fig. 5d). However, the topographically-based map seems to indicate higher seismic amplification potential in much of the densely populated Los Angeles Basin.

It is interesting to note that the resolution of the topography (30 arc sec) allows for detailed maps of site-conditions. Many of these details come from small-scale topographic features that are likely to be manifestations of real site differences, such as basin edges and hills protruding into basins and valleys, and are thus easily visible due to their significant slope change signatures. Typically, these edges are important for predicting ground motion variations due to earthquakes. Again, because higher resolution topography is available for this area of the world, additional details could be resolved.

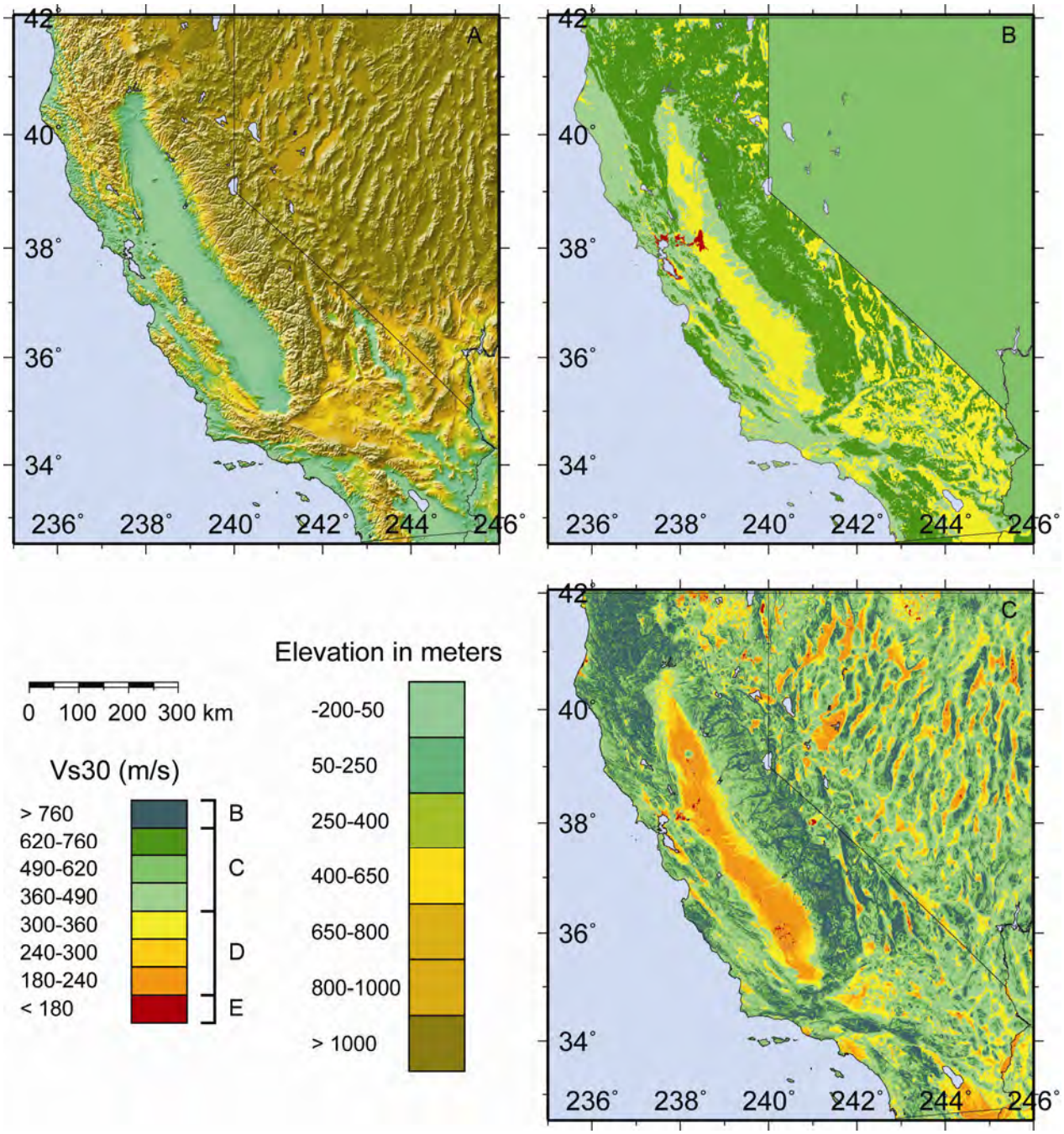

Figure 1. *A*, The topographic relief map for the State of California with elevation in meters (see legend). *B*, Site-condition map for California based on geology and V_S observations (modified from Wills and others, 2000). *C*, Site-condition map derived from topographic slope using the correlations indicated in table 2.

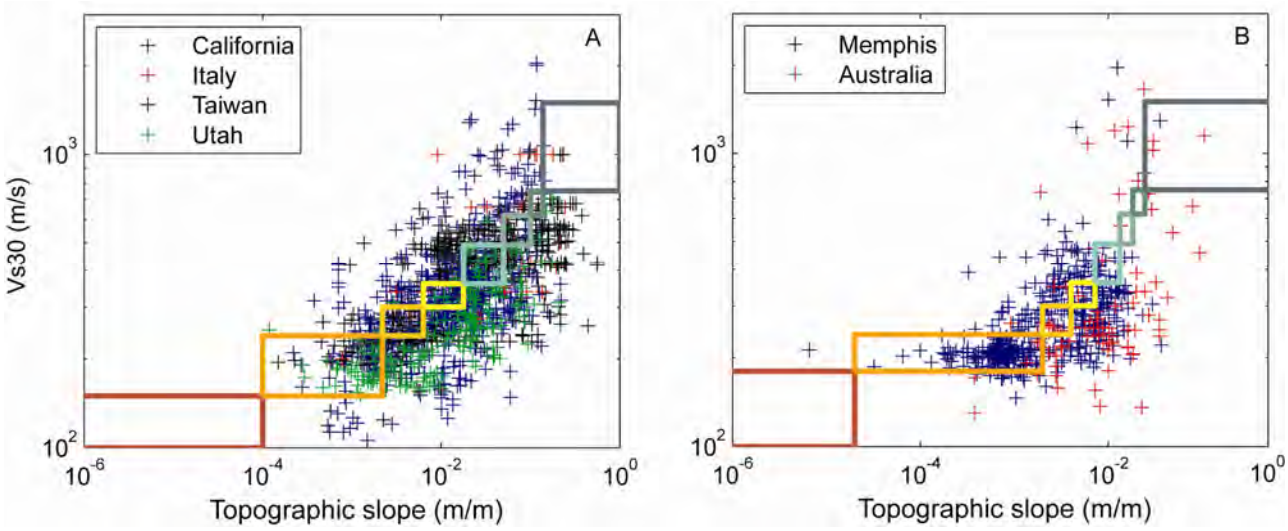

Figure 2. Correlations of measured $V_S{}^{30}$ (m/s) versus topographic slope (m/m) for *A*, active tectonic, and *B*, stable continental regions. Color-coded polygons represent $V_S{}^{30}$ and slope ranges consistent with ranges given in table 2 and also consistent with the $V_S{}^{30}$ legends for all geologic- and topographic-based maps throughout this paper.

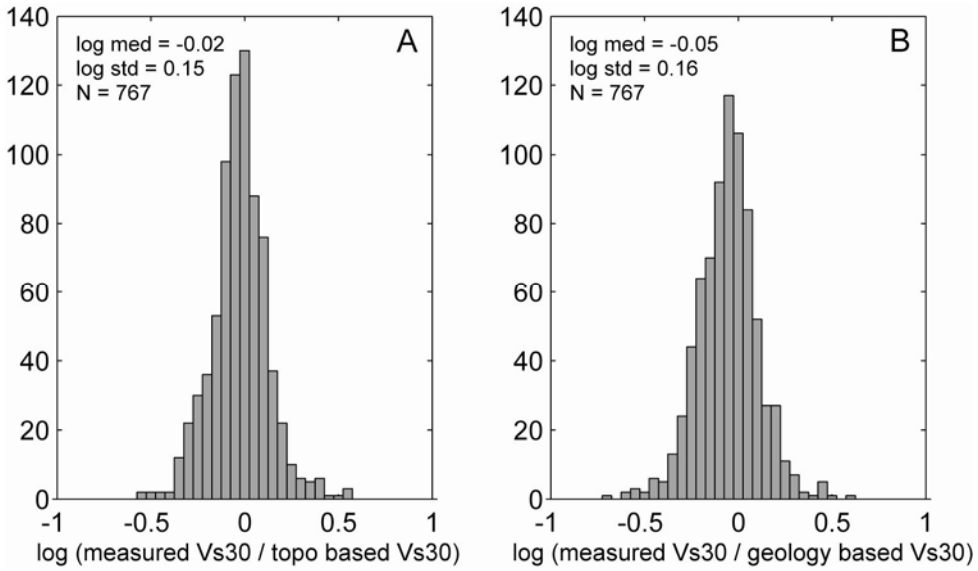

Figure 3. Histograms indicating logarithmic differences of measured Californian $V_S{}^{30}$ values compared with *A*, values derived from topographic slope correlations and, *B*, values based on existing $V_S{}^{30}$ site-condition maps. *N* is the number of $V_S{}^{30}$ measurements.

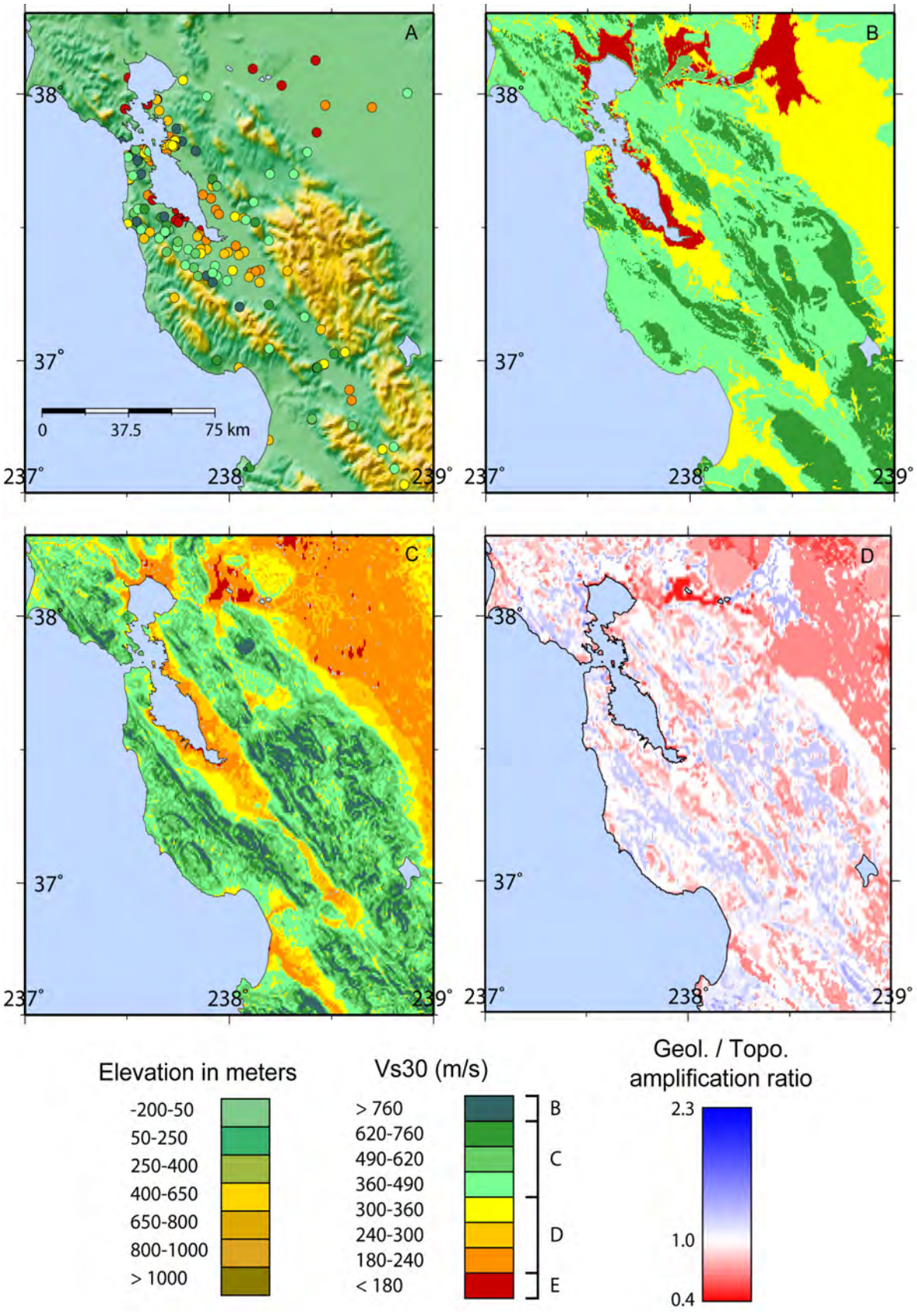
A
B
C
D
38°
37°
237°
238°
239°
0
37.5
75 km
Elevation in meters
-200-50
50-250
250-400
400-650
650-800
800-1000
> 1000
Vs30 (m/s)
> 760
620-760
490-620
360-490
300-360
240-300
180-240
< 180
B
C
D
E
Geol. / Topo.
amplification ratio
2.3
1.0
0.4

Figure 4. *A*, Topographic map of the San Francisco Bay Area. Circles indicate the location of measurements, color-coded by V_S30 in m/s (see left legend). *B*, Site-condition map based on geology and V_S30 observations (modified from Wills and others, 2000). *C*, Site-condition map derived from topographic slope. *D*, The ratio of the predicted amplification for a uniform PGA of 250 cm/s^2 for the geologically- and topographically-based V_S30 maps. Blues indicate that the Wills and others (2000) map predicts higher amplification, whereas reds indicate higher amplifications are predicted from the topographically-based map. White indicated where the two V_S30 maps predict the same amplification.

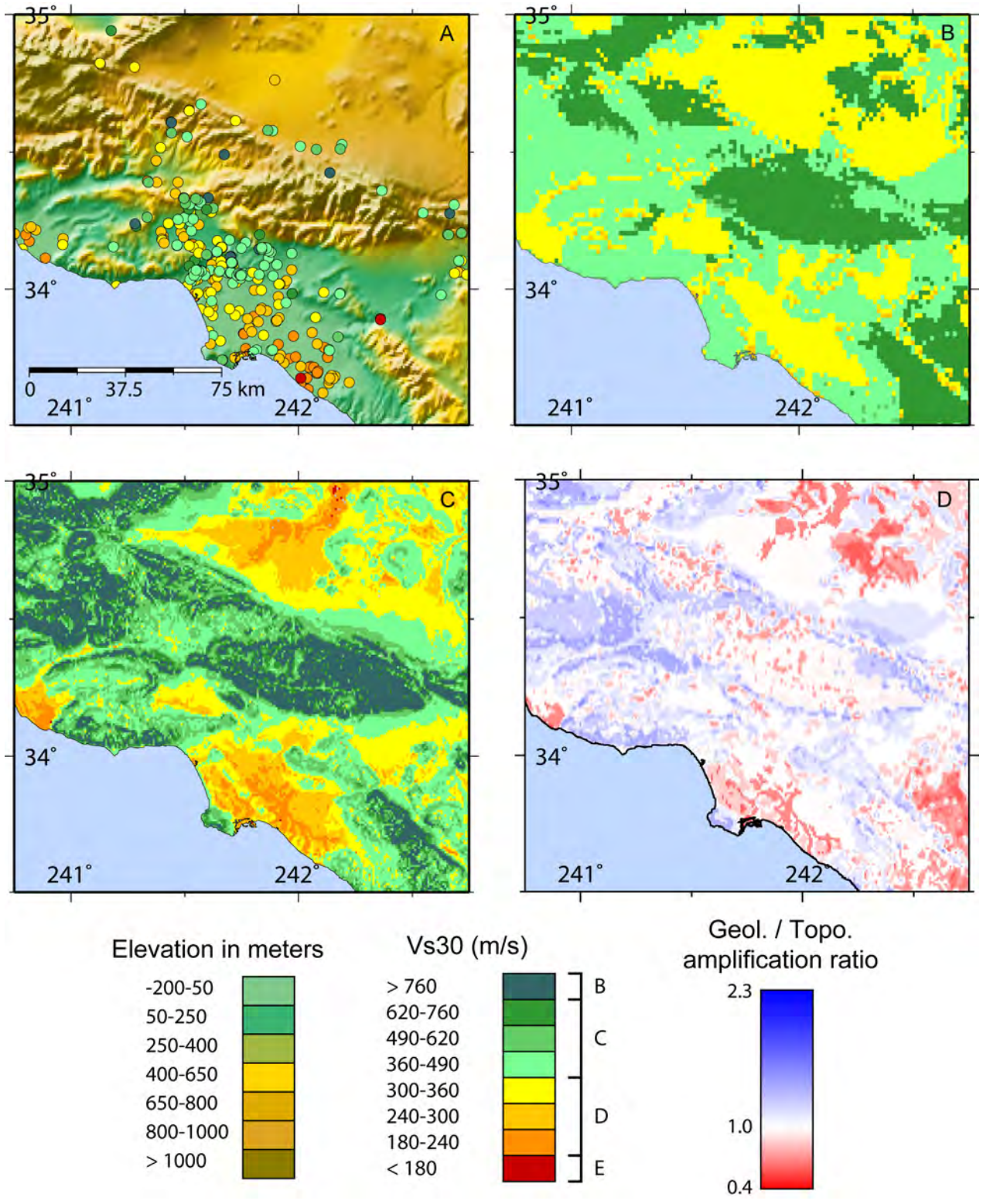

Figure 5. *A*, Topographic map of the Los Angeles region. Circles indicate the location of measurements, color-coded by V_S^{30} in m/s. *B*, site-condition map based on geology and V_S^{30} observations (modified from Wills and others, 2000). *C*, Site-condition map derived from topographic slope. *D*, The ratio of the predicted amplification for a uniform PGA of 250 cm/s^2 for the geologically- and topographically-based V_S^{30} maps.

Taiwan

The next question we address is whether the correlations hold in areas that have similar overall topographic expression but exhibit different geology, tectonics, and geomorphology. Taiwan was chosen to test this hypothesis, primarily because the site classes on a national scale are well-understood from prior studies (for example, Lee and others, 2001) and are available for direct comparison. The high seismicity in Taiwan results from the convergence of the Philippine Sea plate and the Eurasian plate. The Philippine plate is moving NW at a rate of about 7 cm/yr relative to the Eurasian plate.

The abundance of shear-wave observations used in our correlations provides us with a valuable validation case study to ensure that the slope calibration with $V_S{}^{30}$ is robust among our base data sets. Figure 6 shows the topographic map superimposed with color-coded $V_S{}^{30}$ measurements (fig. 6a), the national site-condition map (fig. 6b; modified from Lee *et al*., 2001), and the topographic-gradient derived $V_S{}^{30}$ map for the island of Taiwan (fig. 6c). Shallow shear-wave velocities around Taiwan vary widely, but they do so with rather systematic trends that are well-recovered using topographic slope.

Figure 7a provides the ratio of measured versus slope-derived $V_S{}^{30}$ values. The mean and standard deviation are comparable to those evaluated for California sites (fig. 3a). In presenting the Taiwanese site-condition map, we have assigned median shear velocities based on the NEHRP categories adopted by Lee and others (2001), the exception for this being site class E, where we assigned a $V_S{}^{30}$ of 150 m/s. Statistically, the topographically-derived site-condition map for Taiwan performs very well (fig. 7a) relative to the geologically-based map (fig. 7b). The Taiwanese are currently working on a revised site classification scheme that should further improve comparisons to measured data (C.-T. Lee, written commun., 2007). The correlations derived jointly from California and Taiwan shear-wave observations and topographic slope seem to apply in areas of similar overall topographic expression independent of other factors that may be contributing.

It is interesting to note that, in a significant number of the examples represented in this report, population exposure tends to correlate very well with slower $V_S{}^{30}$ site-conditions calculated from the slope of topography. Intuitively, the correlation between population density and seismic site-condition is not surprising since steep hill slopes are not usually as desirable for building structures, while flat-to-gently sloping lands tend to consist of more fertile soils suitable for agricultural purposes and have traditionally been inhabited. Using Taiwan as an example, we compare seismic site-condition to population exposure as derived from the Oak Ridge National Laboratory's LandScan 2005 database (Dobson and others, 2000; Bhaduri and others, 2002) (fig. 6d). We see that urban communities appear to be most dense in the flat-lying lands that correspond to lower $V_S{}^{30}$. In particular, the region around Taipei possesses significant amplification potential owing to its location on primarily NEHRP site class D surficial material. Population becomes less dense as we grade from gently sloping to steeper terrains. This figure serves to remind urban planners, disaster mitigators, and emergency responders why we must consider seismic site-conditions as an important component in earthquake hazard assessment, since those areas with the densest populations are also likely to have the strongest site amplifications.

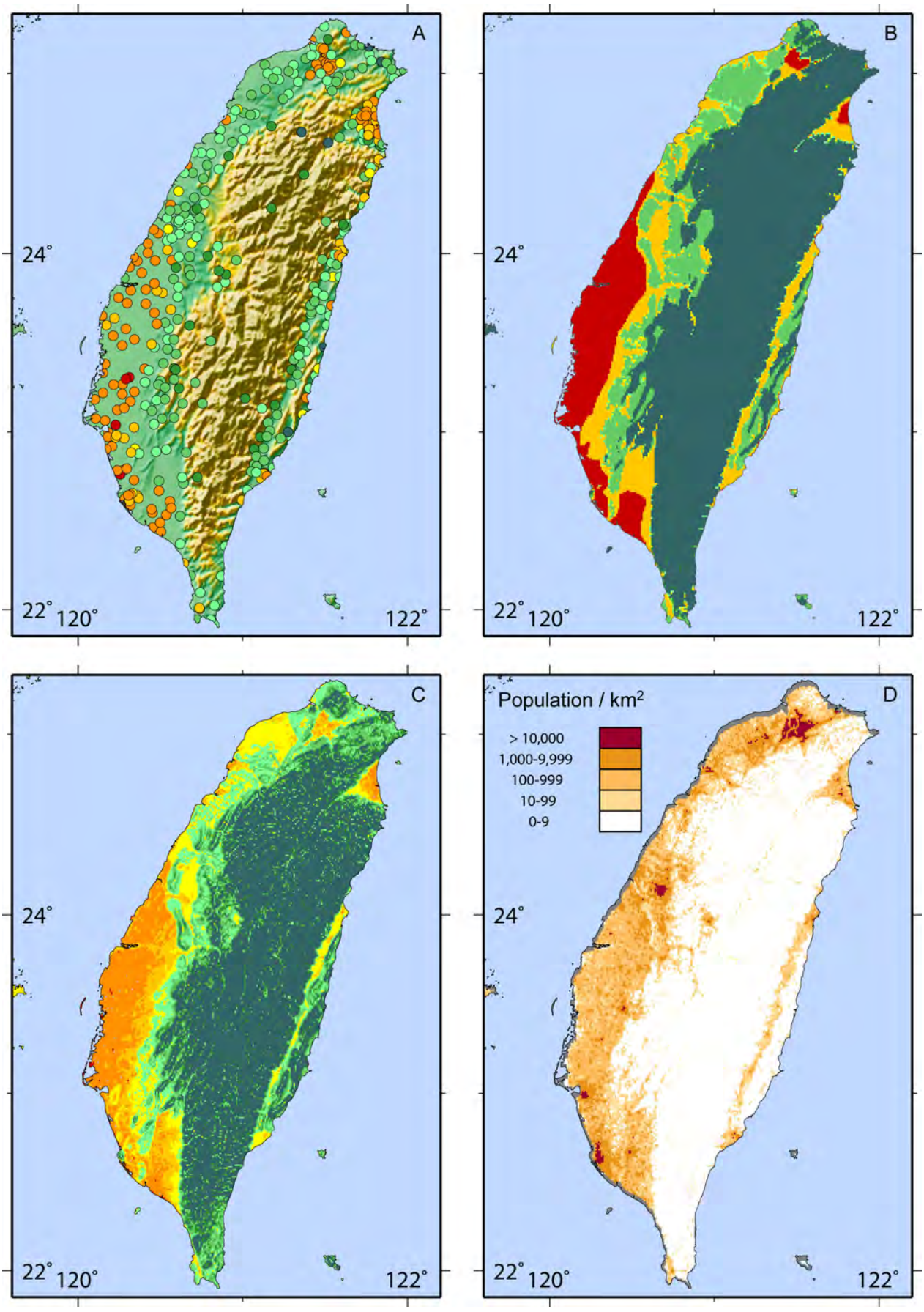
A
B
C
D
24°
22°
120°
122°
Population / km²
> 10,000
1,000-9,999
100-999
10-99
0-9

Figure 6. *A*, Topographic map of Taiwan with elevation in meters. Circles indicate the location of measurements, color-coded by V_S30 in m/s. *B*, Site-condition map based on geology and V_S30 observations (modified from Lee and others, 2001). *C*, Site-condition map derived from topographic slope. *D*, Population density map of Taiwan derived from the LandScan 2005 population database (for example, Dobson and others, 2000; Bhaduri and others, 2002). See figure 1 for topography and V_S30 legends.

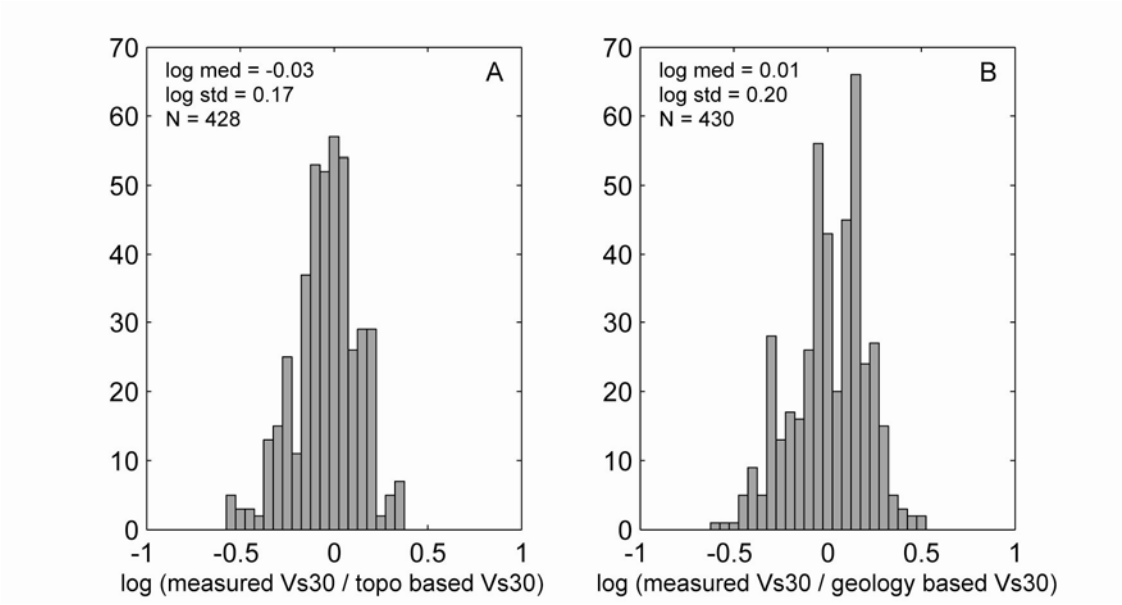

Figure 7. Histograms indicating logarithmic differences of measured Taiwanese V_S30 values compared with *A*, values derived from topographic slope correlations and, *B*, values based on existing V_S30 site-condition maps. *N* is the number of V_S30 measurements. Differences in *N* between *A* and *B* arise when the grid point referred to is not defined within the selected map grid.

Alaska

Alaska is the most seismically active state in the United States, largely because of the active subduction of the Pacific plate beneath the North American plate at a rate of about 5–7 cm/yr. The region has hosted two great-magnitude ($M > 9.0$) earthquakes since 1957 along this tectonic plate boundary (Wesson and others, 1999). In addition to earthquakes occurring along the subduction zone, significant seismicity also occurs throughout Alaska as a result of stresses imposed by interaction of the plates. Much of this relative motion is accommodated at the principal boundary between the two plates in the Gulf of Alaska, but there is also substantial crustal deformation and earthquake activity inland of the plate boundary in central Alaska. In addition to occurring on major mapped faults such as the Denali fault, shallow-focus earthquakes in central Alaska also occur on lesser, unmapped faults.

Many studies have been undertaken that examine site response within Anchorage, given its high seismic hazard, relatively high exposure, and geographic setting within a sedimentary basin (for example, Nath and others, 1997; Dutta and others, 2000; Combellick, 2001; Dutta and others, 2001; Martirosyan and others, 2002; Dutta and others, 2003; Badal and others, 2004). Indeed, ground failure in Anchorage following the 1964 Prince William Sound earthquake was widely reported (Martirosyan and others, 2002; Dutta and others, 2003). Such studies, however, are only available on a very localized scale. A state wide site-condition map for Alaska has been developed by Martirosyan and Hansen (2007) for use in ShakeMap applications. However, this map was unavailable for comparison at the time this report was written.

We generate a $V_S{}^{30}$ map for the State of Alaska using our topographically based approach. In general, we observe that much of the southern margin of the state, adjacent to the subduction zone, indicates relatively fast material, consistent with the dynamic topographic relief (fig. 8). Another feature that can clearly be identified in our $V_S{}^{30}$ map of Alaska is the Yukon delta in western Alaska. This region indicates slower-velocity surficial material consistent with fluvial processes of the Yukon River. Also of note in figure 8 is the low velocity of the braided river systems throughout the Mackenzie River Basin in northwestern Canada.

Next we investigate the seismic site-conditions of Anchorage in more detail and superimpose combined $V_S{}^{30}$ values from Dutta and others (2000) and the PEER NGA database (fig. 9a). Despite the limited resolution, much of Anchorage indicates lower-velocity surficial materials (fig. 9b) consistent with the city's location within a sedimentary basin. In general, our result is consistent with the more detailed studies in Anchorage mentioned above, with mapped $V_S{}^{30}$ grading from fast to slower velocities westward towards the harbor. Statistically, our predictions of $V_S{}^{30}$ compare very well with observed $V_S{}^{30}$ values at strong-motion sites across Alaska and with measurements taken in Anchorage (fig. 10).

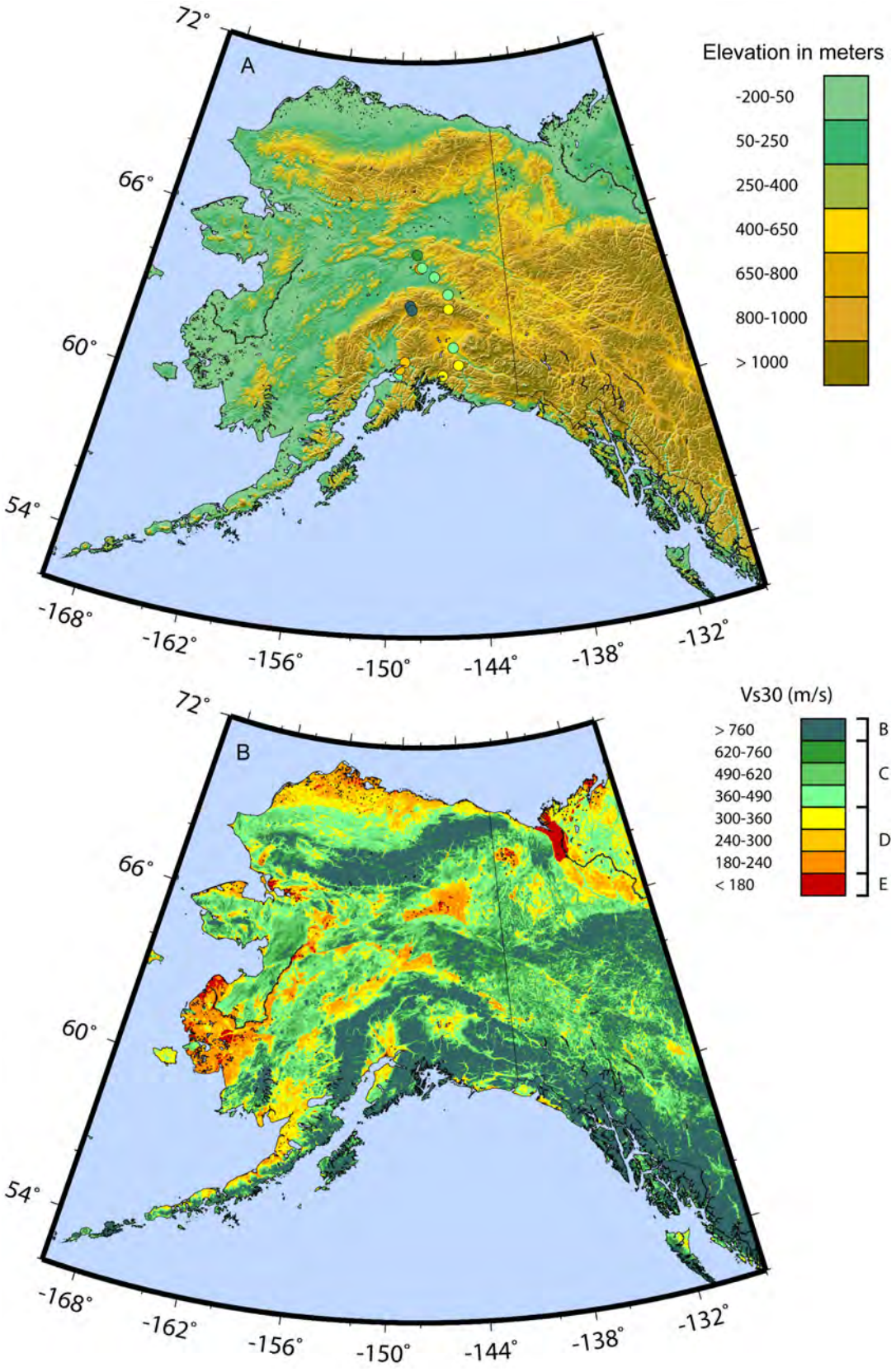

Figure 8. *A*, The topographic relief map for the State of Alaska. *B*, Site-condition map derived from topographic slope.

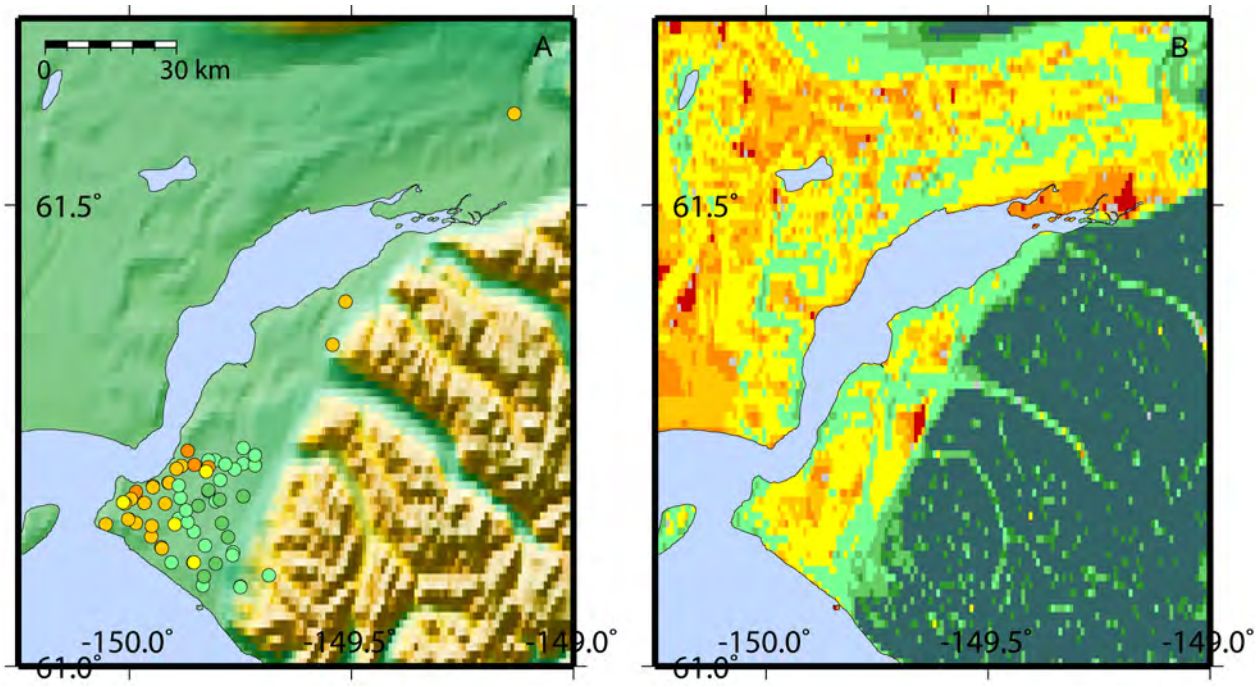

Figure 9. *A*, Topographic map of the Anchorage, Alaska region. Circles indicate the location of $V_S{}^{30}$ measurements, color-coded by velocity in m/s. *B*, Site-condition map derived from topographic slope. See figure 1 for figure legends.

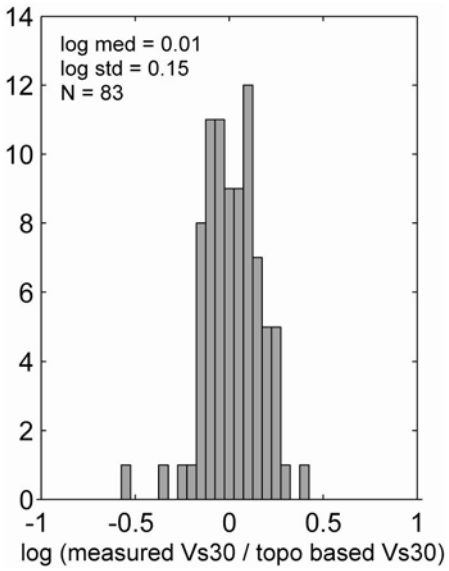

Figure 10. Histogram indicating logarithmic differences of combined Anchorage (Dutta and others (2000) and NGA $V_S{}^{30}$ values compared with values derived from topographic slope correlations.

Nevada

Scott and others (2004) describe the collection of V_S^{30} data on a transect along the Truckee River in Reno, Nevada. These results, based on microtremor analysis, suggest that V_S^{30} is higher than that expected from alluvium-filled basins, based on NEHRP previsions. Scott and others, (2004) concluded that mapped surficial geology is not necessarily a reliable predictor of V_S^{30}, owing to stiffer underlying Tertiary sediments. The location of this survey, closely following an erosive river environment, may be a possible explanation for these results. Consequently, we observed that the Nevada data indicated systematically higher velocities with topographic slope than our reference dataset for California and Taiwan. We use no data from Nevada in our correlations between slope and V_S^{30}. A local adjustment factor may have to be applied to the V_S^{30} map based on topographic slope.

We have not developed a separate topographic slope-based map for the State of Nevada. However, the State is largely represented in the northeast quadrant of the California map (fig. 1). Site classifications for Nevada appear to be highly variable, with spatially periodic changes in site class that are associated with the Basin and Range tectonic province (fig. 1c).

Salt Lake City, Utah

The next example within active tectonic regions is that of the Salt Lake City, Wasatch Front region of Utah. This site-condition map can also be considered a forward prediction since, unlike California and Taiwan, no V_S^{30} data for this region were used in our calibration analysis. The data, which were obtained from the Utah Geological Survey, appeared to have V_S^{30} values systematically lower than mean values from other active regions with similar slope (fig. 2a). The geologically- and topographic slope-based maps (figs. 11b and 11c, respectively) demonstrate similar trends. However, there appears to be a significant trend towards lower velocities in the geologically-based site map, west of the Wasatch Front. This observation is consistent with the measured data. On average, the geology-based map (fig. 12b) represents the measured data better than does the slope-derived map (fig. 12a). The latter shows an overall bias indicating that V_S^{30} predictions in the Salt Lake City region are on average over-predicted by the topographic-slope approach employing the current correlations. It is possible that near-surface shear velocities in the region are lower for a given slope angle than in California and Taiwan, and thus require slight modification to the slope versus V_S^{30} correlation. Alternatively, the V_S^{30} measurements underestimate actual in situ velocities for some other reason, not yet established.

While we observe that the slope-derived map (fig. 11c) indicates a more natural progression of V_S^{30} grading towards higher values in steeper topographic relief, it is also possible that Lake Bonneville deposits that abut the mountain front, rather than sloping, may violate the basic assumption on which our correlations are based (K. Pankow, written commun., 2007). The small overall bias in the Salt Lake City region could be removed with an overall shift of about 25 percent in predicted V_S^{30} values, though it is possible that these biases are concentrated in particular geological units.

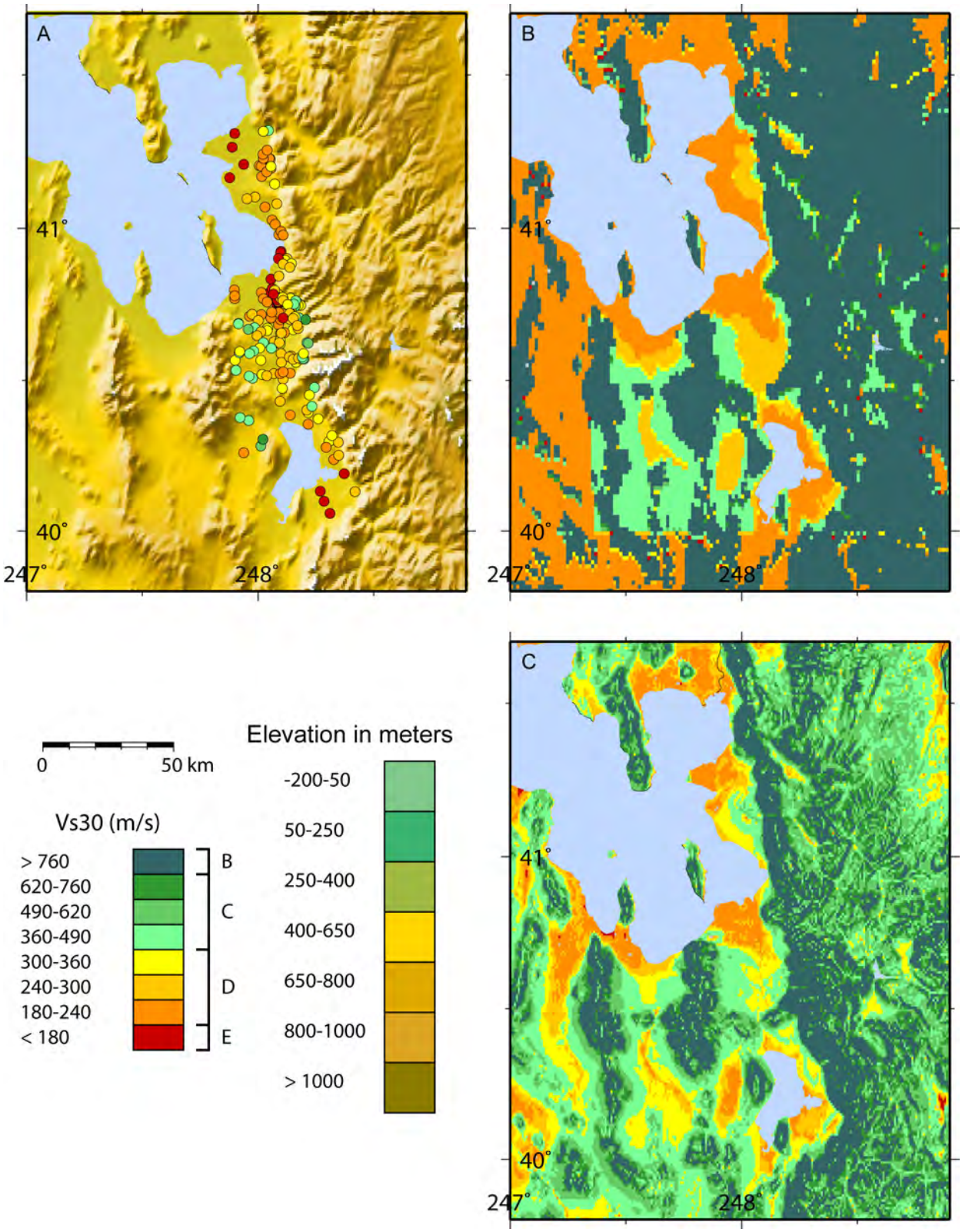

Figure 11. *A*, Topographic map of the Salt Lake City, Wasatch Front region of Utah. Circles indicate the location of measurements, color-coded by V_S^{30} in m/s. *B*, Site-condition map based on geology and V_S observations. *C*, Site-condition map derived from topographic slope.

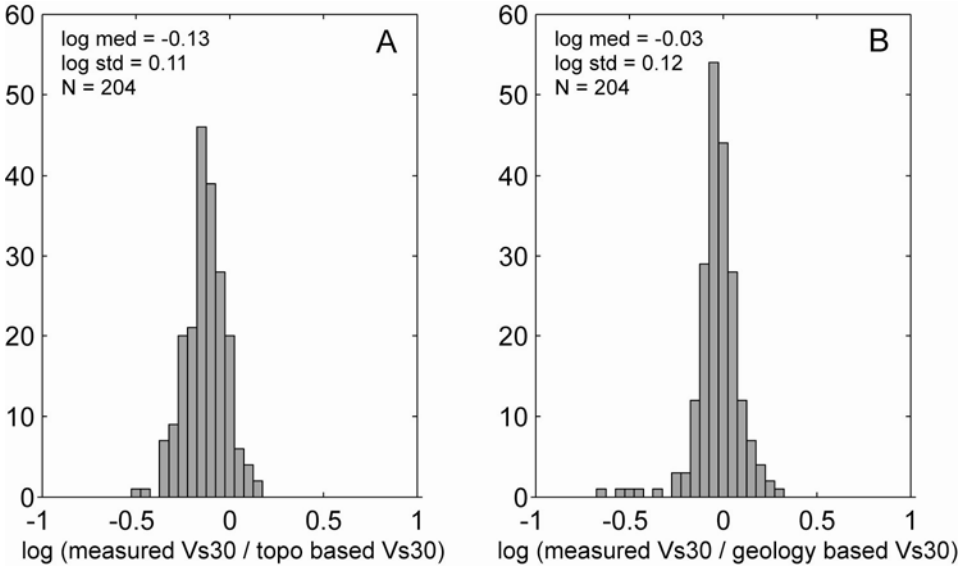

Figure 12. Histograms indicating logarithmic differences of measured Utah V_S^{30} values compared with *A*, values derived from topographic slope correlations and, *B*, values based on existing V_S^{30} site-condition maps. *N* is the number of V_S^{30} measurements.

Seattle, Washington

The Cascadia subduction zone lies just off the coast of Oregon and Washington. This subduction zone is the main tectonic feature in the geologically active Pacific Northwest. On shore, the (continental) North American plate overlays the subducting (oceanic) Juan de Fuca plate. Assessment of the regional shaking impact of an anticipated great Cascadia subduction zone earthquake requires at least a first-order approximation of site-conditions.

The contribution of site response to the observed ground shaking is well recognized in the Seattle region (Frankel and others, 1999). Assessment of site characteristics has found that sites on artificial fill are likely to experience significant response from an input ground motion. Given that no Seattle data were used in the model development, our topographically-based assessment of V_S^{30} can be considered as forward prediction of seismic site-conditions. Visually, the topographically-based map appears to recover many of the key features in the geology-based map (figs. 13b and 13c). The former does indicate greater variability in predicted V_S^{30} than the latter, particularly in the lower-lying regions to the southwest of downtown Seattle, where a higher proportion of slower D class material is predicted. However, the geologically-based map predicts more slow E class material. The topographic approach also predicts more higher-velocity B class material within the mountains that bound the city. Statistically, the topographically-based map represents the observed values relatively well (fig. 14a) however, there is not a strong correlation. The geologically-based map has a strong peak about the median value consistent with the fact that it was based on these observed V_S^{30} values (fig. 14b). These results suggest that V_S^{30} maps based on topography alone can serve as a suitable proxy in the absence of more detailed geologically-based site-condition maps.

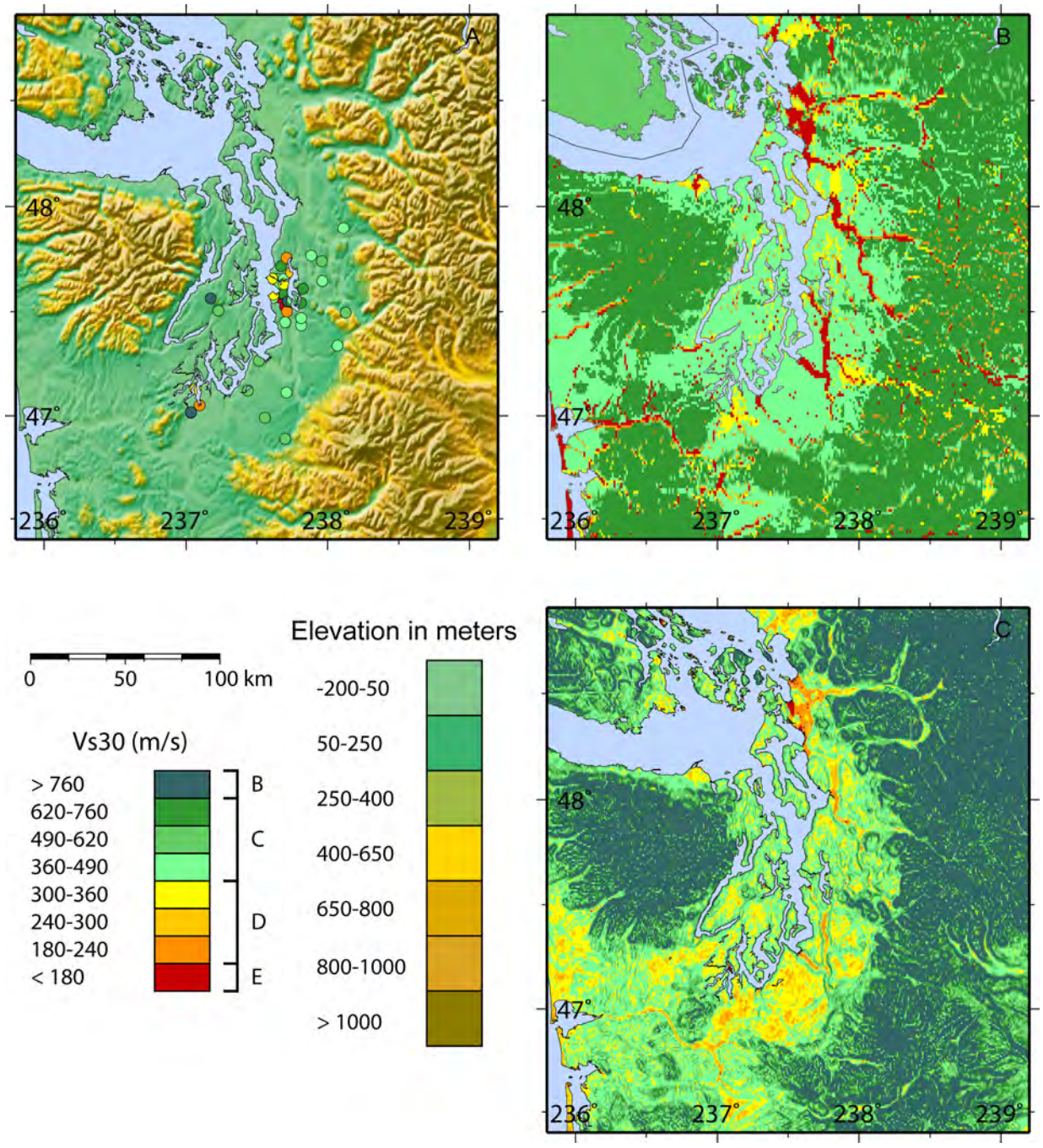

Figure 13. *A*, Topographic map of the Seattle, Washington, region. Circles indicate the location of measurements, color-coded by V_S^{30} in m/s. *B*, Site-condition map based on geology and V_S observations. *C*, Site-condition map derived from topographic slope.

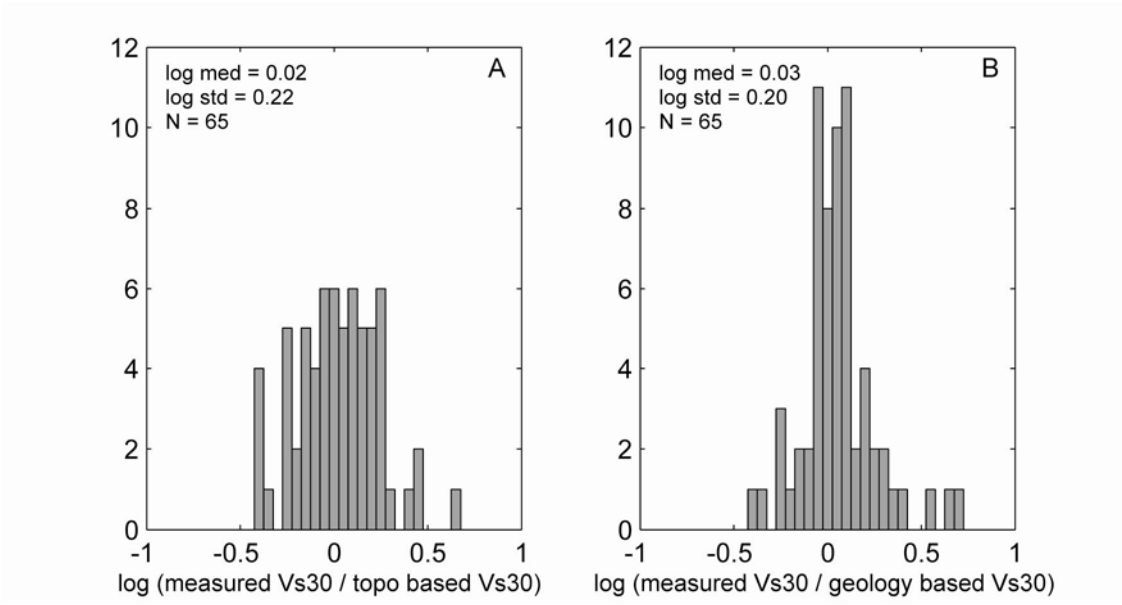

Figure 14. Histograms indicating logarithmic differences of measured Seattle, Washington V_S^{30} values compared with *A*, values derived from topographic slope correlations and, *B*, values based on existing V_S^{30} site-condition maps. *N* is the number of V_S^{30} measurements.

Indonesia

The origin of the Indonesian Archipelago about the Sunda Arc results from the active subduction of the Indo-Australian tectonic plate beneath the Eurasian plate. The high rate of destructive seismicity that accompanies this plate motion has been recently demonstrated by several catastrophic earthquakes including the 2004 M_w 9.0 and 2005 M_w 8.7 Sumatra-Andaman Islands earthquakes, and the 2006 M_w 6.3 Yogyakarta earthquake. Little information regarding the response of near-surface geology to strong ground shaking in Indonesia is available. However, a reconnaissance report following the 2006 Yogyakarta earthquake notes that the most heavily damaged areas were underlain by young volcanic deposits consisting of undifferentiated tuff, ash, breccia, agglomerates, and lava flows (Earthquake Engineering Research Institute, 2006). Moreover, the report explicitly states that the most pronounced effects were associated with directivity and soil amplification. Consequently, first-order estimates of seismic site-conditions for Indonesia will be important to assess earthquake hazard in future studies. A pilot hazard study performed in the Sulawesi Province also suggested significant potential for ground motion amplification owing to effects of surficial geology (Thenhaus and others, 1993).

Figure 15a shows the topographic relief of Indonesia. Because of the active subduction of the Indo-Australian plate beneath the island arc, the topographic signature of the islands is dominated by a chain of active volcanoes adjacent to the subduction zone. The margin most distant from the active subduction indicates more subdued topography grading to relatively flat slopes near the coastlines. This subdued topography is particularly apparent for the island of Sumatra. The corresponding V_S^{30} map derived from the slope of topography (fig. 15b) indicates broad regions of low-velocity surficial materials (NEHRP site class D). The steeper volcanic chain is indicated by faster BC to B surficial materials. We also note narrow zones of lower V_S^{30} along the margins nearest the Sunda Arc.

Figure 15c shows the population density map for Indonesia, one of the most densely populated nations on Earth. The island of Java is particularly heavily populated, with much of the exposure correlating to NEHRP site classes C and D. High exposure rates are also observed in southeastern Sumatra, which again is largely mapped as site class D.

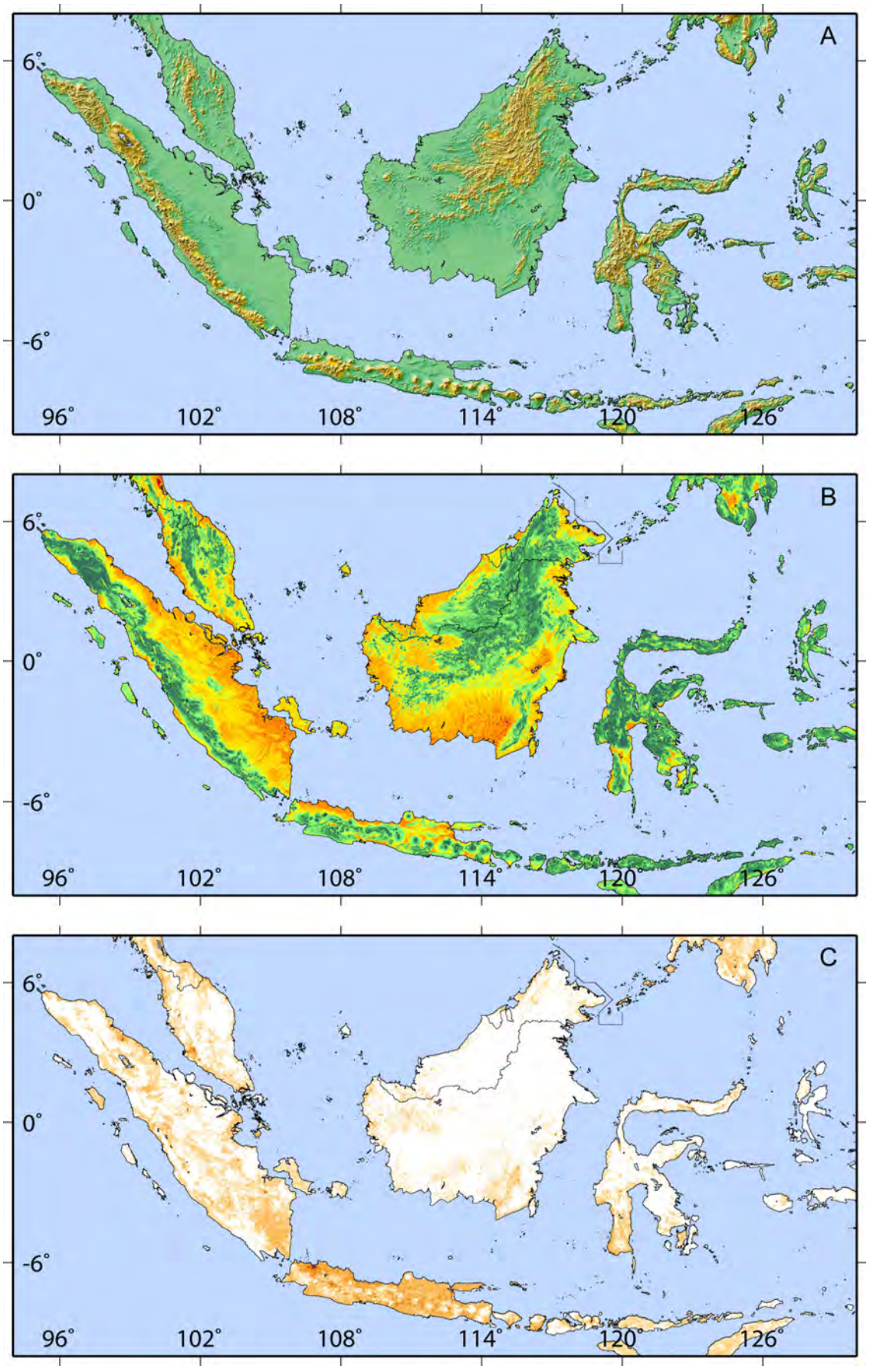
A
B
C
6°
0°
-6°
96°
102°
108°
114°
120°
126°

Figure 15. (Facing page) *A*, Topographic map of Indonesia. *B*, Site-condition map derived from topographic slope. *C*, Population density map of Indonesia. See figure 6 for map legends.

Iran

This highly seismic region forms the north-west trending boundary between the Arabian and Eurasian tectonic plates. The Arabian plate is a small plate split from the African plate by rifting along the Red Sea. As it underthrusts the Eurasian Plate it causes uplift of the Zagros Mountains and numerous devastating earthquakes. Iran has suffered many deadly earthquakes in the recent past with death tolls in excess of 1000 each; for example 1962 M_S 7.3 Buyin-Zara; 1968 M_S 7.3 Dasht-e Bay z; 1972 M_S 6.9 Ghir; 1976 M_W 7.0 Iran-Turkey border; 1978 M_W 7.3 Tabas; 1981 M_W 7.2 Sirch; 1990 M_W 7.4 Manjil; 1997 M_W 7.2 Ardakul; and 2003 M_W 6.6 Bam. The combination of high hazard and primarily poorly constructed adobe structures makes Iran an extremely high-risk region.

In almost all of the earthquakes noted above, it was identified that adobe houses located on alluvium suffered greater damage than those located on firm gravels or rock sites (Ambraseys, 1963; Bayer and others, 1969; Dewey and Grantz, 1973; Berberian, 1979; Berberian and others, 1992; Jafari and others, 2005; Building and Housing Research Center, 2007). Consequently, first-order estimates of seismic site-conditions are fundamental for quantifying regions at risk for strong ground shaking from surficial effects.

We superimpose some significant Iranian earthquakes listed above onto the topographic map (fig. 16a). From the seismic site-condition map developed from the slope of topography, we observe that many of these deadly earthquakes have occurred near sites of relatively low V_S^{30} (fig. 16b), consistent with our earlier observation that populations tend to concentrate on flat-lying sedimentary basins. In particular, the deadly Manjil earthquake near the Caspian Sea, which resulted in approximately 35,000 deaths (Utsu, 2002), is located in close proximity to large Quaternary sedimentary deposits, indicated by low V_S^{30} in figure 16b (for example, Niazi and Bozorgnia, 1992). The Dasht-e Bay z and Bam earthquakes, which resulted in very high casualties (15,000 and 26,000 deaths, respectively), also occurred near regions of significant amplification potential, and this is likely to have contributed to the extreme number of fatalities observed. Unfortunately, no V_S^{30} measurements are available from Iran for comparison.

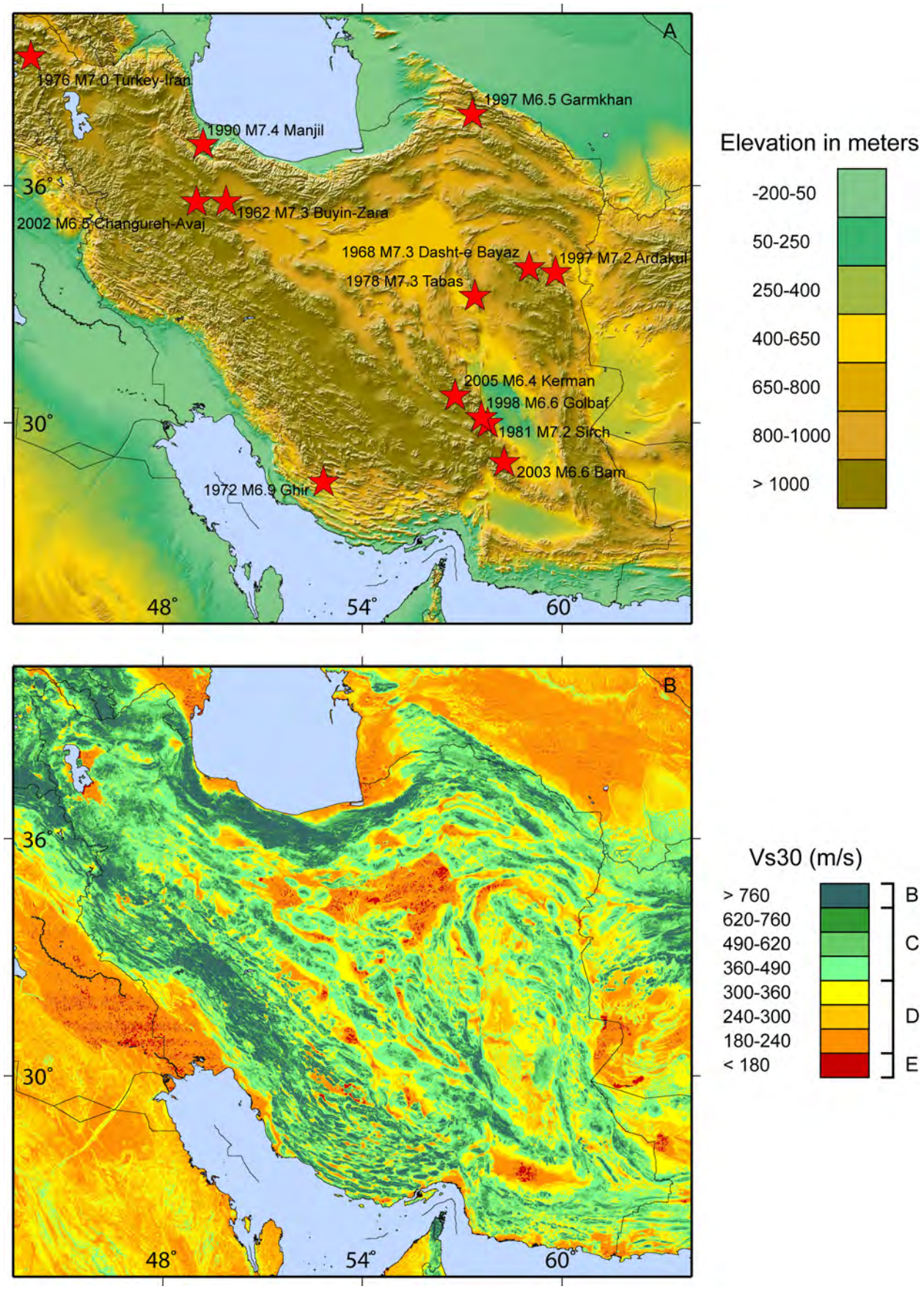
A
1976 M7.0 Turkey-Iran
1997 M6.5 Garmkhan
1990 M7.4 Manjil
36°
1962 M7.3 Buyin-Zara
2002 M6.5 Changureh-Avaj
1968 M7.3 Dasht-e Bayaz
1997 M7.2 Ardakul
1978 M7.3 Tabas
2005 M6.4 Kerman
1998 M6.6 Golbaf
30°
1981 M7.2 Sirch
2003 M6.6 Bam
1972 M6.9 Ghir
48°
54°
60°
Elevation in meters
-200-50
50-250
250-400
400-650
650-800
800-1000
> 1000
B
36°
30°
48°
54°
60°
Vs30 (m/s)
> 760
620-760
490-620
360-490
300-360
240-300
180-240
< 180
B
C
D
E

Figure 16. (Facing page) *A*, Topographic relief map for Iran, superimposed with the epicenters of recent deadly earthquakes (red stars). *B*, Site-condition map derived from topographic slope.

Italy

Primary tectonic activity in Italy results from the collision of the Eurasian and African Plates. The high-topography zone of the central Apennines, which trends NW-SE within peninsular Italy, is dissected by a Quaternary fault system that has hosted several moderate-to-large historical earthquakes (Cello and others, 1997), most recently 1980 M_W 6.9 Iripinia, and 1997 M_W 6.0 Umbria-Marche. Site response effects were documented following the 1997 Umbria-Marche seismic sequence (Caserta and others, 2000; Tertulliani, 2000). In 2002, the Molise and Puglia regions of southern Italy were struck by two moderate-magnitude earthquakes (Cara and others, 2005). The first and largest of the two (M_W 5.7) resulted in 30 casualties in the town of San Giuliano di Puglia. The high intensities observed in this town are largely attributed to local site-conditions (Cara and others, 2005).

The Istituto Nazionale di Geofisica e Vulcanologia (INGV), Italy, has recently installed the ShakeMap system as a routine process of its national earthquake monitoring program. We obtained the national site-condition map that is used in this system (fig. 17b) courtesy of A. Michelini (written commun., 2006). In general, the topographically-derived map (fig. 17c) demonstrates many of the same features as the geologically-derived map. However, there are some discrepancies over the absolute value of V_S^{30} assignments. We observe that the geologically-based map (fig. 17b) has systematically higher velocities than our topographically-based map (fig. 17c). This difference is reflected in figure 18 when we compare V_S^{30} values at Italian strong-motion stations, available from the PEER NGA project, with the respective site-condition maps. Despite a larger spread in the comparisons, the topographically-based map tends to recover individual V_S^{30} values better than the geologically-based map, which is biased towards higher velocities. Again, population density correlates well with flat-lying, low-V_S^{30} areas (fig. 17d).

Although the site-condition maps generally indicate similar trends, one obvious disparity between them occurs in the Puglia region of southeastern Italy, where figure 17b indicates significantly faster velocities than are predicted by the topographic approach. The predominant geology comprises flat-lying Mesozoic shallow-water carbonate and evaporite rocks (de Alteriis and Aiello, 1993). Relative to much of Italy and other Mediterranean regions, the seismicity of Puglia is quite low. This observation is subsequently reflected in the absence of significant topographic relief. Consequently, we can conclude that, in geological conditions dominated by these flat-lying carbonates, the automated topographic approach may not recover V_S^{30} as well as a more rigorous assessment of local surficial geology.

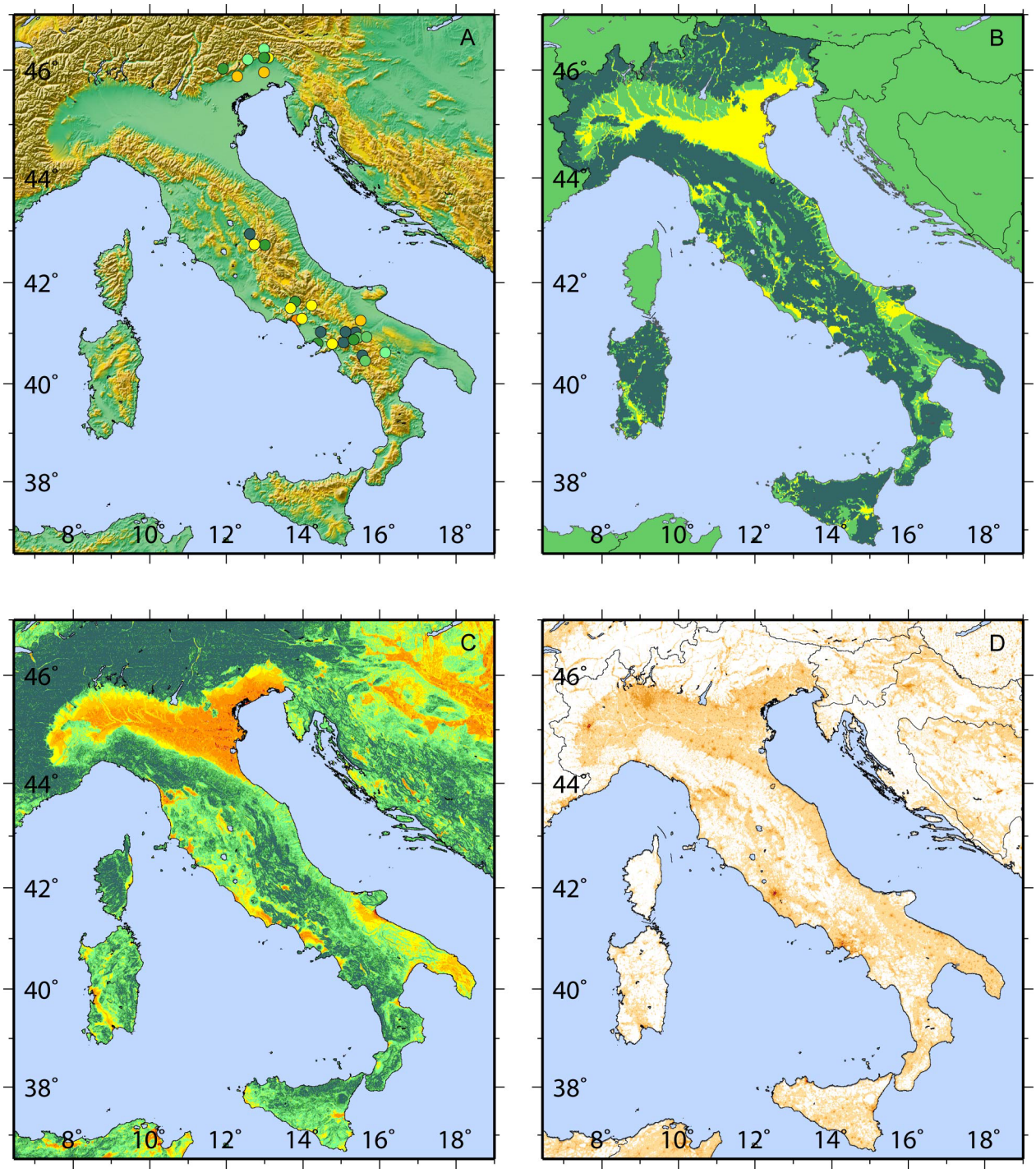

Figure 17. *A*, Topographic map of Italy. Circles indicate the location of measurements, color-coded by V_S^{30}. *B*, Site-condition map based on geology and V_S observations. *C*, Site-condition map derived from topographic slope. *D*, Population density map of Italy. See figures 1 and 6 for map legends.

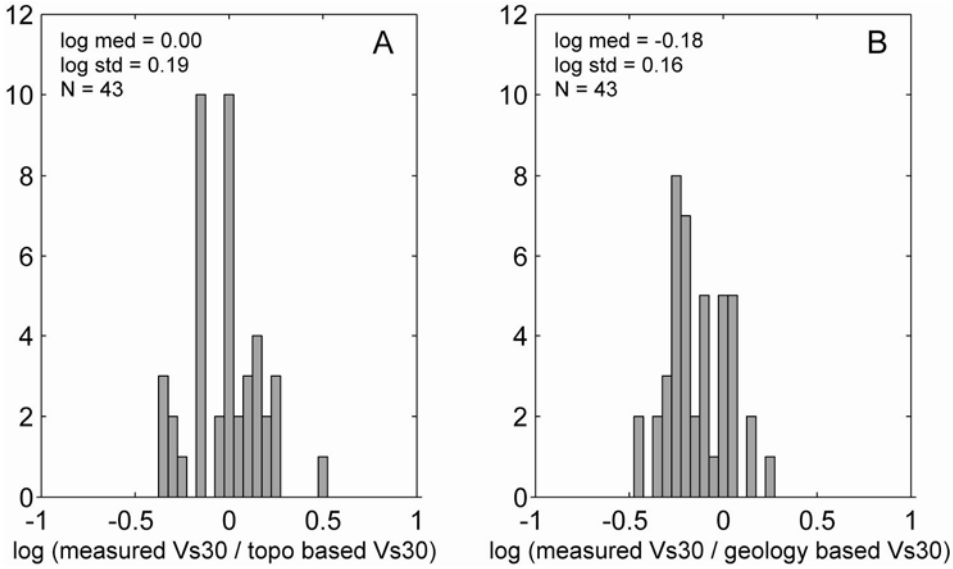

Figure 18. Histograms indicating logarithmic differences of Italian V_S30 values from the NGA dataset, compared with *A*, values derived from topographic slope correlations and, *B*, values based on existing V_S30 site-condition maps. *N* is the number of V_S30 measurements.

Japan

Japan is a densely populated nation that is high in seismic hazard. Much of Japan's population resides on thick sedimentary basins that have significant potential to amplify ground shaking. Tectonically, Japan is located near the junction of the Pacific, Philippine Sea, and Okhotsk tectonic plates. The Pacific plate is moving northwest at a rate of about 8–9 cm/yr relative to, and subducting beneath, the Philippine Sea and Okhotsk plates. In addition, the Philippine Sea plate is subducting northward beneath Japan and the Okhotsk and Amurian plates (Miller and Kennett, 2006). The complex tectonics drive the high rates of seismicity observed in the region, and the subducting slabs provide the source for the many active volcanoes that occupy the island.

Figure 19a shows the topographic map of Japan. We have obtained a geologically-based V_S^{30} map (fig. 19b) of Japan courtesy of M. Matsuoka (written commun., 2006). This map was developed analyzing geomorphic characteristics tied to V_S^{30} measurements (Matsuoka and others, 2005). They further refine this model using multiple linear regression analysis on additional geomorphic indicators; i.e., correlating V_S^{30} with elevation, topographic slope, and the distance from mountain ranges. Our purely topographically-based map (fig. 19c) exhibits many of the same trends as the Matsuoka and others (2005) map. However, the topographic approach does not predict as much slow-velocity material (equivalent to NEHRP site class E) as indicated in figure 19b. As with Taiwan, we also plot the population exposure (fig. 19d) and compare this with the site-condition map. Again we note a strong correlation between population density and assignments of low V_S^{30}.

Shallow shear-wave velocities have been determined for a number of sites within the KiK-Net strong-motion network (Kawase and Matsuo, 2004; H. Kawase, written commun., 2006). Kawase and Matsuo (2004) made these V_S^{30} estimates by first using a spectral inversion of ground motion recordings to determine site factors, and then inverting for the best fit 1-D shear-velocity model using a genetic algorithm. Unlike most other regions studied, many of these sites were located on rock, so the distribution is biased towards higher-velocity V_S^{30} data. The ratio of measured V_S^{30} to predicted V_S^{30} is

compared for both site-condition maps in figure 20. We observe no significant difference between the geologic- and geomorphic-based map of Matsuoka *et al*. (2005) and our site-condition map based on topographic slope. However, it appears that both maps tend to underestimate V_S^{30}, relative to observed data. We note that there is not uniform sampling of V_S^{30} data across all possible site classes, with only a limited number of C and D site classes available for comparison. Furthermore, this strong-motion network was probably designed so that the accelerometers were located at "hard rock" sites. Consequently, it is expected that the location of these sites will be more biased towards faster velocities than average sites of similar topographic slope. Since these V_S^{30} values were not derived from more widely used measurement techniques, we are as yet unsure of the consistency of this approach compared with more standard V_S^{30} measurements; however, the strong correlation of the two V_S^{30} maps (figs. 19*B*, *C*) with each other provides some level of confidence in the overall results. Also, as noted earlier, the differences between observed and topographically-based V_S^{30} may not affect amplification potential significantly since most of the data are of higher velocity, which occurs near or above the BC boundary and where site effects are not as pronounced.

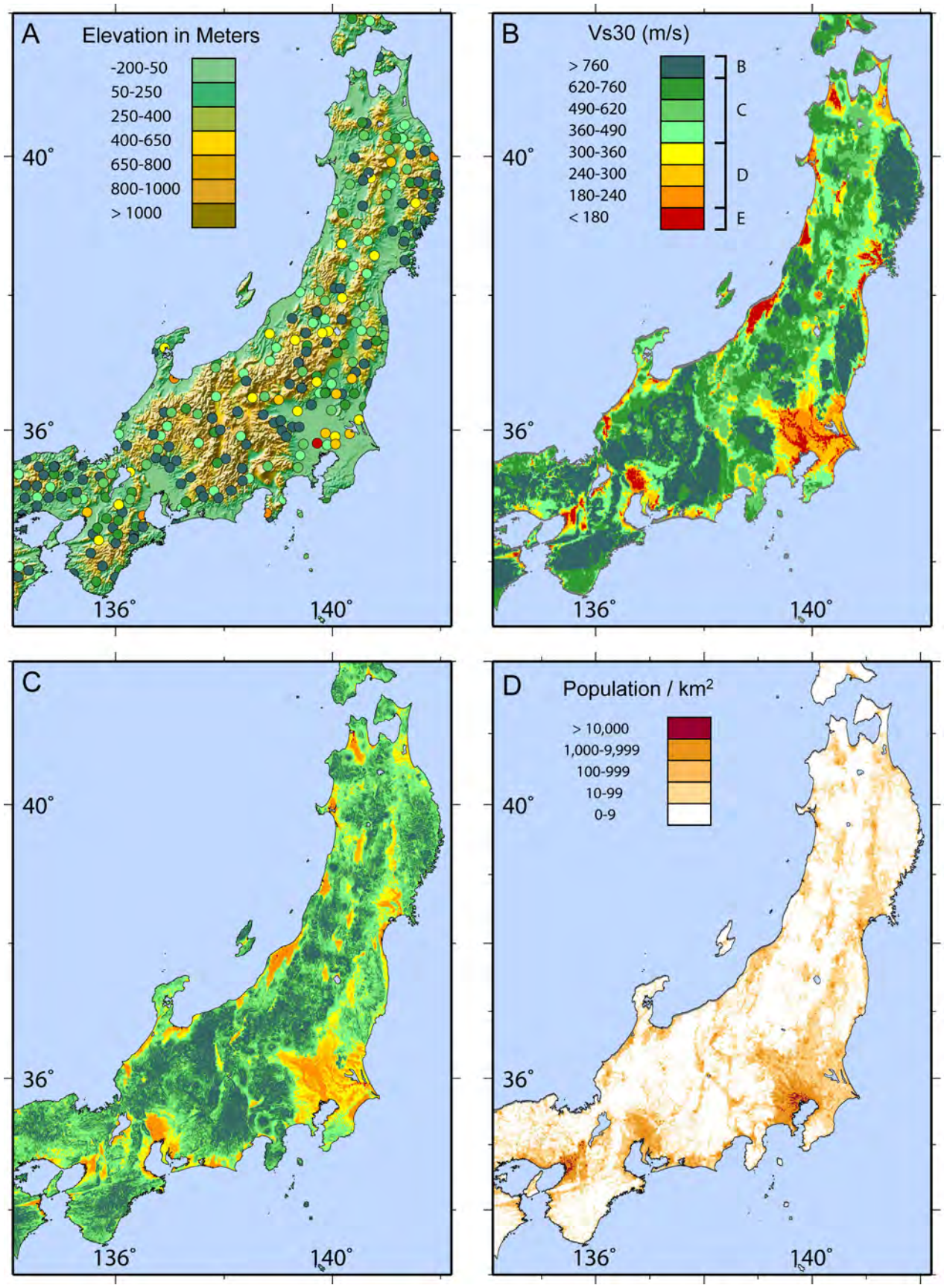
A
Elevation in Meters
-200-50
50-250
250-400
400-650
650-800
800-1000
> 1000
B
Vs30 (m/s)
> 760
620-760
490-620
360-490
300-360
240-300
180-240
< 180
B
C
D
E
C
D
Population / km2
> 10,000
1,000-9,999
100-999
10-99
0-9
40°
36°
136°
140°

Figure 19. *A*, Topographic map of Japan. Circles indicate the location of V_S30 measurements, color-coded by velocity in m/s. *B*, Site-condition map based on geology and V_S30 observations (modified from Matsuoka and others, 2005). *C*, Site-condition map derived from topographic slope. *D*, Population density of Japan.

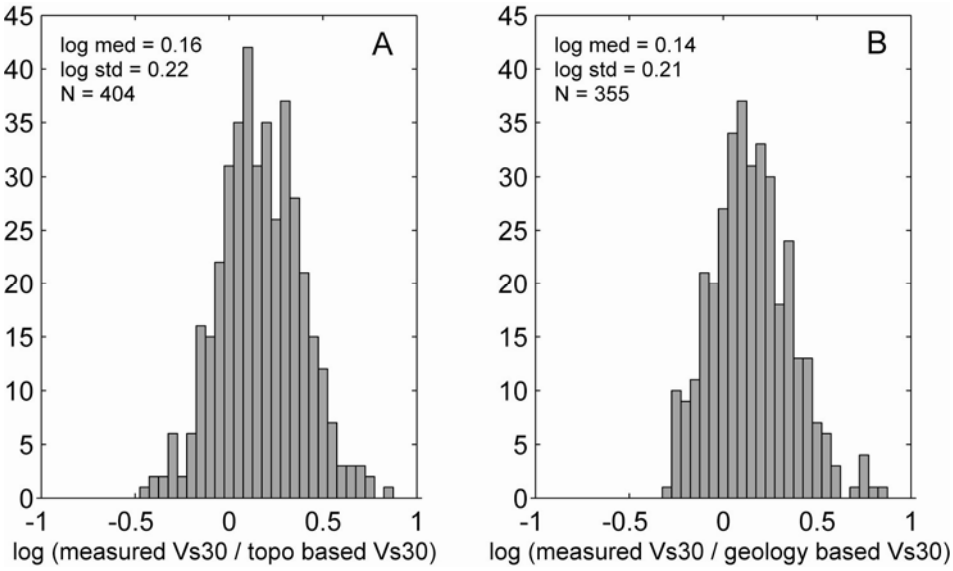

Figure 20. Histograms indicating logarithmic differences of Japanese V_S30 values, compared with *A*, values derived from topographic slope correlations and, *B*, values based on existing V_S30 site-condition maps. *N* is the number of V_S30 measurements. The difference in *N* between the two histograms is because some of the V_S30 measurement points are plotted outside the grid defined by the geologic- and geomorphic-based map of Matsuoka and others (2005).

Mexico

One of the most obvious and most well-documented occurrences of seismic site amplification resulted from the great 1985 M_W 8.1 Michoacan earthquake that devastated Mexico City, some 350 km from the epicenter (for example, Campillo and others, 1989; Glass, 1989; Ordaz and Singh, 1992). In this case, a number of factors contributed to the high damage rates observed, including complex heterogeneous rupture (Campillo and others, 1989), enhanced transmission path (Furumura and Kennett, 1998), basin resonance effects at long periods (2–3 sec), and local site response from lakebed sediments (Campillo and others, 1989).

Much of Mexico's seismicity is driven by the subduction of the Rivera and Cocos microplates beneath the Pacific coast of Mexico (part of the North American plate). The slower subducting Rivera Plate is moving northeast at about 2 cm/yr relative to the North American plate, and the faster Cocos plate is moving in a similar direction at a rate of about 4.5 cm/yr. These microplates interact with the larger Pacific plate via a combination of transform faults and spreading ridges (DeMets and Stein, 1990). Further north, the Gulf of California represents a developing transform-rift margin (Umhoefer and others, 1994).

We calculate a V_S^{30} map for the country of Mexico from the topographic slope employing the coefficients for active tectonic regions (fig. 21). We observe that relatively high V_S^{30} values are associated with the Sierra Madre Occidental and Oriental mountain ranges along the western and eastern margins of the Mexican Plateau, respectively. The Mexican Plateau itself is represented by more complex V_S^{30} patterns, but in general is indicated by slower surficial materials relative to the mountain ranges that bound the plateau. The surficial materials that make up the Mexican Plateau are

most likely weathering products derived from the Sierra Madre Mountains via fluvial processes. Slower velocity materials are also predicted along the western coast of Mexico along the Gulf of California and Pacific coastlines. Again, these surficial materials are most likely derived from weathering processes within the Sierra Madre Occidental Mountains.

Figure 22 shows a more detailed view of the seismic site-conditions about Mexico City. Much of the city is built upon lakebed sediments, which are known to have contributed to seismic wave amplification following the devastating 1985 Michoacan earthquake (Ordaz and Singh, 1992). The topographically-based V_S^{30} map indicates that much of Mexico City is built upon NEHRP site class D. The extent of site class D also corresponds to the regions of highest population density (fig. 22c).

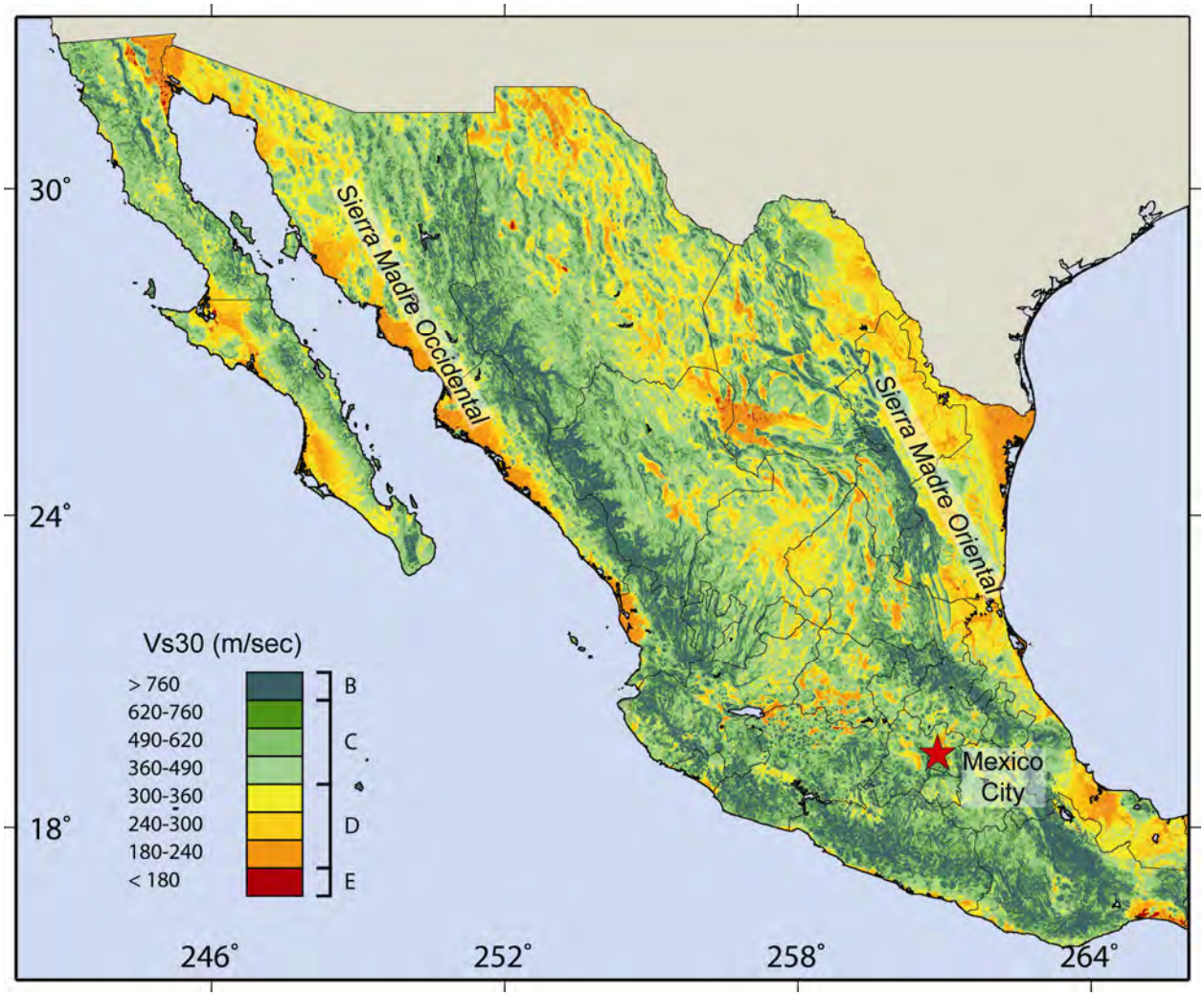

Figure 21. V_S^{30} map for Mexico employing the coefficients for active tectonic regions. See figure 22 for a more detailed view of Mexico City.

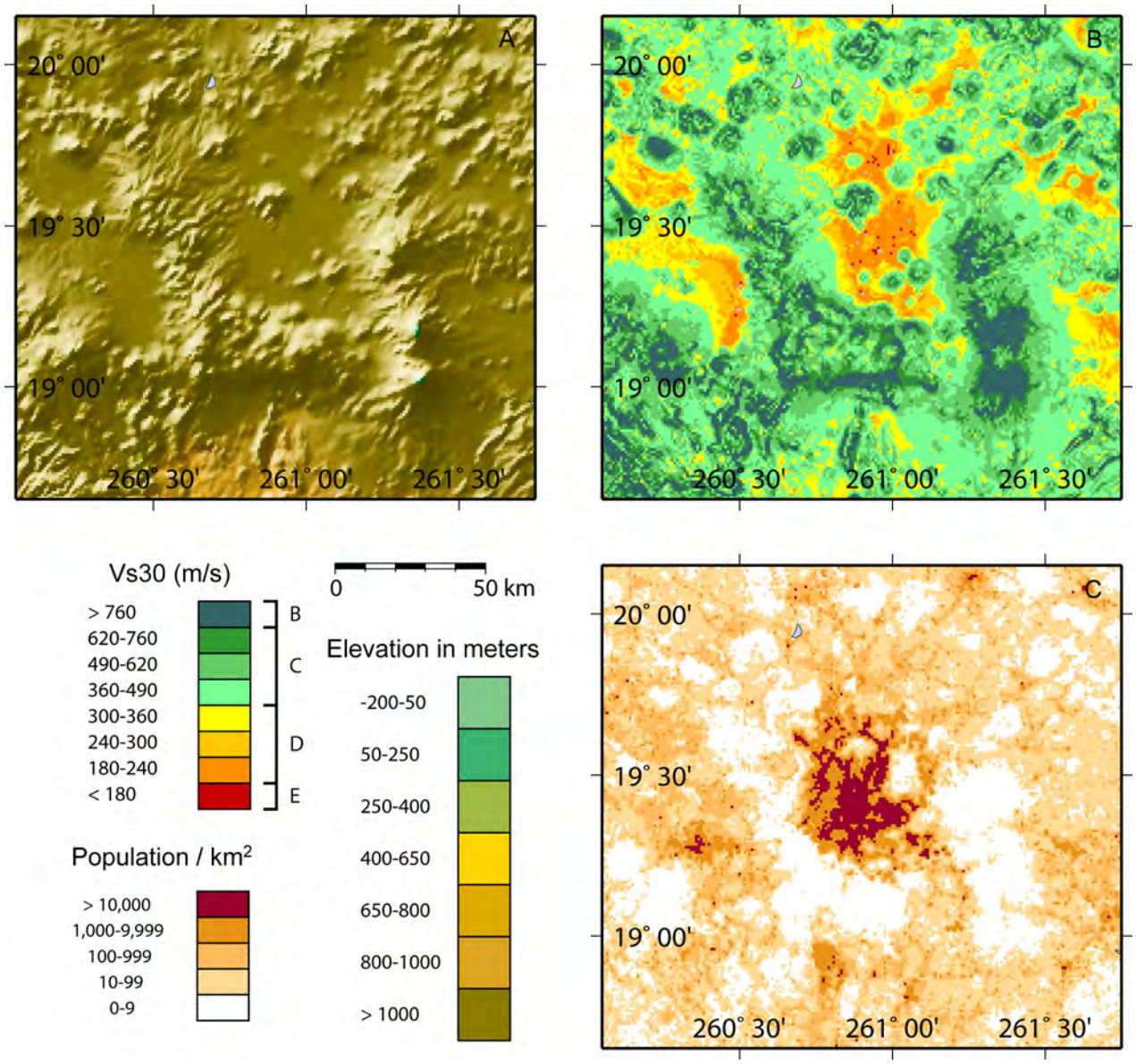

Figure 22. *A*, Topographic relief map of Mexico City. *B*, Site-condition map derived from topographic slope. *C*, Population density map of Mexico City.

New Zealand

New Zealand straddles the boundary between the Indo-Australian and Pacific tectonic plates. The relative plate motion in New Zealand is expressed by a complex assemblage of active faults, coupled with a moderately high rate of seismicity (Stirling and others, 2002). The plate boundary beneath New Zealand comprises the Hikurangi (North Island) and Fiordland (far south of South Island) subduction zones, which dip in the opposite sense relative to each other. Active tectonic motion is accommodated by the faults of the axial tectonic belt that traverse much of the South Island between the subducting slabs (Stirling and others, 2002). The Alpine Fault in the central South Island accommodates the release of much of the strain energy produced by the relative plate motion.

Significant site response effects have been observed from several of New Zealand's large earthquakes. Furthermore, microzoning was clearly recognized following the deadly *M* 7.8 1931 Hawke's Bay earthquake. Dowrick and others (1995) note that the structures most affected by this earthquake were located on rock sites and the least damage occurred on the soft alluvium sites. They conclude that topographic effects may have enhanced the ground shaking in rock locations, and strong ground shaking at high frequencies was attenuated on the deep basin sediments. In contrast to these observations, Abercrombie and Benites (1998) noted that weak-motion data recorded in the cities of Hastings and Napier, both of which were affected by the 1931 quake, exhibited prolonged duration and amplification of shaking owing to the existence of thin soil layers above a Miocene-age sedimentary basin. These data suggest that there may be strong nonlinear behavior of the soils in this region when subjected to increasing levels of ground shaking.

More recently, a reconnaissance report following the M_W 6.5 1987 Edgecumbe, Bay of Plenty earthquake indicated that most of the damage occurred on drained swampland consisting of soft, unconsolidated soils (EQE Incorporated, 1987; Franks, 1988). Based on these observations, it is important that the effects of site response should be considered for hazard and risk assessments in regions such as New Zealand. Based on our topographic approach for defining seismic site-conditions, we observe that many of New Zealand's most developed urban centers appear to be located in regions of significant amplification potential, including Greater Wellington, Christchurch, Hastings, Napier, Dunedin, and Invercargill (figs. 23 and 24).

Limited work in defining V_S^{30} in the Greater Wellington region has been performed through collaborations among the University of Nevada, Reno; Victoria University, Wellington; and the Institute of Geological and Nuclear Sciences (see *http://www.seismo.unr.edu/ hazsurv/#wnlh*). This work culminated in approximately 90 V_S^{30} measurements across the local area, from the city of Wellington to Upper Hutt. We compare our topographically-based map of the Wellington region with these measured values (fig. 25). Despite limitations in the resolution of the topographic data and the tight spatial clustering of the V_S^{30} measurements, we observe the same general trends are recovered by the topographic-based site-condition map. This dataset, however, comprises more E site class material than is predicted with the topographic approach. The availability of higher-resolution topography data in this region may yield site-conditions more comparable to the observed data.

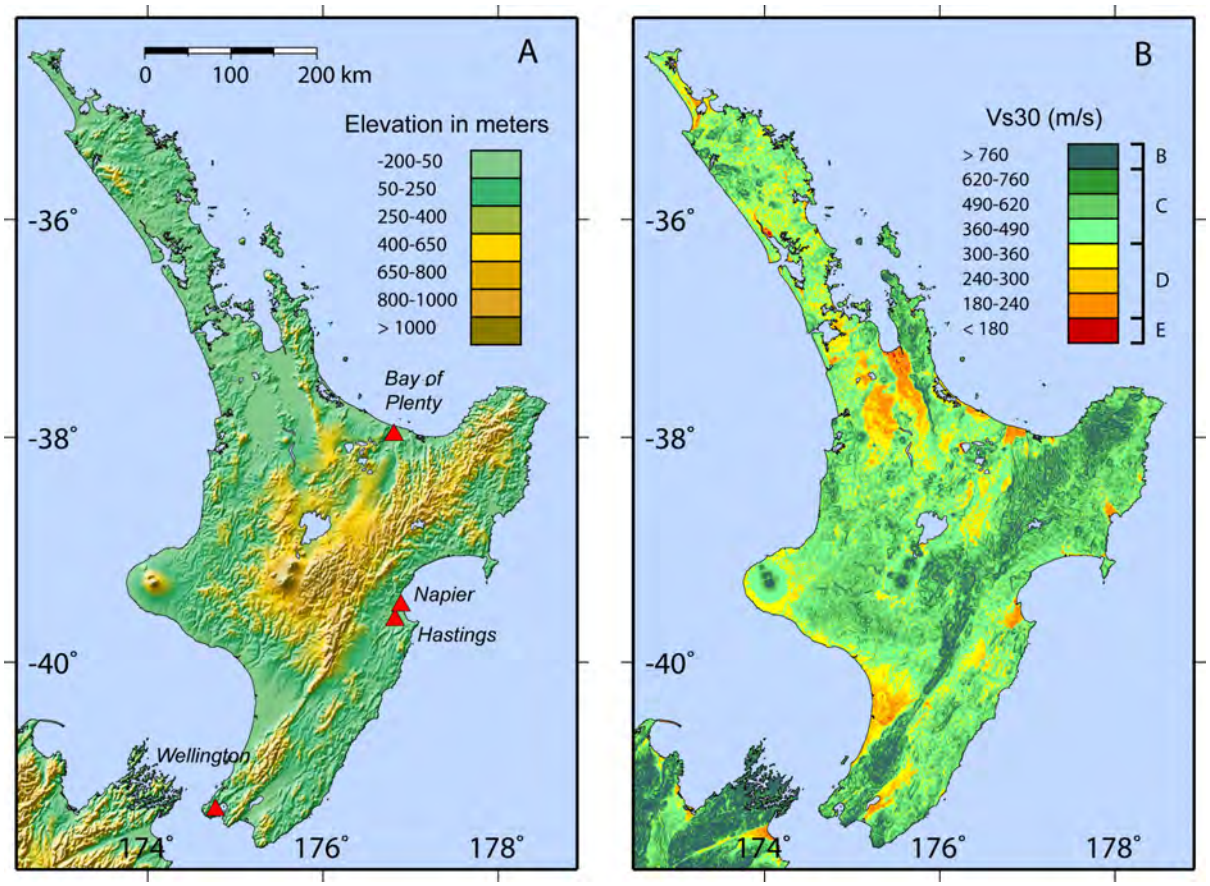

Figure 23. *A*, Topographic relief map for New Zealand's North Island. *B*, Site-condition map derived from topographic slope.

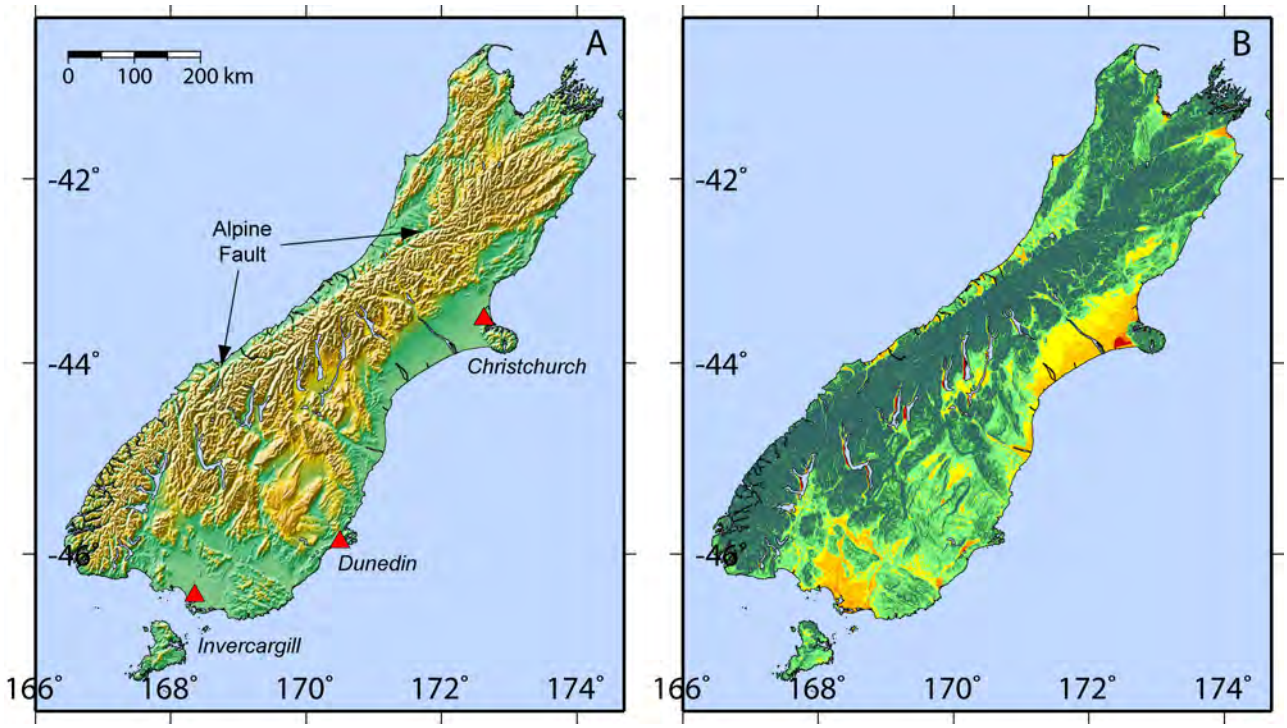

Figure 24. *A*, Topographic relief map for New Zealand's South Island. *B*, Site-condition map derived from topographic slope. See figure 23 for map legends.

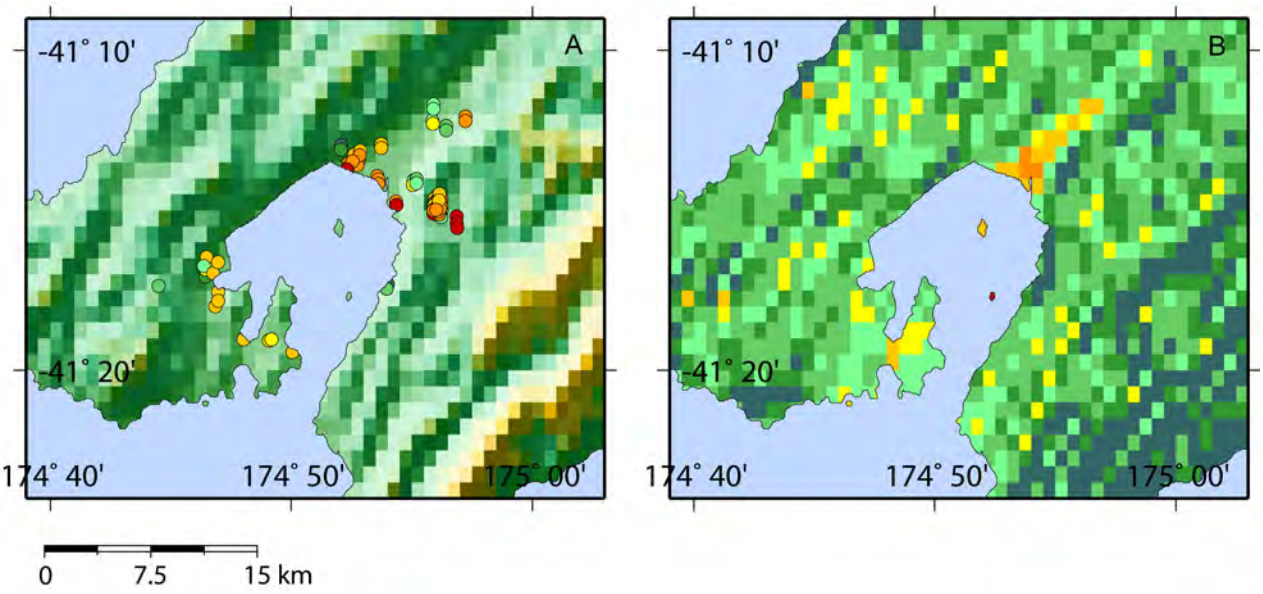

Figure 25. *A*, Topographic map of the Greater Wellington region, New Zealand. Circles indicate the location of measurements, color-coded by $V_S{}^{30}$ (see figure 23). Data were measured through collaborations between the University of Nevada, Reno; Victoria University, Wellington; and the Institute of Geological and Nuclear Sciences. *B*, Site-condition map derived from topographic slope. See figure 23 for map legends.

The Philippines

The Philippine archipelago represents a complex system of microplates that are being compressed between two convergent plate margins that bound the nation: the Philippine Sea and Eurasian plates. Because of its tectonic setting, the Philippines experiences frequent damaging seismic activity. It was reported following the M_W 7.7 1990 Central Luzon earthquake that the most serious damage occurred on soft soil sites (EQE Engineering, 1990).

The seismic site-condition map for the Philippines, derived from topographic slope, indicates several broad regions of low $V_S{}^{30}$ (fig. 26b). Slower $V_S{}^{30}$ values generally tend to mimic the regions of highest population exposure (fig. 26c). Consequently, site response will be an important factor when providing rapid estimates of ground shaking following a large earthquake in the region.

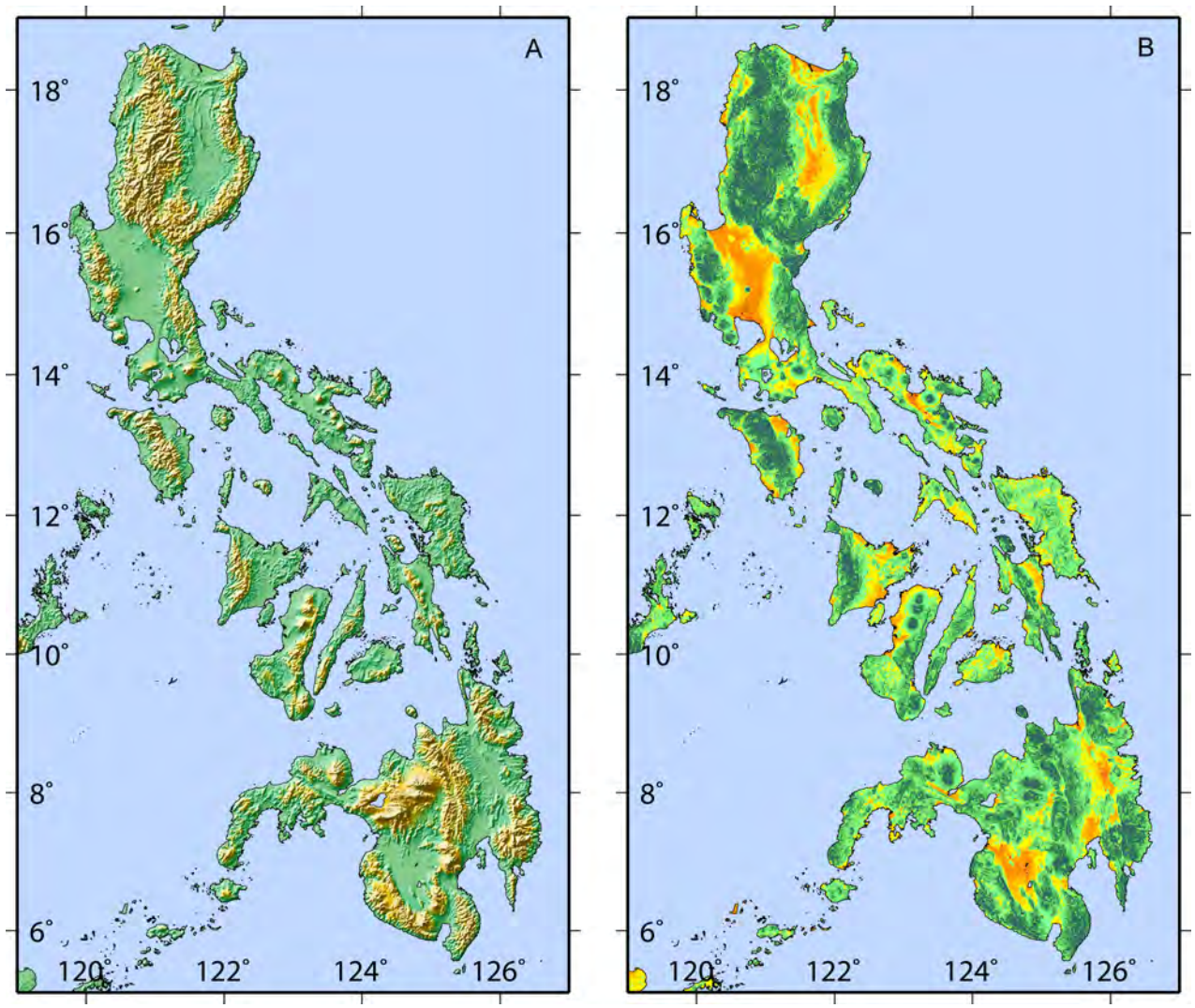

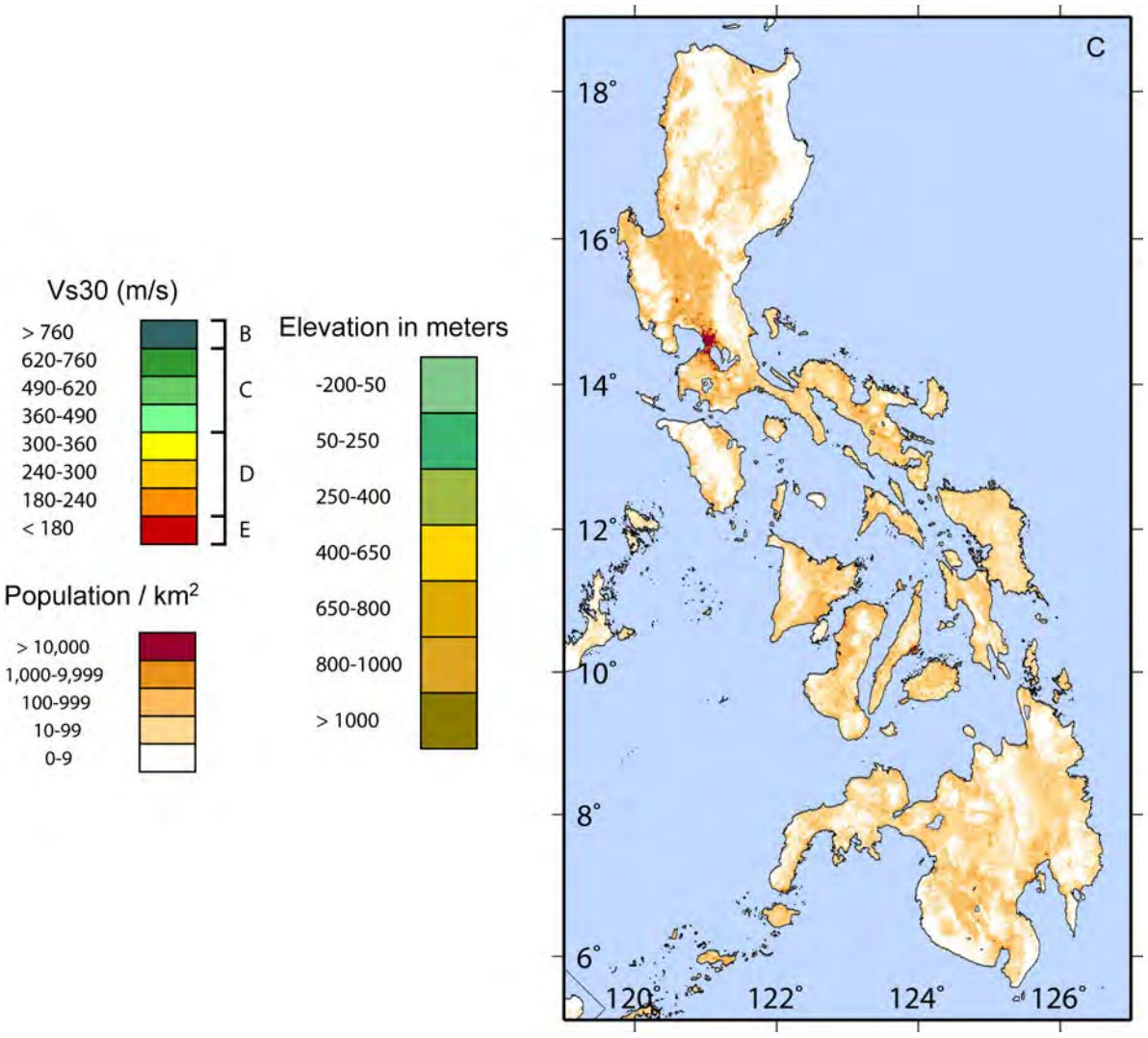

Figure 26. *A*, Topographic map of the Philippines. *B*, Site-condition map derived from topographic slope. *C*, Population density map of the Philippines.

Puerto Rico

The island of Puerto Rico, in the northwest Caribbean, lies within a broad deformation zone between the Caribbean and North American tectonic plates (Masson and Scanlon, 1991). In 1999, the USGS held a workshop to develop strategies to mitigate against earthquake and tsunami hazards in the region (Brink and others, 1999; Mueller and others, 2003). One of the key outcomes from this workshop was the need to develop a site response map for Puerto Rico. Puerto Rico has recently installed the ShakeMap system (Clinton and others, 2006) that incorporates a national site-condition map (fig. 27b). This map is based upon V_S^{30} measurements conducted by Odum and others (2007).

We compare the topographically-derived site-condition map (fig. 27c) with the map based on geology and V_S^{30} measurements (fig. 27b). The first thing that is apparent from figure 27b is the absence of any significant lateral variability in V_S^{30} assignments. Except for minor variations along coastlines and tributaries, existing ShakeMap V_S^{30} site-conditions are mapped almost entirely between 360–490 m/s. The topographically-derived map, however, demonstrates significant variability, and

mapped extents appear consistent with the mapped geology where harder plutonic and volcanic rocks are recovered with fast V_S^{30}, while Quaternary alluvial deposits are recovered with slower V_S^{30} (see Fig. 2 in Odum and others, 2007).

The number of V_S^{30} measurements are limited for the island of Puerto Rico. However, we use data from two recent studies (Pérez-Marcial, 2005; Odum and others, 2007) to evaluate both site-condition maps. We find a good correlation between measured V_S^{30} and predicted V_S^{30} from the topographic slope method (fig. 28a). The geologically-based map, however, appears to be a very poor predictor of V_S^{30} (fig. 28b).

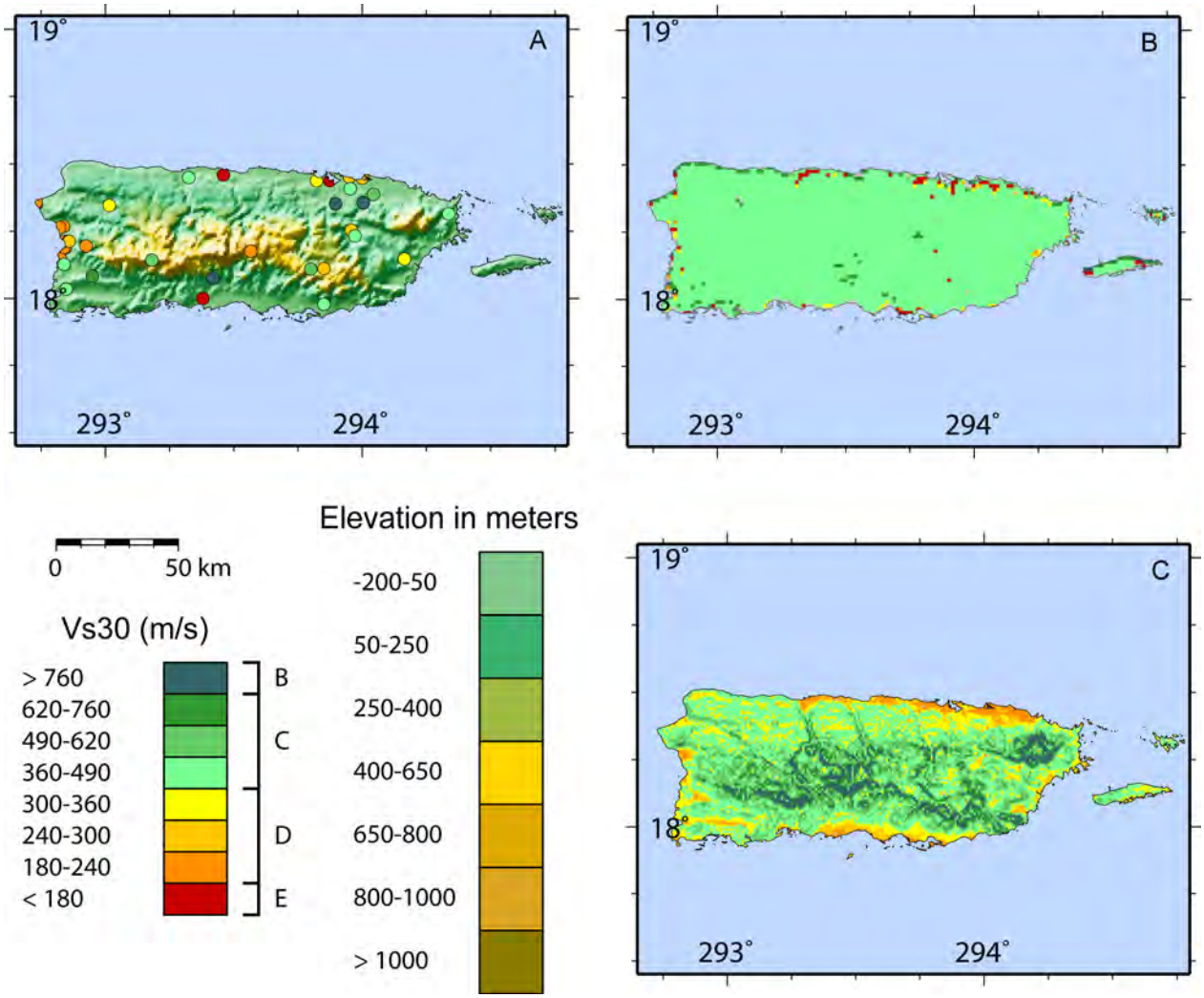

Figure 27. *A*, Topographic map of Puerto Rico. Circles indicate the location of measurements, color-coded by V_S^{30} in m/s. *B*, Site-condition map based on geology and V_S observations. *C*, Site-condition map derived from topographic slope.

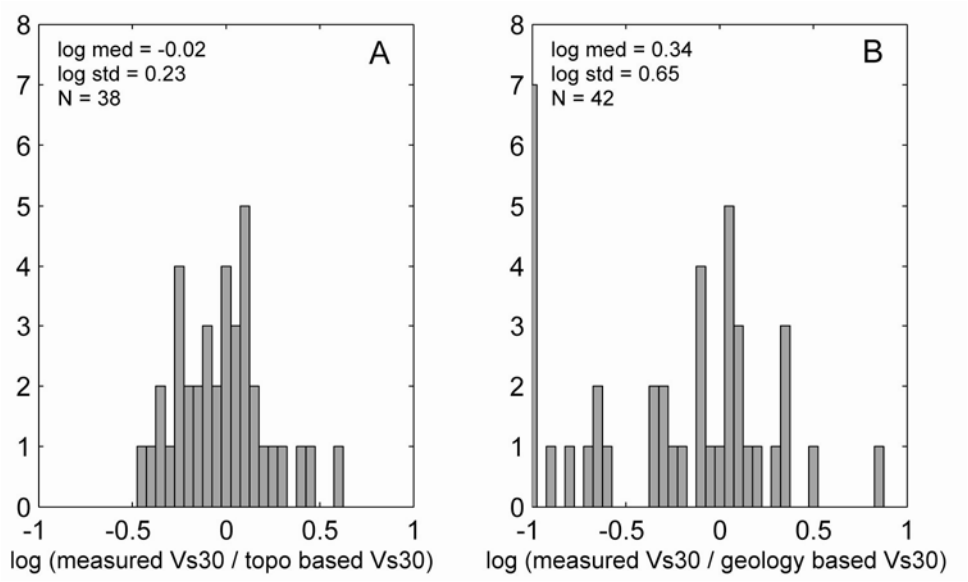

Figure 28. Histograms indicating logarithmic differences of Puerto Rican V_S30 values from Pérez-Marcial (2005) and Odum and others (2007), compared with *A*, values derived from topographic slope correlations and, *B*, values based on existing V_S30 site-condition maps. *N* is the number of V_S30 measurements.

Turkey

Turkey is a tectonically active region that experiences frequent destructive earthquakes. First-order tectonics are controlled by the collision of the Arabian plate and the Eurasian plate. A large piece of continental crust almost the size of Turkey, called the Anatolian block, is being compressed in a westerly direction. The block is bounded to the north by the North Anatolian Fault and to the southeast by the East Anatolian Fault. It was observed following the deadly 1999 zmit earthquake that site effects were a significant contributor to the high human losses (Bray and Stewart, 2000; Rathje, 2000; Bakır and others, 2002).

We compare the national site-conditions map for Turkey compiled by Department of Earthquake Engineering, Kandilli Observatory and Earthquake Research Institute (KOERI; Z. Cagnan, written commun., 2007), derived from geologically-based data (fig. 29b), with our topographically-derived map (fig. 29c). The former was prepared using the correlations of NEHRP site classifications as a function of lithologic age, as described by Wills and Silva (1998). From this work, Turkey was assigned three different site classes: B, C, and DE. We assign V_S^{30} to the Turkish geologically-based map by taking the median NEHRP value for classes B and C, while the DE site class was assigned on the basis of the range given by Wills *et al*. (2000). The topographic-slope technique recovers most of the features indicated by the geology-based approach. Shear-wave values obtained from the NGA dataset are compared to the topographically-based approach (fig. 30a). In general, the topographic slope method tends to overestimate V_S^{30} with respect to the values given in the NGA database. However, there are reservations over the quality of these assignments since they were not derived from in situ measurement techniques. The same comparison using the Turkish national site-condition map appears to overestimate V_S^{30} as well, but yields a better overall median value with a slightly higher standard deviation (fig. 30b).

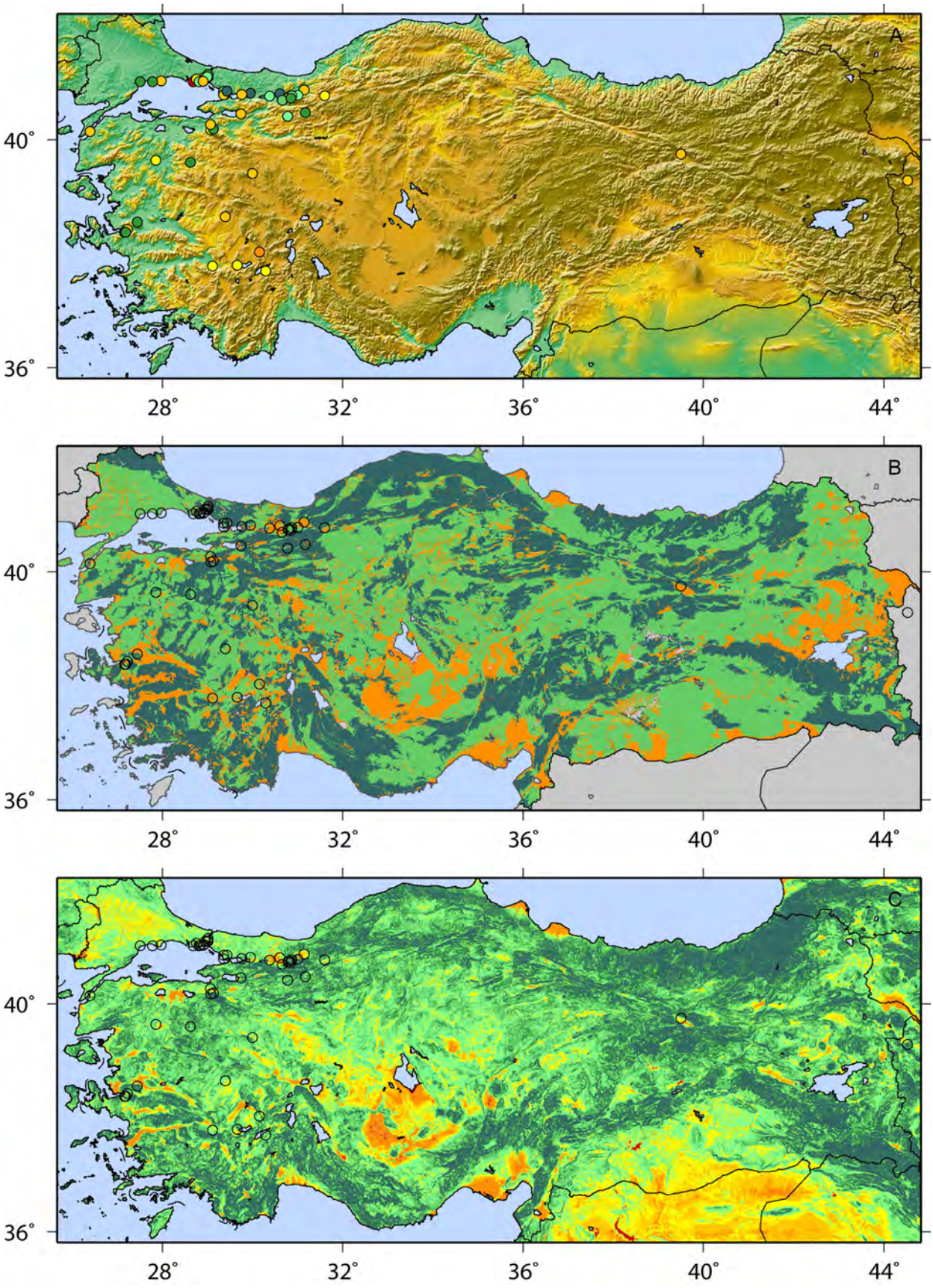
A
B
C
40°
36°
28°
32°
36°
40°
44°

Figure 29. *A*, Topographic map of Turkey. Circles indicate the location of measurements, color-coded by V_S30 in m/s. *B*, Site-condition map based on surficial geology from KOERI (Z. Cagnan, written commun., 2007). *C*, Site-condition map derived from topographic slope. See figure 1 for map legends.

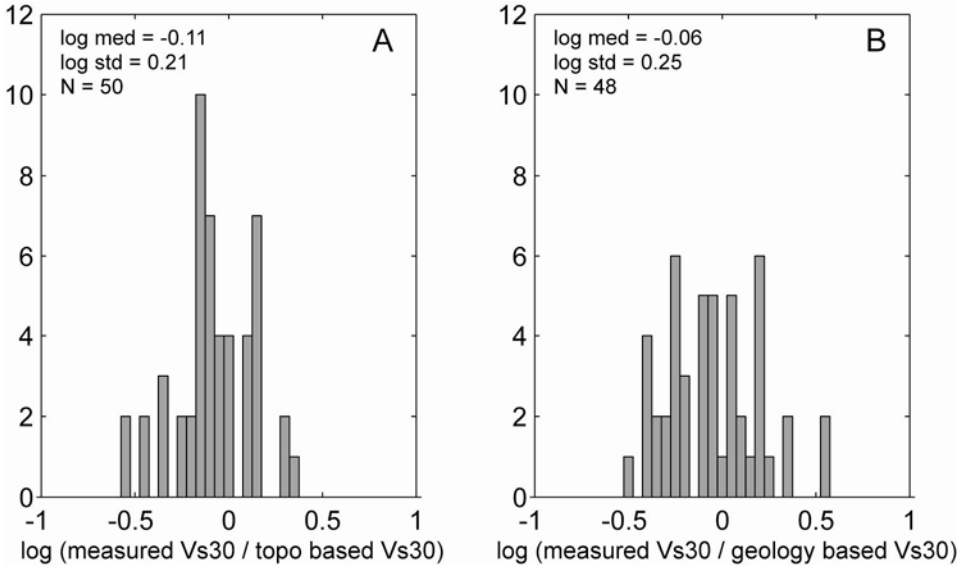

Figure 30. Histograms indicating logarithmic differences of Turkish V_S30 values taken from the NGA database, compared with *A*, values derived from topographic slope correlations and, *B*, values based on existing V_S30 site-condition maps. *N* is the number of V_S30 measurements.

Southern Europe

The moderate-to-high rate of seismicity in the Mediterranean region originates from the convergence of the African and Eurasian tectonic plates at a rate of about 6 mm/year. To date, little work available to the public has been done to constrain parameters for regional site-conditions.

Using the active tectonic V_S^{30}-slope relations (fig. 31), we observe that many features of the southern European and northern African geologic landscape are well recovered using our technique. Major mountain belts are clearly identified as high velocity zones, including the Alps, Pyrenees (France and Spain), Apennines (Italy), Dinaride (Greece), and Atlas (Morocco, Algeria, and Tunisia) mountain ranges. Other features such as the Po Basin (Italy) and Nile River Delta (Egypt) are clearly identified as low velocity zones. Less obvious at this scale, the Rhône (France) and Rhine (France and Germany) River Valleys can also be identified as a low seismic velocity zone.

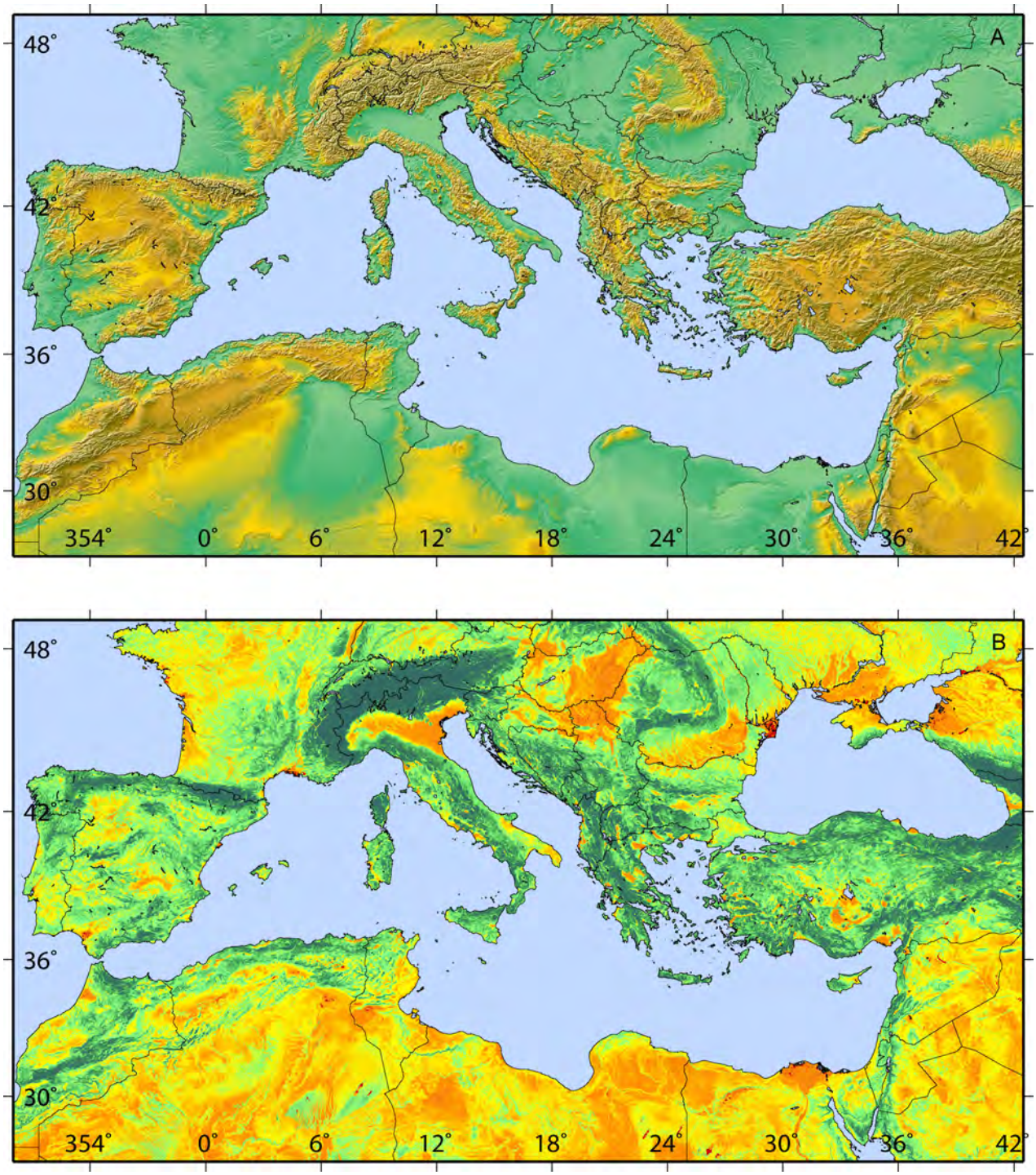

Figure 31. A, Topographic relief map for Southern Europe, Anatolia, and Northern Africa. B, Site-condition map derived from topographic slope. See figure 1 for map legends.

Application in Intraplate Regions

Mississippi Embayment Region

As expected from basic geomorphology, in areas of significant relief, mountains correlate well with rock and basins correlate well with sediments. Will this approach work in areas of lower overall relief? While a similar range of shear-velocity measurements, from hard rock to soft sediments, exist in the Mississippi Embayment, the associated topography as captured by the 30 arc sec (approximately 1 km resolution) SRTM30 data is much more subdued, as indicated by the narrow range in elevation (fig. 32a). Hence, there is less variation in slope and consequently, it might be expected that it would be more difficult to assign slope ranges that define the $V_S{}^{30}$ categories. Furthermore, as in the active tectonic regions, few $V_S{}^{30}$ measurements are available for high-velocity, hard rock sites. Nonetheless, there does appear to be a natural progression among $V_S{}^{30}$ values plotted against slope for both the central Australia and United States (fig. 2b), and we use these limits to produce the slope-based site-condition map for the Mississippi Embayment region shown in figure 32. We compare the 432 $V_S{}^{30}$ measurements with topography (fig. 29a), the $V_S{}^{30}$ site-condition map (fig. 32b) used for the regional ShakeMap installation (Bauer and others, 2001; Brackman, 2005), and the slope-derived $V_S{}^{30}$ map (fig. 32c) at sites in the Mississippi Embayment.

We find excellent correspondence of measured and slope-estimated $V_S{}^{30}$ values. The lowest $V_S{}^{30}$ regions, particularly those along river channels and in the Mississippi Embayment itself, are recovered, as are the few relatively high-velocity $V_S{}^{30}$ values in the southwestern corner of the map. On average there is very little bias to the estimates (fig. 33a). The same cannot be said of the geology-based site-condition map (fig. 32c), which shows an overall bias, having significantly lower $V_S{}^{30}$ values with respect to those measured (fig. 33b). Likewise, there is a more continuous progression of varying $V_S{}^{30}$ in the topography-based map (fig. 32c) than in the geology-based map (fig. 32b). Furthermore, the current map shown in figure 32b, used by the Central United States Earthquake Consortium (CUSEC), itself shows significant inconsistencies across state borders because they were mapped independently by different researchers. These inconsistencies are mostly observed outside the embayment itself.

Consequently, it appears that the slope versus $V_S{}^{30}$ categories for this region of low topographic relief can successfully be used as a proxy for basic site-conditions, just as for tectonically active regions. Another redeeming feature is that either the slope range or the mean slope values for a given region can provide simple quantitative diagnostics for the nature of the appropriate $V_S{}^{30}$-slope coefficients applied to the region. For example, mean slope values for the active tectonic regions are about 0.07; for the Mississippi Embayment region the mean slope is much lower, at 0.01, and over the entire continental United States east of the Rocky Mountains, the slope mean is about 0.04. Hence, we can use the mean slope to establish which slope correlations should be employed: active tectonic or stable continent. Alternatively, simplified characterizations of tectonically active versus stable continent domains could suffice in choosing between the coefficients employed for slope-based $V_S{}^{30}$ assignments.

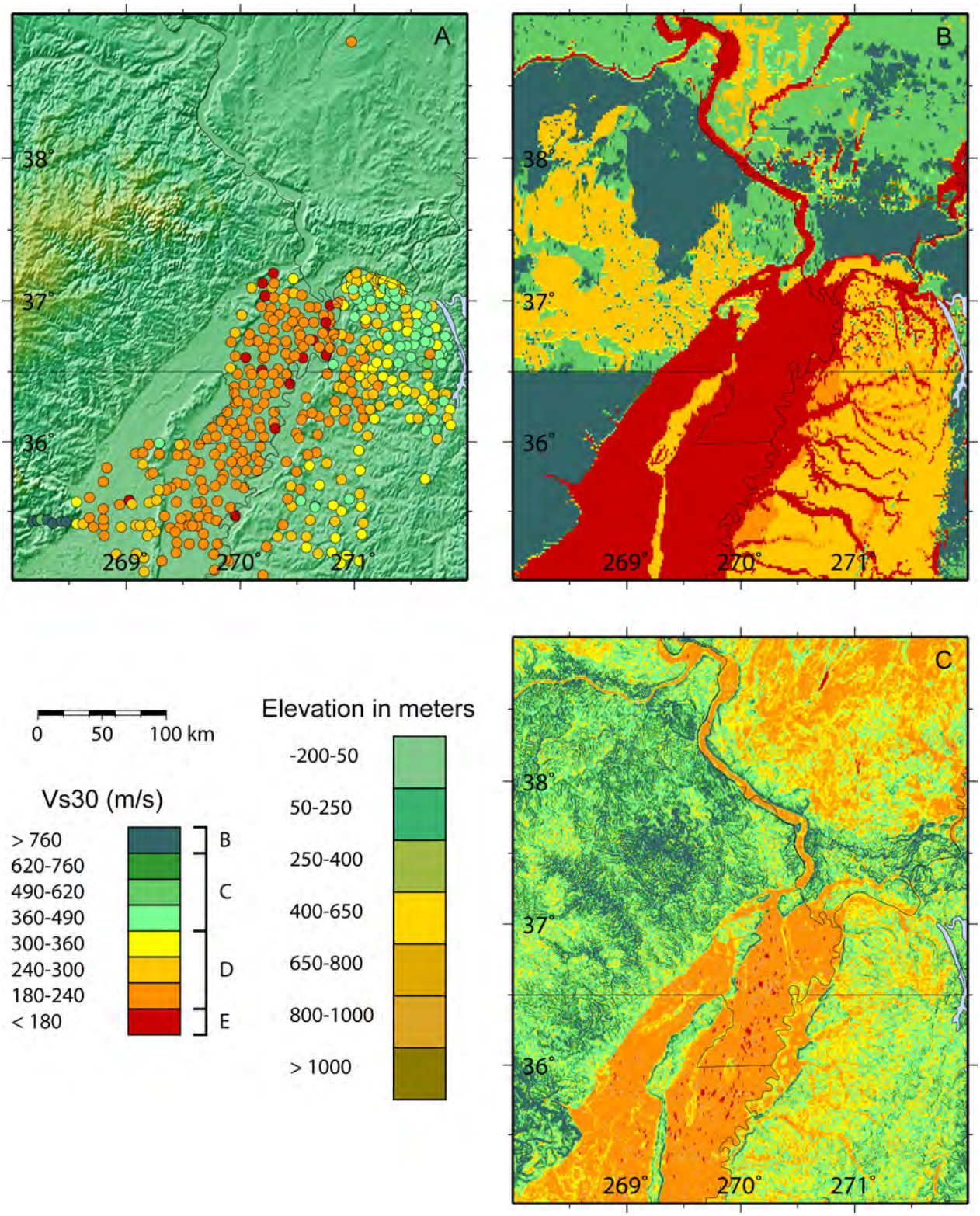

Figure 32. *A*, Topographic map showing the Mississippi Embayment region of the central United States. Circles indicate the location of measurements, color-coded by V_S^{30} in m/s. *B*, Site-condition map based on geology and V_S observations (modified from Bauer and others, 2001). *C*, Site-condition map derived from topographic slope.

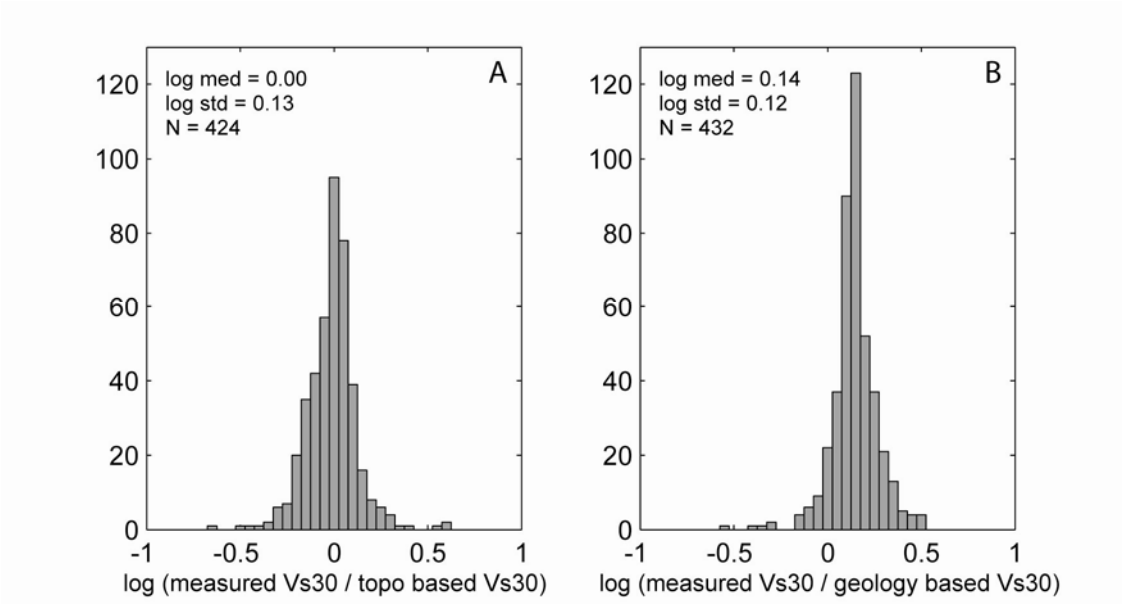

Figure 33. Histograms indicating logarithmic differences of V_S^{30} values for the Mississippi Embayment region, compared with *A*, values derived from topographic slope correlations and, *B*, values based on existing V_S^{30} site-condition maps. *N* is the number of V_S^{30} measurements.

Australia

Despite Australia's stable continental setting, it has hosted several large earthquakes in the past 50 yrs (for example, McCue, 1990; Clark and McCue, 2003). In contrast to most stable continental regions, where the largest magnitude earthquakes ($M > 6.0$) are concentrated in failed rifts or passive margins, Australia's largest onshore earthquakes have occurred largely in the ancient Proterozoic and Archean terranes of western and central Australia (Johnston and Kanter, 1990).

We estimate seismic site-conditions for Australia (fig. 34) using the stable continental relationships employed for the Mississippi Embayment region. Many geological features are well-recovered, including the high-velocity Eastern Highlands; Adelaide Fold Belt (South Australia); and the adjacent low-velocity playa lakes–Eyre, Frome, Torrens and Gairdner–which largely remain dry for almost the whole year. The Kimberly, Pilbra, and Yilgarn Cratons (Western Australia) are also recovered as faster velocity material. Visually, this map compares quite well with the national site condition map of A. McPherson and L. Hall (unpub. manuscript, 2007). However, their map grid was unavailable for direct comparison at the time this report was written. One region where these two maps disagree is in the Nullarbor Plain region of southeastern Western Australia and southwestern South Australia. This zone comprises very flat-lying carbonate-dominated sediments that A. McPherson and L. Hall (unpub. manuscript, 2007) have classified as NEHRP class C. In contrast, the topographically-based approach classifies this region near the DE boundary. Nevertheless, the topographically-based approach appears to be a good predictor of V_S^{30} relative to the map of A. McPherson and L. Hall (unpub. manuscript, 2007).

Comparing measured V_S^{30} data to the Australian topographically-based site-condition map, we find a good correlation between observed and predicted values within moderate confidence limits (fig. 35). Most of these data were obtained from the urban regions of Sydney, Newcastle, and Perth; however, some scattered SASW data from ground motion recording sites across the continent were also included (Collins and others, 2006). This analysis suggests that the approach does recover first-order site-conditions relatively well within the stable continental setting of Australia.

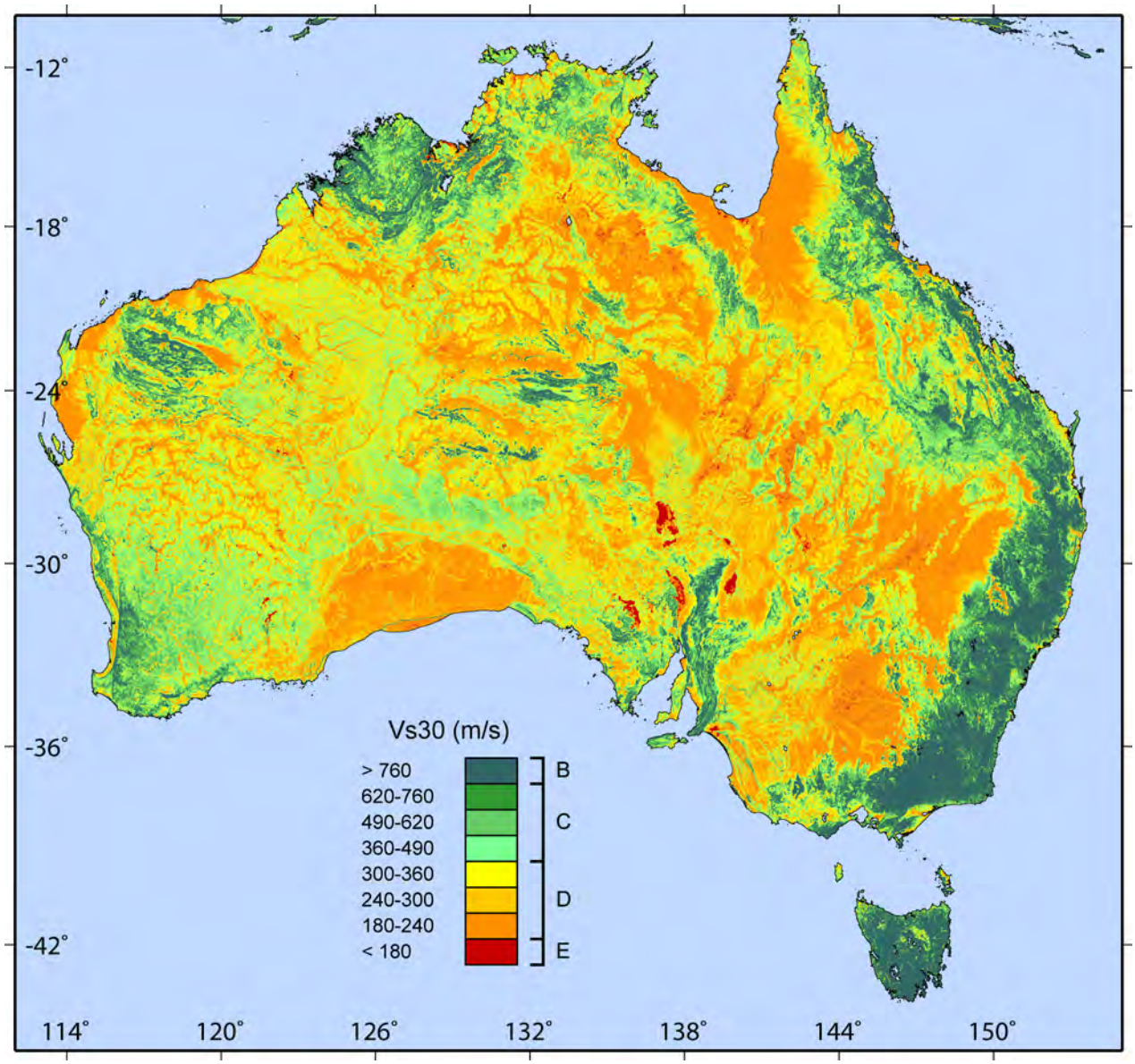

Figure 34. Site-condition map for Australia derived from topographic slope and the stable continent relations.

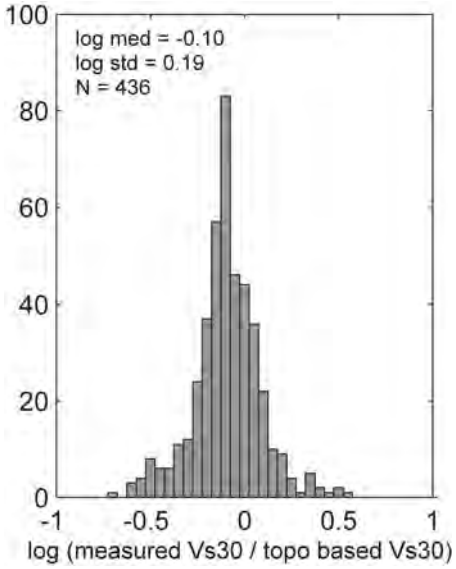

Figure 35. Histogram indicating logarithmic differences of Australian $V_S{}^{30}$ data compared with values derived from topographic slope correlations. *N* is the number of $V_S{}^{30}$ measurements.

Scandinavia

With the (geologically) recent deglaciation of the Fennoscandian Shield, the Scandinavian region is now considered to have potential for significant tectonic activity (for example from postglacial rebound), despite its stable continental setting (Bungum and others, 2005). This potential hazard is further exacerbated by its proximity to both a rifted passive continental margin and to failed rift zones. Although the region has not observed any large magnitude earthquakes ($M > 5.8$) in the past century, there is growing neotectonic evidence for several large earthquakes ($M > 7.0$) in recent prehistoric times (Olesen and others, 2000; Bungum and others, 2005).

We derive a site-condition map for Norway employing the stable continent relations (fig. 36). Owing to its significant topographic relief, we observe that much of the country can be classified as NEHRP site class B. Intuitively, this makes sense given that the recent glaciation scoured much of the preexisting surficial materials, exposing fresh unweathered rock. In contrast, interspersed glacial valleys, composed of glacial till eroded from adjacent mountains, are low-lying and are marked by low $V_S{}^{30}$.

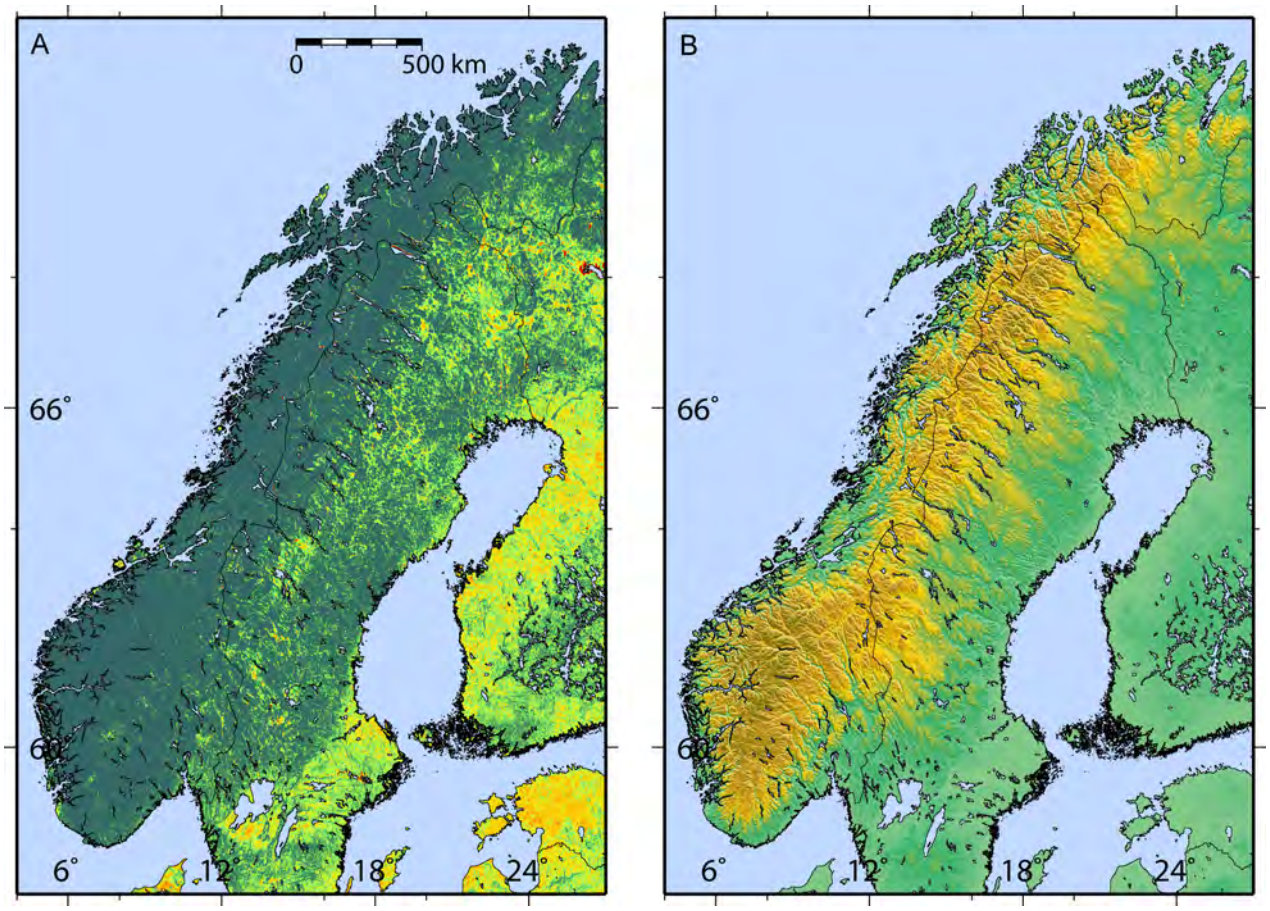

Figure 36. *A*, Topographic relief map for the stable continental setting of Norway. *B*, Site-condition map derived from topographic slope. See figure 1 for map legends.

Application for the Continental United States

Equipped with these correlations between topographic slope and V_S^{30}, and assuming either stable continent or tectonic coefficients for slope versus V_S^{30} apply, we can readily generate maps of estimated V_S^{30} velocities for any region around the globe. As an example, we describe regional evaluation of site classes for the continental United States below. At present, V_S^{30} maps for the entire continental United States are not available. Consequently, these maps, despite inherent limitations, will be an important starting point for many regional and national hazards analyses if extended beyond hazard on bedrock.

Western United States

We now apply the slope and V_S^{30} relations developed for active tectonic regions for the western margin of the continental United States, west of the front range of the Rocky Mountains (fig. 37). The regional topographically-based site-condition map indicates broad regions of contrasting site-conditions throughout the western United States, with faster material associated with much of the Rocky and Cascade Mountain ranges, and slower material interspersed in the lower-lying basins. In Nevada, in particular, we observe highly variable and spatially periodic changes in site class associated with the Basin and Range Province (also see Fig. 1c). It is also noteworthy that this map has excellent correspondence with the United States national surficial materials map (Soller and Reheis, 2004). We observe that regions of different surficial material tend to produce different site class signatures. For example, lacustrine sediments that cover much of western Utah are also well recovered.

As noted in northeast California (fig. 1), regions of recent volcanism are interpreted as having relatively slow velocities on our topographically-based site-condition map. This is because the associated lava flows have relatively low topographic gradient. In addition to areas of northern California, areas of low V_S^{30} due to recent volcanism is particularly apparent in southern Idaho, central Oregon, and southeastern Washington, east of the Cascades. This observation highlights one of the limitations in using this technique in broad scale applications. One must be aware of existing geological conditions within the region of interest that may affect the reliability of this approach.

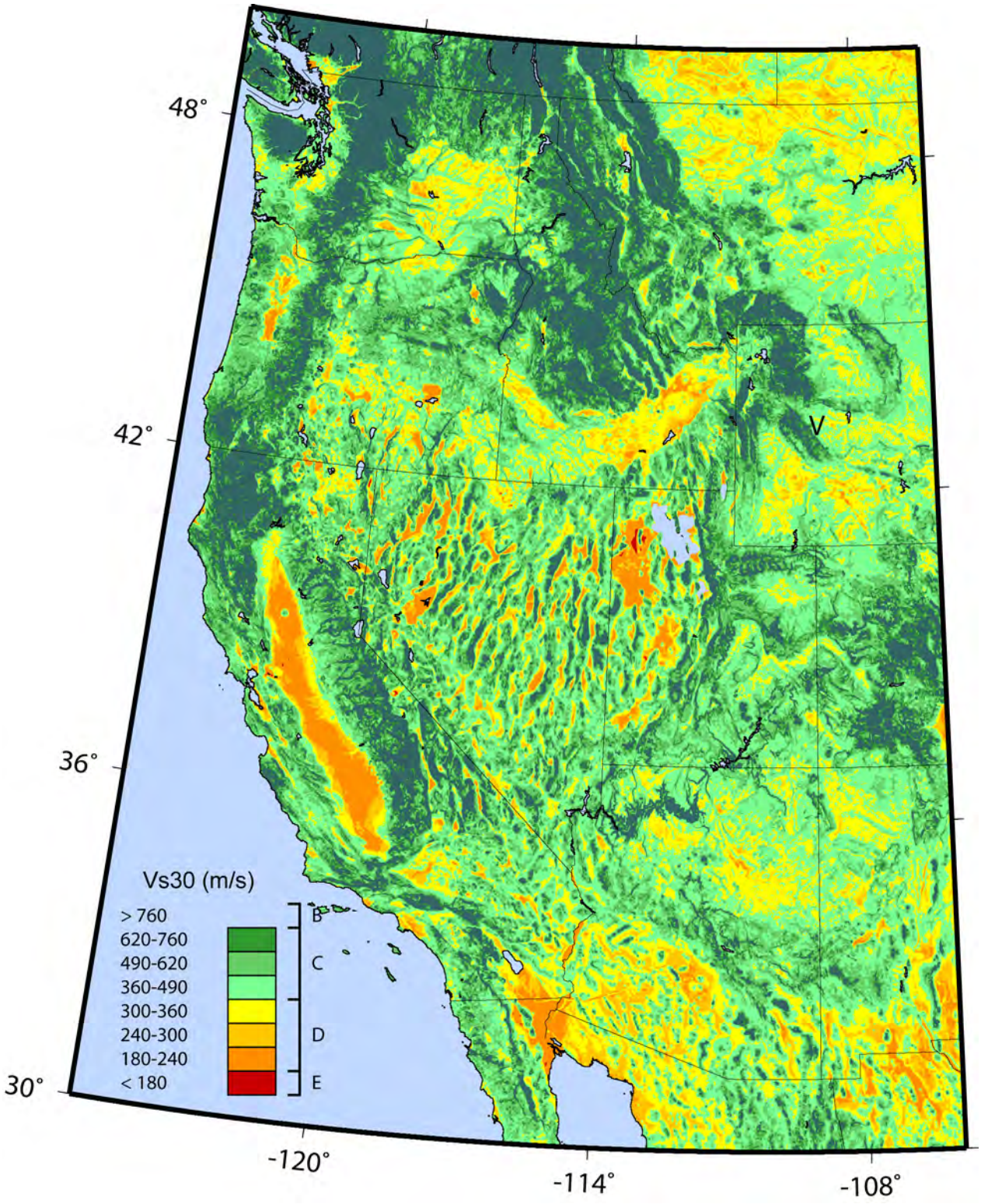

Figure 37. Estimated site-condition map for the continental United States, west of and including the Rocky Mountains, derived from topographic slope and slope-$V_S{}^{30}$ correlations for active tectonic regions.

Eastern United States

We also apply our approach using the stable-shield slope-$V_S{}^{30}$ correlations to produce a seismic site-condition map of the entire continental United States, east of the Rocky Mountains (fig. 38). Again, the seismic site-condition map produced recovers many of the surficial features described by Soller and Reheis (2004). In particular, the Appalachians indicate relatively fast velocity material, consistent with their steeper terrain and relatively high topographic relief. The Atlantic and Gulf coasts indicate slower material, corresponding to Coastal Plain sediments. Glacial deposits adjacent to the Great Lakes region, in addition to Minnesota, North Dakota and South Dakota, are also well-recovered (Soller and Reheis, 2004). It is likely that our topographic slope correlations under-predict $V_S{}^{30}$ in areas where flat-lying carbonate rocks dominate (for example, southern Florida), but the absence of $V_S{}^{30}$ measurements or site-condition maps precludes direct comparison. These carbonates may have varying degrees of lithification or weathering and surficial deposits that preclude regional, broad-brush $V_S{}^{30}$ classification (for example, A. McPherson and L. Hall, unpub. manuscript, 2007). It is worth noting that had southern Florida ranked high for earthquake hazards, such information would likely be more readily available; its low-hazard status warrants a more regional approach at this time.

While some aspects of these maps may be very approximate, they do provide first-order $V_S{}^{30}$ site-condition maps for the continental United States, with very little effort. One obvious side-benefit of this approach is that this map requires only our correlation, a digital 30-sec topographic map, and a few seconds of computer time to produce. Greater detail, and perhaps greater accuracy, might be obtained with higher-resolution elevation data.

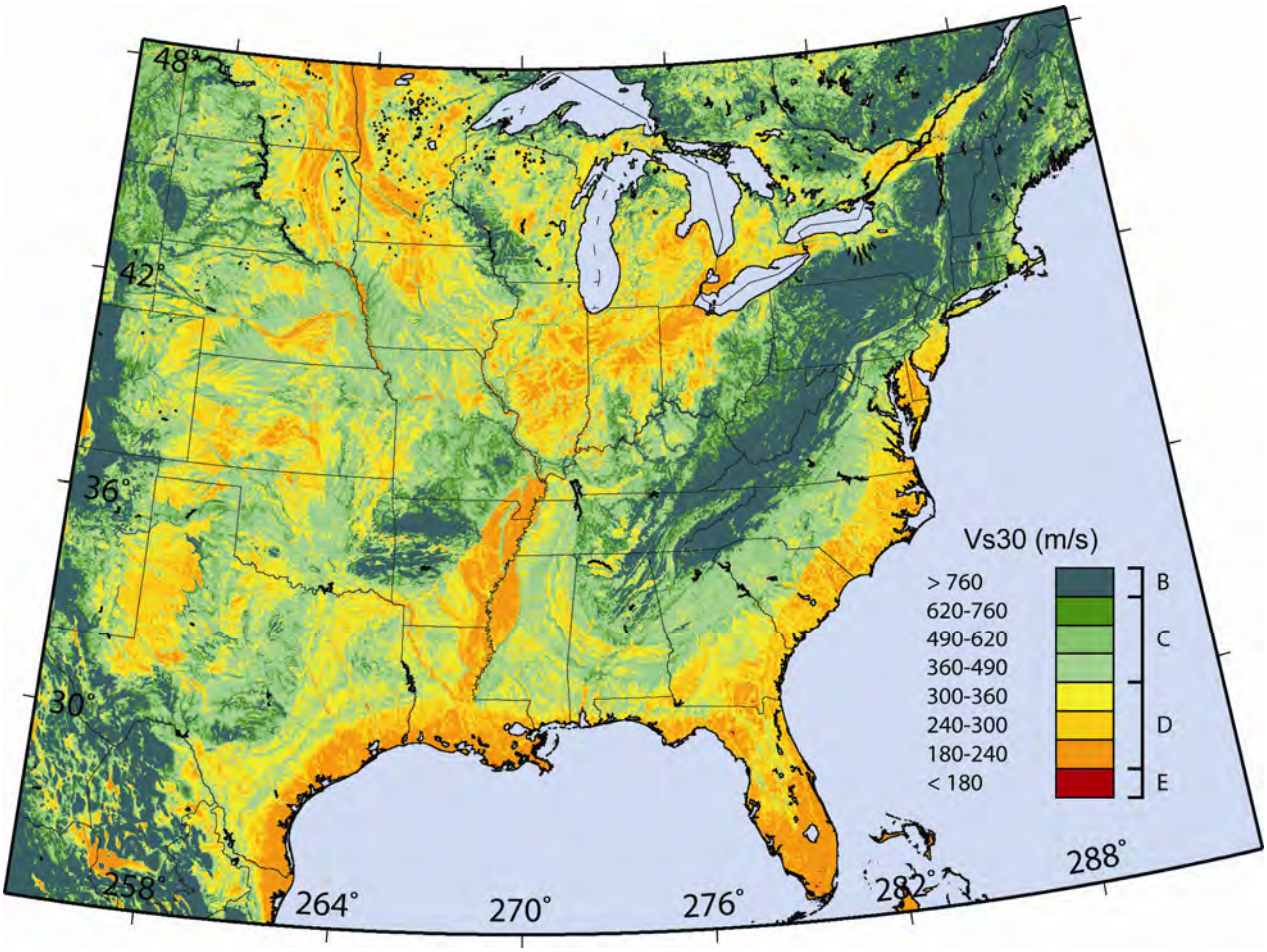

Figure 38. Estimated site-condition map for the continental United States east of the Rocky Mountains, derived from topographic slope and slope-$V_S{}^{30}$ correlations for stable continental regions.

Web Delivery of Global $V_S{}^{30}$ Maps

Given that we expect a significant demand for these simplified topographically-based $V_S{}^{30}$ maps for regional as well as global hazard and risk studies, we have chosen to make the $V_S{}^{30}$ grids available via a web delivery service. Motivation for providing this service is also to avoid any possible misinterpretation in duplicating our method; while duplication should be straight-forward, differences may ensue when processing large topographic data sets. Users of this service will be able to choose from three styles of global $V_S{}^{30}$ maps: USGS topographic slope, a compiled mosaic, and user-specified customized maps. Maps of specified dimensions (lon1/lon2/lat1/lat2) will be individually computed and will subsequently be available for download from the web server (fig. 39).

The three categories of site-condition maps are briefly described below. Access to all maps is provided at:

http://earthquake.usgs.gov/ vs30/

USGS Topographic Slope V_S^{30} Model

The USGS topographic slope-based V_S^{30} model is currently the default site-condition map being used in global ShakeMap applications. It comprises the maps indicated in this report using the coefficients described in table 2. Users can access the predefined maps and grids (those presented in this report) or generate a V_S^{30} grid for selected map extents anywhere around the globe, specifying either active tectonic or stable continent coefficients on the interactive user interface (fig. 39).

Mosaic V_S^{30} Model

Several regional seismic site-condition maps already exist that have been developed by independent researchers (for example, Wills and others, 2000; Bauer and others, 2001; Lee and others, 2001; Matsuoka and others, 2005; Martirosyan and Hansen, 2007). Furthermore, the use of higher-resolution topographic data than the SRTM30 data presently used may provide significant improvements to our current site-condition maps. Where we have confidence that these site-condition maps are better than what we can achieve employing the topographic-based approach with SRTM30 data, we stitch together these grids within our global grid above, thus creating a mosaic of topographically- and geologically-based V_S^{30} maps. These maps will represent our preferred global site-condition model and will be the model that will be employed for Global ShakeMap applications. At present we do not have the capability to provide the mosaic V_S^{30} model online, and this product will be delivered at a later date. Consequently our preferred site-condition model is presently based purely upon the topographically-derived model described above. However, this will be rectified once we have the resources and permissions to develop the mosaic model further.

Custom V_S^{30} Model

We also enable users to customize site-condition maps. If users derive alternative V_S^{30}-slope correlations from those described in table 2, they may customize a seismic site-condition map for a specified region. Users will have the option to specify the topographic slope ranges that correspond to their predefined V_S^{30} ranges. Once this request is submitted, the Web Service will calculate and return a customized V_S^{30} grid that can subsequently be downloaded from the ftp server.

Vs30 (m/s)	180	240	300	360	490	620	760
Active Tectonic (m/m)	0.000032	0.0022	0.0063	0.018	0.05	0.1	0.138
Stable Shield (m/m)	0.000006	0.002	0.004	0.0072	0.013	0.018	0.025

Site Name		Resolution: 30 arc-sec
Northeast Point	Latitude:	Longitude:
Southwest Point	Latitude:	Longitude:
Slope Type	◉ Active Tectonic	○ Stable Shield
Slope Values	0.000032 | 0.0022 | 0.0063 | 0.018 | 0.05 | 0.1 | 0.138	
Output Type	☐ ASCII Output ☐ GMT Output ☐ JPEG Output	
	Generate and View Map/Grid	Start Over

Figure 39. Screenshot of the web page for the global topographically-based V_S30 grid delivery service.

Discussion

Why would topographic slope provide such a good proxy for the average shear velocity in the top 30 meters of the ground? A discussion of a wide range of geological materials and erosional and depositional domains, and their influence on the physical properties controlling shear velocity, is beyond the scope of this discussion. However, some limited examples of widespread geomorphic domains are warranted. We consider the physical properties that most influence shallow shear velocities in soil and rock separately.

Why Topographic Slope Works as a Proxy for V_S^{30}

Of the physical properties of soils, those that have a strong effect on shear modulus are most pertinent to shear velocity. In general, void space and effective mean stress dominate shear modulus changes, since density variations tend to be rather small in soils (Fumal and Tinsley, 1985). When considering only shallow (top 30 m) conditions, mean principal effective stresses do not vary dramatically. Hence, among physical parameters, void ratio is one of the most important affecting shear modulus. Fumal and Tinsley (1985) found that the soil texture and the relative grain-size distribution can be a good measure of void ratio. For the San Francisco Bay area, they divided the soils into four textural categories based on grain-size distribution and found that shear-velocity generally increases as mean grain size increases. That shear velocity increases with increasing grain size goes a long way in explaining why lower shear velocity and lower topographic slope correlate so well: particle size decreases as the available energy in the depositional environment decreases at lower slopes.

In rock, Fumal and Tinsley (1985) show that the two dominant physical properties determining shear velocity are hardness and fracture spacing, with greater hardness and spacing resulting in higher velocities. Here too, we would expect that these parameters would be correlative with topographic slope as hard rock and coarse fracture spacing both resist weathering, allowing rocks with higher shear velocities to hold a steeper slope.

In semiarid alluvial fan systems, found in much of the western United States, mountain fronts typically grade from steep bedrock slopes to the outer fan, where channels are very shallow and braided (for example, Blatt and others, 1980). Generally, there is a decrease in grain size down-fan as the importance of stream-flow deposits dominates that of debris-flow deposition. With increasing distance from the mountain front, floodplain deposits continue to decrease in particle size as deposited at decreasing slopes by less energetic fluvial and pluvial processes.

Naturally, our above generalization applies only to the overall trend of fining particle size with lower gradients, and hence lower V_S^{30} with lower slope within a particular depositional setting. There are also several reasons why topographic slope should be limited in its ability to recover V_S^{30} by a number of known geologic processes and overall variations in geologic materials. Clearly, other processes can modify or control particle size and other factors that determine V_S^{30} in any depositional environment, such as variable source material, sorting, cementing, channeling, etc. These processes and material properties will presumably lead to substantial variation on the overall trend we observe. For example, in many western United States soils, the age of the soil development and weathering will influence V_S^{30}, with perhaps little change in topographic slope. Soil aging, particularly calcite cementation of soils (a.k.a. caliche) in the Las Vegas Basin, Nevada, has been shown to elevate V_S^{30} values to 500–600 m/s (Scott and others, 2004), despite relatively low slopes. Fortunately, such rigid soil should be expected to hold considerable slope under erosional (stream cutting) influences, so the overall trend may still be consistent with our simple assumptions.

Thelen and others (2006), based on V_S^{30} profiles in the Los Angeles Basin, suggest that slope also controls the distribution of clay minerals in the basin, which they describe as key in the designation of mappable soil units, and that slope also controls texture, which in turn affects porosity of the type of soil formed. Thelen *et al*. (2006) further conclude that the best surface indicator of V_S^{30} may be the hydraulic gradient of the San Gabriel River, another manifestation of the influence of slope. Yet, they rightly caution that to the extent that soils are predictors of hydraulic gradient, they may also be considered only rough predictors of V_S^{30}.

Our simple assumption on the correlation of slope with V_S^{30} will break down for some obvious topographic and geomorphic combinations. For example, in continental glaciated terrains, topography alone cannot distinguish between topographically similar depositional (glacial till) drumlins and erosional (bedrock) roche moutonnées. Likewise, and more extensive in area, nominally flat volcanic plateaus may not be recognized as rock since they can have low overall slope. The latter case happens to be quite common for much of northeastern California, where significant areas of hard rock (fig. 1c) are assigned to soft rock or soil based on our procedure because of regions of low slope (fig. 1a). Since our goal is to quantify shaking in populated areas, and glacial formations and unweathered volcanic plateaus tend to be sparsely populated, particularly in comparison to the many urbanized low-sloping alluvial basins, this misclassification may not lead to significant uncertainties in loss or damage assessments.

Alternatively, it is likely that other readily-available characteristics of topography may further elucidate the difference, even between low gradient soils and rocks. For example, spatial roughness determined at high resolution may allow one to distinguish between smooth depositional sediments and rougher volcanic rock despite similar slopes. Additional digital geographic and (or) geomorphic data may also be exploited to this end as well; in particular, land use data may distinguish among comparable slopes of varying materials in many cases. For example, Matsuoka *et al*. (2005) found a good correlation between slope, along with geomorphic indicators (for example, man-made fill versus natural fill, distance to mountain front, etc.), and V_S^{30} in Japan. However, we have purposely limited our study to easily exploited topography data; further analysis is underway to provide additional constraints on V_S^{30} in areas that may violate our simple topographic slope versus V_S^{30} assumptions.

Comparison with Geologically-Based V_S^{30} Maps

We should emphasize that our direct comparison with other V_S^{30} maps derived from maps of regolith and basement geology does not imply that we have full confidence in the details of either. Rather, consistencies and inconsistencies become more apparent with direct side-by-side comparison. Only on very local scales with dense V_S^{30} sampling are V_S^{30} maps fully constrained, and then typically only along profiles (for example, Scott and others, 2004; Thelen and others, 2006).

Since geology-based maps are typically developed with completely different goals in mind than constraining seismic site amplification, there are some obvious drawbacks to using them as a starting point for mapping site-conditions. Standard geologic maps ordinarily contain little information about the hardness or fracture spacing of bedrock units, so estimating shear-velocity is difficult (Fumal and Tinsley, 1985). Since bedrock V_S^{30} values are sparse, assignments to mapped bedrock units from observational V_S^{30} measurements are often uncertain. In soils, geotechnical properties (including cone penetration test results, thickness, and grain size) beneficial for detailed V_S^{30} assignments (for example, Holzer and others, 2005) are often lacking and V_S^{30} measurement localities are often poorly dispersed.

In our analyses we have shown to some degree that geologically-based V_S^{30} maps can have deficiencies with respect to predicting V_S^{30} measurements. These deficiencies are in part because assignments of single V_S^{30} values to an individual geological unit do not capture the potential variability of shear-wave velocity within the unit. One clear limitation is the lack of information on the depth

variations of particular units; these thickness variations result in variable V_S^{30} values that are not accommodated. Furthermore, geology maps often ignore thin veneers of regolith that are important for constraining ground motion amplification, where the underlying bedrock is well-known. Another concern with geology-based maps is that variations in grain size within a unit (often associated with variable weathering profiles) can alter wave speeds, yet geological units are assigned single V_S^{30} values. Topographic slope, however, does correlate with grain size, so aspects of this variability are captured with our approach to mapping V_S^{30}. At the very least, slope-based V_S^{30} maps allow more continuous changes in V_S^{30} within single mapped geological units if the unit exhibits measurable variations in slope.

Most existing site-condition maps have been derived primarily from existing or reinterpreted geological maps (for example, Fumal and Tinsley, 1985; Park and Elrick, 1998; Wills and others, 2000; Wills and Clahan, 2006). Fumal and Tinsley (1985) predicted shear wave velocities across southern California from geology based on 84 velocity borehole profiles. Their approach involved interpretation of different Quaternary alluvial units along with their lithologic characteristics. Such an approach precludes assigning V_S^{30} values without assigning such characteristics, usually from borehole logs, so substantial geotechnical information is required. Alternatively, Park and Elrick (1998) also predicted V_S^{30} values in southern California from more detailed geologic maps and found that their more numerous (196) V_S^{30} measurements warranted only three age-designated subdivisions (Quaternary, Tertiary, Mesozoic) to fully separate the measured V_S^{30} ranges.

Wills *et al*. (2000) used V_S^{30} measurements from 556 profiles in conjunction with California geologic maps to produce a California statewide V_S^{30} site-condition map by grouping geologic units with similar physical properties into categories that were expected to have comparable shear-velocity values. Like Park and Elrick's approach, no additional geotechnical information is required for units once their geologic versus V_S^{30} correspondence is ascertained, making their approach tractable for a statewide application. The Wills *et al*. (2000) V_S^{30} maps have been widely used for hazard studies and form the basis for site correction in ShakeMap in California (Wald and others, 2005).

More recently, Wills and Clahan (2006) further distinguished between geologic units by grouping geologic units by age and then splitting units by texture and thickness of alluvial deposits. While this approach may reduce the number of misclassified sites, it also requires additional effort and more geotechnical information than simply sorting geologic units from existing geologic maps. A full map for California using this approach is under development according to Wills and Clahan, (2006), a substantial effort that is certainly warranted given the earthquake hazard and risk to major urban centers in California. In comparison, our approach is readily available for our global ShakeMap efforts. We expect to supplant our topographic-based V_S^{30} maps with more detailed regional V_S^{30} maps as they are further developed.

Conclusions

We have developed a simple, inexpensive method for delivering first-order seismic site-condition maps that can be used, in the absence of detailed geologically-based maps, to rapidly estimate potential ground shaking following large global earthquakes. This process has been developed primarily for ShakeMap and PAGER applications. However, the technique has potential to be used more widely in scenario and probabilistic earthquake hazard and risk assessments for disaster response and mitigation programs anywhere in the world.

We exploit the simple and natural correlation between topography and surficial geology to derive topographic slope bounds that allow automatic mapping of V_S^{30} suitable on a regional scale anywhere on the globe. Since we are concerned with earthquake ground motions, and earthquakes occur predominantly in regions with significant tectonic relief, the V_S^{30} versus topographic slope

correlation for tectonic regions (dominated by data from California and Taiwan) should hold under most circumstances. In stable continental regions that tend to exhibit more subdued topography (like the central United States), $V_S{}^{30}$ values can also be recovered, but the correlation with slope is modified to accommodate the general observation that rock sites occupy lower slopes than in the active tectonic regions. Despite the overall lower range of slopes, the correspondence of $V_S{}^{30}$ and slope in stable continental areas suggests that the results in these regions will also be beneficial for site-condition mapping. Analysis of any additional $V_S{}^{30}$ measurements in stable continental areas that become available will allow us to better quantify the uncertainty as well as establish over what types of geologic and geomorphic regimes this method applies and where it is most limited.

While these relationships for estimating $V_S{}^{30}$ are calibrated against a particular resolution topography (30 arc sec global), they hold approximately for both lower- and higher-resolution maps. Beneficial attributes of the topographic-based site-condition maps, in addition to the obvious ease with which they can be produced, include both consistency and spatial continuity of resolution when making $V_S{}^{30}$ assignments. Unlike geology-based maps, which typically assign a constant velocity to a particular geologic unit or units, the topographic-slope approach allows for variable $V_S{}^{30}$ across a geologic unit, characterizing the presumed change in particle size with topographic gradient (alluvial fans or plains, for example). At the same time, with sharp, well-defined topographic features, there is also the ability to show discrete boundaries, for example, at mountain/basin interfaces.

While the topographic slope approach provides adequate first-order estimates of regional site amplification for the entire globe, there are noted discrepancies. For example, we note a difference in geologically and topographically derived $V_S{}^{30}$ values between soft and hard rock (NEHRP classes BC and C), and the correlation is made difficult for these units by the lack of shear-wave measurements. Fortunately, corresponding differences in site amplification for these site classes are relatively small (approximately 10 percent amplification in PGV for an input PGA of 200 cm/s^2; see table 1), so distinguishing between them is not as critical as it is for other site classes. Again, additional $V_S{}^{30}$ data for rock sites should improve our ability to recover $V_S{}^{30}$ from slope for areas with fast $V_S{}^{30}$ values. We have also identified some specific geologic terrains and processes for which topographic slope and $V_S{}^{30}$ are unlikely to correlate, and caution is urged in applying our approach without consideration of the geological units and environment. Although we have not made a systematic effort to establish over which geology and erosional and depositional environments our approach is applicable, we anticipate that additional $V_S{}^{30}$ data acquisition over time will allow us and others to do so. In the mean time, for larger-scale site-condition mapping using higher-resolution topography, additional analysis is required and refined slope ranges will be needed to assign $V_S{}^{30}$ values.

Empirically-based global ShakeMaps benefit from the amplification assigned with this approach. Interestingly, Wald and others (1999b) originally settled on using topography as the base layer for ShakeMap since topography tends to highlight areas of amplified shaking in basins from those less amplified mountainous areas. They had not anticipated the additional benefit of these base maps for constraining the site factors directly.

Topographic gradients can be easily converted to NEHRP site amplification factors for estimating ground motions in direct conjunction with standard ground motion prediction equations. In summary, our simple recipe for computing site amplification is:

1. Calculate the maximum slope of topography using GMT command “grdgradient.”
2. Determine map extent and compute mean slope over the domain (conveniently, GMT “grdinfo –L2” returns slope mean and standard deviation). For mean slopes less than 0.05, use the stable continent slope ranges for site class assignments; otherwise use the active tectonic slope ranges for site class assignments (table 2). Alternatively, simply assign table 2 coefficients based on knowledge of the tectonic regime.

3. Assign V_S^{30} to all sites using the slope and V_S^{30} ranges tabulated in table 2.
4. For ShakeMap, amplify empirically-based ground motions based on the combinations of site class, ground motion period, and input amplitude based on the Borcherdt (1994) amplification factors given in table 1 (see Wald and others, 2005, for detailed use in ShakeMap).

In addition to the shallowest site-conditions, seismic waves are also known to be strongly influenced by sediment thickness and basin structure (for example, Frankel and others, 1991; Field, 2000). In order to automatically derive an estimate of soil thickness as well as its shallow velocity, we are investigating the potential for topography to characterize basin structures and their depth. It may also be possible to characterize basins in low, slow regions, by fitting simple functions or shapes (for example ellipses) whose aspect ratios should provide an estimate of basin location and orientation, in addition to depth. In the process of analyzing global earthquakes using ShakeMap, we are examining the effects of basin amplification while looking for topographic signatures that might be exploited with routine, uniform processing of globally available data.

We have not fully exploited this topographic slope-based approach for mapping V_S^{30} by using the highest resolution topographic data available, which could be done for many areas. In addition, geomorphic, land-use, and other data sets could be brought to bear for some areas where such data exist. Local or regional-scale modifications to the correlations may provide improved V_S^{30} maps with little additional effort. In areas where numerous V_S^{30} measurements are available, or become available, minor modifications in the form of an overall static shift to slope-based V_S^{30} predictions or adjustments to the slope versus V_S^{30} correspondence ranges may be warranted.

Finally, to avoid confusion in the duplication of our method, we have provided a web service to deliver specified global site-condition maps uniformly. Users can choose from three styles of site-condition mapping: topography-based only, a mosaic of topography- and geologically-based maps, and maps customized to user specifications (that is, V_S^{30}-slope coefficients). We envisage that such a service will be of significant value at all levels of government and private industry for many applications of global earthquake hazard and risk assessments.

Acknowledgments

Chris Wills of the California Geological Survey kindly provided his database of V_S^{30} values for California, Ron Street generously compiled and provided his collection of V_S^{30} values for the central United States, Walt Silva provided an early copy of the NGA database, Kris Pankow provided the Utah V_S^{30} data and ShakeMap V_S^{30} grid, Tom Brackman provided Mississippi Embayment regional ShakeMap V_S^{30} grid, and Lisa Hall and Andrew McPherson provided Australian V_S^{30} data. Discussions with Vincent Quitoriano, Chris Wills, Kris Pankow, Lisa Hall and Andrew McPherson were very beneficial. Internal reviews by Chuck Mueller, Rus Wheeler, and Steve Harmsen improved this manuscript. The maps produced in this analysis were made using Generic Mapping Tools (GMT; Wessel and Smith, 1991). We also appreciate the constructive reviews of our more concise BSSA manuscript by Kris Pankow, Ivan Wong, and Chris Wills that led to significant improvements to the manuscript. Special thanks also goes to Eric Martinez and Vincent Quitoriano, who built the interactive V_S^{30} webpage and underlying PERL script to calculate the V_S^{30} maps on the fly.

References Cited

Abercrombie, R.E., and Benites, R.A., 1998, Strong motion modelling of the 1993 Tikokino earthquake, southern Hawke's Bay, New Zealand: New Zealand J. Geol. Geophy., v. 41, p. 259–270.

Ambraseys, N.N., 1963, The Buyin-Zara (Iran) earthquake of September, 1962 – a field report: Bull. Seism. Soc. Am., v. 53, no. 4, p. 705–740.

Ashland, F.X., and McDonald, G.N., 2003, Interim map showing shear-wave-velocity characteristic of engineering geologic units in the Salt Lake City, Utah, metropolitan area: Utah Geological Survey Open-File Report 424, 43 p.

Badal, J., Dutta, U., Serón, F., and Biswas, N., 2004, Three-dimensional imaging of shear wave velocity in the uppermost 30 m of the soil column in Anchorage, Alaska: Geophys. J. Int., v. 158, p. 983–997.

Bakır, S.B., Sucuoğlu, H., and Yılmaz, T., 2002, An overview of local site effects and the associated building damage in Adapazarı during the 17 August 1999 İzmit Earthquake: Bull. Seism. Soc. Am., v. 92, no. 1, p. 509–526.

Bauer, R.A., Kiefer, J., and Hester, N., 2001, Soil amplification maps for estimating earthquake ground motions in the Central US: Engineering Geol., v. 62, p. 7–17.

Bayer, K.C., Heuckroth, L.E., and Karim, R.A., 1969, An investigation of the Dasht-e Bayāz, Iran earthquake of August 31, 1968: Bull. Seism. Soc. Am., v. 59, no. 5, p. 1793–1822.

Berberian, M., 1979, Earthquake faulting and bedding thrust associated with the Tabas-e-Golshan (Iran) earthquake of September 16, 1978: Bull. Seism. Soc. Am., v. 69, no. 6, p. 1861–1188.

Berberian, M., Qorashi, M., Jackson, J.A., Priestley, K., and Wallace, T., 1992, The Rudbar-Tarom earthquake of 20 June 1990 in NW Persia: preliminary field and seismological observations, and its tectonic significance: Bull. Seism. Soc. Am., v. 82, no. 4, p. 1726–1755.

Bhaduri, B., Bright, E., Coleman, P., and Dobson, J., 2002, LandScan – locating people is what matters: Geoinformatics, v. 5, no. 2, p. 34–37.

Blatt, H., Middleton, G., and Murray, R., 1980, Origin of sedimentary rocks (2nd ed.): Englewood Cliffs, Prentice-Hall, Inc., 768. p.

Boore, D.M., Joyner, W.B., and Fumal, T.E., 1997, Equations for estimating horizontal response spectra and peak acceleration from Western North American earthquakes: A summary of recent work: Seismological Research Letters, v. 68, no. 1, p. 128–153.

Borcherdt, R.D., 1994, Estimates of site-dependent response spectra for design (methodology and justification): Earthquake Spectra, v. 10, no. 4, p. 617–653.

Brackman, T., 2005, ShakeMap implementation for the upper Mississippi Embayment: Memphis, Tenn., University of Memphis, 102 p.

Bray, J.D., and Stewart, J.P., 2000, Damage patterns and foundation performance in Adapazari, *in* Youd, T.L., Bardet, J.-P., and Bray, J.D., eds., Kocaeli, Turkey, earthquake of August 17, 1999 Reconnaissance report: Earthquake Engineering Research Institute: Earthquake Spectra, p. 163–189.

Brink, U., Dillon, W., Frankel, A., Mueller, C., and Rodriguez, R.W., 1999, Seismic and tsunami hazard in Puerto Rico and the Virgin Islands: U.S. Geological Survey Open-File Report 99–353.

Building and Housing Research Center, 2007, Ardakul (Khorasan) earthquake May 10 1997, Islamic Republic of Iran, Ministry of Building and Urban Development, Building and Housing Research Center, *http://www.bhrc.ac.ir/ISMN/SHABAKEH/accelerograms/earthquake/ten_years/ARDAKOL/Ardakol.htm*, October 2007.

Building Seismic Safety Council, 1995, NEHRP recommended provisions for seismic regulations for new buildings, 1994 edition: Federal Emergency Management Agency, FEMA 222A Report.

Building Seismic Safety Council, 2000, National Earthquake Hazards Reduction Program (NEHRP) Part 1 – Recommended provisions for seismic regulations for new buildings and other structures: Federal Emergency Management Agency.

Bungum, H., Lindholma, C., and Faleide, J.I., 2005, Postglacial seismicity offshore mid-Norway with emphasis on spatio-temporal–magnitudal variations: Marine Petrol. Geol., v. 22, p. 137–148.

Campillo, M., Gariel, G.C., Nzi, K., and Sanchez-Sesma, F.J., 1989, Destructive strong ground motion in Mexico City: source, path, and site effects during great 1985 Michoacan earthquake: Bull. Seism. Soc. Am., v. 79, no. 6, p. 1718–1735.

Cara, F., Rovelli, A., Di Giulio, G., Marra, F., Braun, T., Cultrera, G., Azzara, R., and Boschi, E., 2005, The role of site effects on the intensity anomaly of San Giuliano di Puglia inferred from aftershocks of the Molise, central southern Italy, sequence, November 2002: Bull. Seism. Soc. Am., v. 95, no. 4, p. 1457–1468.

Caserta, A., Bellucci, F., Cultrera, G., Donati, S., Marra, F., Mele, G., Palombo, B., and Rovelli, A., 2000, Study of site effects in the area of Nocera Umbra (Central Italy) during the 1997 Umbria-Marche seismic sequence: J. Seismology, v. 4, p. 555–565.

Cello, G., Mazzoli, S., Tondi, E., and Turco, E., 1997, Active tectonics in the central Apennines and possible implications for seismic hazard analysis in peninsular Italy: Tectonophys., v. 272, p. 43–68.

Chiou, B.S.-J., and Youngs, R.R., 2006, PEER-NGA empirical ground motion model for the average horizontal component of peak acceleration and psuedo-spectral acceleration for spectral periods of 0.01 to 10 seconds; Interim report for USGS review: Richmond, Calif., Pacific Earthquake Engineering Research Center, Interim Reports of Next Generation Attenuation (NGA) Models, 219 p.

Clark, D., and McCue, K., 2003, Australian paleoseismology: towards a better basis for seismic hazard estimation: Annals Geophys., v. 46, no. 5, p. 1087–1105.

Clinton, J.F., Cua, G., Huérfano, V., von Hillebrandt-Andrade, C.G., and Martínez-Cruzado, J., 2006, The current state of seismic monitoring in Puerto Rico: Seism. Res. Lett., v. 77, no. 5, p. 532–543.

Collins, C., Kayen, R., Carken, B., Allen, T., Cummins, P., and McPherson, A., 2006, Shear wave velocity measurement at Australian ground motion seismometer sites by the spectral analysis of surface waves (SASW) method, in Earthquake Engineering in Australia, Canberra, ACT, November 24-26, 2006, Proceedings: Australian Earthquake Engineering Society, p. 173–178.

Combellick, R., 2001, Liquefaction-susceptibility and seismic soil-type maps of Anchorage, Alaska: Alaska Division of Geological and Geophysical Surveys, Fairbanks, 5 p.

de Alteriis, G., and Aiello, G., 1993, Stratigraphy and tectonics offshore of Puglia (Italy, southern Adriatic Sea): Marine Geol., v. 113, p. 233–253.

DeMets, C., and Stein, S., 1990, Present-day kinematics of the Rivera Plate and implications for tectonics in southwestern Mexico: J. Geophys. Res., v. 95, no. B13, p. 21,931–921,948.

Dewey, J.W., and Grantz, A., 1973, The Ghir earthquake of April 10, 1972 in the Zagros Mountains of southern Iran: seismotectonic aspects and some results of a field reconnaissance: Bull. Seism. Soc. Am., v. 63, no. 6, p. 2071–2090.

Dhu, T., and Jones, T., 2002, Earthquake risk in Newcastle and Lake Macquarie: Geoscience Australia Record 2002/15.

Dobry, R., Borcherdt, R.D., Crouse, C.B., Idriss, I.M., Joyner, W.B., Martin, G.R., Power, M.S., Rinne, E.E., and Seed, R.B., 2000, New site coefficients and site classification system used in recent Building Seismic Code provisions: Earthquake Spectra, v. 16, no. 1, p. 41–67.

Dobson, J.E., Bright, E.A., Coleman, P.R., Durfee, R.C., and Worley, B.A., 2000, LandScan: A global population database for estimating populations at risk: Photogrammetric Engineering & Remote Sensing, v. 66, no. 7, p. 849–857.

Dowrick, D.J., Rhoads, D.A., Babor, J., and Beetham, R.D., 1995, Damage ratios for houses and microzoning effects in Napier in the magnitude 7.8 Hawke's Bay, New Zealand earthquake of 1931: Bull. N.Z. Nat. Soc. Earthquake Eng., v. 28, no. 2, p. 134–145.

Dutta, U., Biswas, N., Martirosyan, A., Nath, S., Papageorgiou, A., and Combellick, R., 2000, Delineation of spatial variation of shear wave velocity with high-frequency Rayleigh waves in Anchorage, Alaska: Geophys. J. Int., v. 143, p. 365–375.

Dutta, U., Biswas, N., Martirosyan, A., Papageorgiou, A., and Kinoshita, S., 2003, Estimation of earthquake source parameters and site response in Anchorage, Alaska from strong-motion network data using generalized inversion method: Phys. Earth Planet. Inter., v. 137, p. 13–29.

Dutta, U., Martirosyan, A., Biswas, N., Papageorgiou, A., and Combellick, R., 2001, Estimation of S-wave site response in Anchorage, Alaska, from weak-motion data using generalized inversion method: Bull. Seism. Soc. Am., v. 91, no. 2, p. 335–346.

Earthquake Engineering Research Institute, 2006, The Mw 6.3 Java, Indonesia, Earthquake of May 27, 2006: Earthquake Engineering Research Institute, Special Earthquake Report, 8 p.

EQE Engineering, 1990, The July 16 1990 Philippines Earthquake: EQE Engineering, San Francisco, Calif., 47 p.

EQE Incorporated, 1987, Summary of the 1987 Bay of Plenty, New Zealand Earthquake: EQE Incorporated, San Francisco, Calif., 29 p.

Farr, T.G., and Kobrick, M., 2000, Shuttle Radar Topography Mission produces a wealth of data: EOS Trans., v. 81, p. 583–585.

Field, E.H., 2000, A modified ground-motion attenuation relationship for southern California that accounts for detailed site classification and a basin-depth effect: Bull. Seism. Soc. Am., v. 90, no. 6, p. S209–S221.

Frankel, A., Carver, D., Cranswick, E., Meremonte, M., Bice, T., and Overturf, D., 1999, Site response for Seattle and source parameters of earthquakes in the Puget Sound region: Bull. Seism. Soc. Am., v. 89, no. 2, p. 468–483.

Frankel, A.D., Hough, S., Friberg, P., and Busby, R., 1991, Observations of Loma Prieta's aftershocks from a dense array in Sunnyvale, California: Bull. Seism. Soc. Am., v. 81, p. 1990–1922.

Franks, C.A.M., 1988, Engineering geological aspects of the Edgecumbe, New Zealand earthquake of 2 March 1987: Q. J. Eng. Geol., v. 21, p. 337–345.

Fumal, T.E., and Tinsley, J.C., 1985, Mapping shear-wave velocities of near-surface geologic materials, *in* Ziony, J.I., ed., Evaluating earthquake hazards in the Los Angeles region–An earth-science perspective: U.S. Geological Survey Professional Paper 1360, p. 101–126.

Furumura, T., and Kennett, B.L.N., 1998, On the nature of regional seismic phases—III. The influence of crustal heterogeneity on the wavefield for subduction earthquakes: the 1985 Michoacan and 1995 Copala, Guerrero, Mexico earthquakes: Geophys. J. Int., v. 135, no. 3, p. 1060–1084.

Gallant, J.C., and Dowling, T.I., 2003, A multiresolution index of valley bottom flatness for mapping depositional areas: Water Resour. Res., v. 39, p. doi:10.1029/2002WR001426.

Glass, C.E., 1989, Seismic wave attenuation during the 19 September 1985 Michoacan, Mexico earthquake: Int. J. Mining Geol. Eng., v. 7, p. 9-15.

Harmandar, E., Oye, V., Lindholm, C., and Bungum, H., 2007, Soil condition maps based on topographic slope: Network of Earthquake Research Institutes for Earthquake Seismology (NERIES) JRA3 Report, 20 p.

Holzer, T.L., Padovani, A.C., Bennett, M.J., Noce, T.E., and Tinsley, J.C., 2005, Mapping Vs30 site classes: Earthquake Spectra, v. 21, no. 2, p. 353–370.

Jafari, M.K., Ghayamghamian, M.R., Davoodi, M., Kamalian, M., and Sohrabi-Bidar, A., 2005, Site effects of the 2003 Bam, Iran, earthquake: Earthquake Spectra, v. 21, no. S1, p. S125–S136.

Johnston, A.C., and Kanter, L.R., 1990, Earthquakes in stable continental crust: Scientific American, v. 262, p. 42–49.

Jones, T., Middelmann, M., and Corby, N., 2005, Natural hazard risk in Perth, Western Australia: Canberra, Geoscience Australia, 352 p.

Kawase, H., and Matsuo, H., 2004, Amplification characteristics of K-Net, KiK-Net, and JMA Shindokei network sites based on the spectral inversion technique, World Conference on Earthquake Engineering, 13, Vancouver, British Columbia, Canada, August 1-6, 2004, Proceedings: Canadian Association for Earthquake Engineering, International Association for Earthquake Engineering, no. 454.

Lee, C.-T., Cheng, C.-T., Liao, C.-W., and Tsai, Y.-B., 2001, Site classification of Taiwan free-field strong-motion stations: Bull. Seism. Soc. Am., v. 91, p. 1283–1297.

Martirosyan, A., Dutta, U., Biswas, N., Papageorgiou, A., and Combellick, R., 2002, Determination of site response in Anchorage, Alaska, on the basis of spectral ratio methods: Earthquake Spectra, v. 18, no. 1, p. 85–104.

Martirosyan, A., and Hansen, R., 2007, Seismic site classification in Alaska for generation of real-time ground shaking maps: Geophys. Res. Abstr., v. 9, p. 11009.

Masson, D.G., and Scanlon, K.M., 1991, The neotectonic setting of Puerto Rico: Geol. Soc. Am. Bull., v. 103, p. 144–154.

Matsuoka, M., Wakamatsu, K., Fujimoto, K., and Midorikawa, S., 2005, Nationwide site amplification zoning using GIS-based Japan engineering geomorphologic classification map, International Conference on Structural Safety and Reliability, 9, Rome, Italy, June 19-23, 2005, Proceedings: Rotterdam, Netherlands, Millpress, p. 239–246.

McCue, K., 1990, Australia's large earthquakes and recent fault scarps: J. Structural Geol, v. 12, p. 761–766.

Miller, M.S., and Kennett, B.L.N., 2006, Evolution of mantle structure beneath the northwest Pacific: Evidence from seismic tomography and paleogeographic reconstructions: Tectonics, v. 25, p. doi:10.1029/2005TC001909.

Mueller, C.S., Frankel, A.D., Petersen, M.D., and Leyendecker, E.V., 2003, Documentation for 2003 USGS seismic hazard maps for Puerto Rico and the U.S. Virgin Islands: U.S.Geological Society Open-File Report 03-379, 12 p.

Nath, S.K., Chatterjee, D., Biswas, N.N., Dravinski, M., Cole, D.A., Papageorgiou, A., Rodriguez, J.A., and Poran, C.J., 1997, Correlation study of shear wave velocity in near surface geological formations in Anchorage, Alaska: Earthquake Spectra, v. 13, no. 1, p. 55–75.

Niazi, M., and Bozorgnia, Y., 1992, The 1990 Manjil, Iran, earthquake: geology and seismology overview, PGA attenuation, and observed damage: Bull. Seism. Soc. Am., v. 82, no. 2, p. 774–799.

Odum, J.K., Williams, R.A., Stephenson, W.J., Worley, D.M., von Hillebrandt-Andrade, C., Asencio, E., Irizarry, H., and Cameron, A., 2007, Near-surface shear wave velocity versus depth profiles, Vs30, and NEHRP classifications for 27 sites in Puerto Rico: U.S. Geological Survey Open-File Report 2007-1174, 46 p.

Olesen, O., Dehls, J., Bungum, H., Riis, F., Hicks, E., Blikra, L.H., Fjeldskaar, W., Lindholm, C., Olsson, L., Longva, O., Faleide, J.I., Bockmann, L., Rise, L., Roberts, D., Braathen, D., and Brekke, H., 2000, Neotectonics in Norway – final report from the NEONOR project: Geological Survey of Norway Report 2000.002 2000.002, 134 p.

Ordaz, M., and Singh, S.K., 1992, Source spectra and spectral attenuation of seismic waves from Mexican earthquakes, and evidence of amplification in the hill zone of Mexico City: Bull. Seism. Soc. Am., v. 82, no. 1, p. 24–43.

Park, S., and Elrick, S., 1998, Predictions of shear-wave velocities in southern California using surface geology: Bull. Seism. Soc. Am., v. 88, p. 677–685.

Pérez-Marcial, E.J., 2005, Ground response spectra at surface for Mayagüez considering in-situ soil dynamic properties: Mayagüez, Puerto Rico, University of Puerto Rico, Department of Civil Engineering, M.S. thesis, 135 p.

Rathje, E., 2000, Strong ground motions and site effects, *in* Youd, T.L., Bardet, J.-P., and Bray, J.D., eds., Kocaeli, Turkey, earthquake of August 17, 1999–Reconnaissance report: Earthquake Spectra 16, Supplement A, p. 65–96.

Scott, J.B., Clark, M., Rennie, T., Pancha, A., Park, H., and Louie, J.N., 2004, A shallow shear-wave velocity transect across the Reno, Nevada, area basin: Bull. Seism. Soc. Am., v. 94, no. 6, p. 2222-2228.

Soller, D.R., and Reheis, M.C., 2004, Surficial materials in the conterminous United States: U.S. Geological Survey Open-File Report 03-275, scale 1:5,000,000.

Stirling, M.W., McVerry, G.H., and Berryman, K.R., 2002, A new seismic hazard model for New Zealand: Bull. Seism. Soc. Am., v. 92, no. 5, p. 1878–1903.

Street, R., Woolery, E.W., Wang, Z., and Harris, J.B., 2001, NEHRP site classifications for estimating site-dependent seismic coefficients in the Upper Mississippi Embayment: Engineering Geology, v. 62, p. 123–135.

Tertulliani, A., 2000, Qualitative effects of local geology on damage pattern: Bull. Seism. Soc. Am., v. 90, no. 6, p. 1543–1548.

Thelen, W.A., Clark, M., Lopez, C.T., Loughner, C., Park, H., Scott, J.B., Smith, S.B., Greschke, B., and Louie, J.N., 2006, A transect of 200 shallow shear-velocity profiles across the Los Angeles basin: Bull. Seism. Soc. Am., v. 96, no. 3, p. 1055–1067.

Thenhaus, P.C., Hanson, S.L., Effendi, I., Kertapati, E.K., and Algermissen, S.T., 1993, Pilot studies of seismic hazard and risk in north Sulawesi Province, Indonesia: Earthquake Spectra, v. 9, no. 1, p. 97–120.

Umhoefer, P.J., Dorsey, R.J., and Renne, P., 1994, Tectonics of the Pliocene Lorento Basin, Baja California Sur, Mexico, and evolution of the Gulf of California: Geology, v. 22, p. 649–652.

Utsu, T., 2002, A list of deadly earthquakes in the World: 1500-2000, *in* Lee, W.K., Kanamori, H., Jennings, P.C., and Kisslinger, C., eds., International handbook of earthquake engineering and seismology: Amsterdam, Academic Press, p. 691–717.

Wald, D.J., and Allen, T.I., 2007, Topographic slope as a proxy for seismic site conditions and amplification: Bull. Seism. Soc. Am., v. 97, no. 5, p. 1379–1395.

Wald, D.J., Earle, P.E., Lin, K., Quitoriano, V., and Worden, B., 2006, Challenges in rapid ground motion estimation for the prompt assessment of global urban earthquakes: Bull. Earthq. Res. Inst., v. 81, p. 272–281.

Wald, D.J., Quitoriano, V., Heaton, T.H., and Kanamori, H., 1999a, Relationship between Peak Ground Acceleration, Peak Ground Velocity, and Modified Mercalli Intensity in California: Earthquake Spectra, v. 15, no. 3, p. 557–564.

Wald, D.J., Quitoriano, V., Heaton, T.H., Kanamori, H., Scrivner, C.W., and Worden, B.C., 1999b, TriNet "ShakeMaps": Rapid generation of peak ground-motion and intensity maps for earthquakes in southern California: Earthquake Spectra, v. 15, no. 3, p. 537–556.

Wald, D.J., Worden, B.C., Quitoriano, V., and Pankow, K.L., 2005, ShakeMap manual: technical manual, user's guide, and software guide: U.S. Geological Survey, 132 p.

Wessel, P., and Smith, W.H.F., 1991, Generic Mapping Tools: EOS, v. 72, p. 441.

Wesson, R.L., Frankel, A.D., Mueller, C.S., and Harmsen, S.C., 1999, Probabilistic seismic hazard maps of Alaska: U.S. Geological Survey Open-File Report 99–36, 20 p.

Wills, C.J., and Clahan, K.B., 2006, Developing a map of geologically defined site-condition categories for California: Bull. Seism. Soc. Am., v. 96, no. 4A, p. 1483–1501.

Wills, C.J., Petersen, M., Bryant, W.A., Reichle, M., Saucedo, G.J., Tan, S., Taylor, G., and Treiman, J., 2000, A site-conditions map for California based on geology and shear-wave velocity: Bull. Seism. Soc. Am., v. 90, no. 6B, p. S187–S208.

Wills, C.J., and Silva, W., 1998, Shear-wave velocity characteristics of geologic untis in California: Earthquake Spectra, v. 14, no. 3, p. 533–556.

Glossary

Amplification factor Numerical factor to which bedrock ground motion is scaled owing to surficial materials. Factor is dependent on both amplitude and period of input bedrock motion.

NEHRP National Earthquake Hazards Reduction Program

PGA Peak Ground Acceleration

PGV Peak Ground Velocity

Site class Classification of surficial material used to assign amplification factors.

SRTM Shuttle Radar Topography Mission

V_S^{30} Average shear-velocity down to 30 m from the surface.